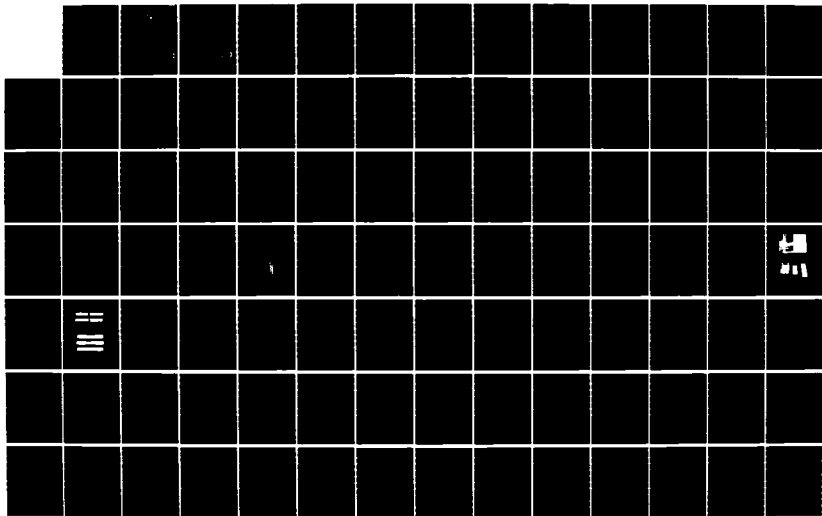
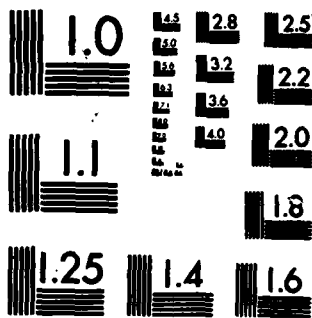


AD-A164 833

COMPARISON OF NOTCH STRENGTH BETWEEN GR/PEEK (APC-1 AND APC-2) AND GR/EPD. (U) AIR FORCE INST OF TECH 1/3  
WRIGHT-PATTERSON AFB OH SCHOOL OF ENGI... J E RAMEY  
DEC 85 AFIT/GAE/AA/85D-12 F/G 11/4 NL

UNCLASSIFIED





MICROCOPY RESOLUTION TEST CHART  
NATIONAL BUREAU OF STANDARDS-1963-A

1

AD-A164 033



COMPARISON OF NOTCH STRENGTH  
 BETWEEN GR/PEEK (APC-1 AND APC-2)  
 AND GR/EPOXY COMPOSITE MATERIALS  
 AT ELEVATED TEMPERATURE

THESIS

Joe E. Ramey, Jr.  
 Captain, USAF

AFIT/GAE/AA/85D-12

**DTIC**  
**ELECTE**  
 FEB 13 1986

*[Handwritten signature]* **S**

DTIC FILE COPY

UNITED STATES AIR FORCE  
 AIR UNIVERSITY

B.

**AIR FORCE INSTITUTE OF TECHNOLOGY**

Wright-Patterson Air Force Base, Ohio

**DISTRIBUTION STATEMENT A**  
 Approved for public release  
 Distribution Unlimited

86 2 12 - 046

AFIT/GAE/AA/85D-12

COMPARISON OF NOTCH STRENGTH  
BETWEEN GR/PEEK (APC-1 AND APC-2)  
AND GR/EPOXY COMPOSITE MATERIALS  
AT ELEVATED TEMPERATURE

THESIS

Joe E. Ramey, Jr.  
Captain, USAF

AFIT/GAE/AA/85D-12

**S** DTIC  
ELECTE **D**  
FEB 13 1986  
**B**

Approved for public release; distribution unlimited

## **DISCLAIMER NOTICE**

**THIS DOCUMENT IS BEST QUALITY PRACTICABLE. THE COPY FURNISHED TO DTIC CONTAINED A SIGNIFICANT NUMBER OF PAGES WHICH DO NOT REPRODUCE LEGIBLY.**

AFIT/GAE/AA/85D-12

COMPARISON OF NOTCH STRENGTH BETWEEN GR/PEEK  
(APC-1 AND APC-2) AND GR/EPOXY COMPOSITE  
MATERIAL AT ELEVATED TEMPERATURE

THESIS

Presented to the Faculty of the School of Engineering  
of the Air Force Institute of Technology

Air University

In Partial Fulfillment of the  
Requirements for the Degree of  
Master of Science in Aeronautical Engineering

Joe. E. Ramey, Jr., B.S.  
Captain, USAF

December 1985

Approved for public release; distribution unlimited

## Preface

In this experimental investigation, the reduction of strength for notched composite laminates of Aromatic Polymer Composite, APC-2, containing the matrix polyetheretherketone (PEEK), was examined. Quasi-isotropic laminates of  $[0/+45/-45/90]_{2S}$  fiber direction plies were tested in tension and compression at room temperature, 250<sup>0</sup>F, 275<sup>0</sup>F and 300<sup>0</sup>F. Three methods of failure strength prediction techniques were compared to experimental results. An extensive investigation of fractured surfaces was performed using a scanning electron microscope. During the SEM investigation, over 500 microphotographs were taken. The hope of this project is to provide insight into the temperature and notch size effects for a composite laminate.

There are several people to whom I am indebted and must single out. I would like to thank Dr. Jim Whitney of the Air Force Materials Lab for his sponsorship of this project. I appreciate the fine technical work of testing the specimens by John Camping and Chuck Fowler from the University of Dayton Research Institute (UDRI). Additionally, Tim Hartness, Dr. Ran Kim, and Satish Kemur from the UDRI staff have graciously provided their expertise. Gary Price, UDRI, was most helpful in the SEM analysis. Steve Donaldson, Dr. Robert Ruh, and Pat Stumpf

provided their fiber fracture expertise to me and provoked many thoughts for evaluating the SEM microphotographs. Dr. Anthony Palazotto, my advisor, is owed a great debt of gratitude. His patience, expertise and encouragement throughout my graduate work are most appreciated.

This paper is dedicated to the people in my life responsible for my happiness, my wife, Freda and my daughter, Tara. Both have suffered personal hardships that allowed me to complete this project and without Freda's typing...I love you both. Thanks

Joe E. Ramey, Jr.

<b>Accession For</b>	
NTIS GRA&I	<input checked="" type="checkbox"/>
DTIC TAB	<input type="checkbox"/>
Unannounced	<input type="checkbox"/>
Justification	
By _____	
Distribution/	
<b>Availability Codes</b>	
<b>Dist</b>	<b>Avail and/or Special</b>
A-1	23



Table of Contents

	Page
Preface . . . . .	ii
List of Figures . . . . .	v
List of Tables . . . . .	xii
List of Symbols . . . . .	xiii
Abstract . . . . .	xv
I. Introduction . . . . .	1
II. Theory . . . . .	12
Failure Prediction . . . . .	12
Point Stress Method . . . . .	15
Average Stress Method . . . . .	17
Three Parameter Method . . . . .	19
Material Analysis . . . . .	22
III. Experimental Procedure . . . . .	32
Material Preparation and Test . . . . .	35
Procedure	
Microscope Analysis . . . . .	38
IV. Results and Discussions . . . . .	40
Strength and Failure Prediction . . . . .	41
Point Stress Results . . . . .	48
Average Stress Results . . . . .	54
Three Parameter Model Results . . . . .	58
Microscopic Evaluation and Stress- Strain Results . . . . .	66
Compression Failure Analysis . . . . .	67
Tension Failure Analysis . . . . .	117
V. Conclusions . . . . .	167
VI. Recommendations . . . . .	170
Bibliography . . . . .	172
Vita . . . . .	176

List of Figures (cont.)

Figure	Page
19. Comparison of Predicted and Experimental Tension Failure Stresses for APC-2.....	51
20. Master 'd' Curve Comparison of Experimental and Predicted Failure Stresses.....	52
21. Comparison of Predicted and Experimental Compression Failure Stresses for APC-2.....	55
22. Comparison of Predicted and Experimental Tension Failure Stresses for APC-2.....	56
23. Master 'a' Curve Comparison of Predicted and Experimental Failure Stresses.....	57
24. Comparison of Predicted and Experimental Tension Failure Stresses for APC-2, Three Parameter Model.....	60
25. Comparison of Predicted and Experimental Tension Failure Stresses for APC-2, Three Parameter Model.....	61
26. Comparison of Predicted and Experimental Compression Failure Stresses for APC-2, Three Parameter Model.....	62
27. Comparison of Predicted and Experimental Compression Failure Stresses for APC-2, Three Parameter Model.....	63
28. Comparison of Predicted and Experimental Failure Stresses for APC-2 Using Three Parameter Model.....	64
29. Three Parameter Model Master Curve Comparison of Predicted and Experimental Failure Stresses for APC-2.....	65
30. Compression Specimen Far Field Strain-Load Data, 0.2" Diameter, Room Temperature.....	69
31. Compression Specimen Strain-Load Data, 0.2" Diameter, Room Temperature, Side-of-Hole Gage and Top-of-Hole Gage.....	70

## List of Figures

Figure	Page
1. Stress Distribution for a Hole in an Infinite Isotropic Plate.....	14
2. Infinite Plate Containing an Elliptical Hole Under Remote Uniform Tension.....	14
3. Point Stress Failure Criteria.....	16
4. Average Stress Failure Criteria.....	18
5. Deformation of a Thermoplastic Polymer.....	26
6. PEEK Cell Structure. (a) Repeat Unit of PEEK (b) Unit Cell of PEEK.....	27
7. Two Principal Types of Laminae.....	29
8. Effect of Broken Fiber on Matrix and Fiber Stresses.....	29
9. Typical Geometry of Notched Specimen .....	36
10. Test Equipment, Heat System Set-up.....	37
11. Compression Test Specimen and Anti-buckling Support.....	37
12. Failed APC-2 Tension Specimen.....	39
13. Failed APC-2 Compression Specimen.....	39
14. Strength for Notched and Unnotched Specimen Varying Temperature.....	43
15. Strength for Notched and Unnotched Specimen Varying Temperature.....	44
16. Tensile Failure Stress Normalized with Room Temperature Strength for Various Hole Diameters...	47
17. Compression Failure Stress Normalized with Room Temperature Strength for Various Hole Diameters...	49
18. Comparison of Predicted and Experimental Compression Stresses for APC-2 at Failure.....	50

List of Figures (cont.)

Figure	Page
32. Compression Specimen, Strain-Load Data, 0.2" Diameter 250 <sup>o</sup> F, Far Field Strain Gage.....	71
33. Compression Specimen Strain-Load Data, 0.2" Diameter, 250 <sup>o</sup> F, Side-of-Hole Gage and Top-of-Hole Gage.....	72
34. Compression Specimen, Strain-load Data, 0.2" Diameter, 275 <sup>o</sup> F, Far-Field Side-of-Hole, and Top-of-Hole Gages.....	74
35. Compression Specimen, Top-of-Hole and Side-of-Hole Strain-load Data, 300 <sup>o</sup> F, 0.2" Diameter.....	75
36a. Area of Study for Compression Specimen.....	77
36b. Area of Study for Tension Specimen.....	78
37. 90 Percent of Average Compression Failure Load. Top View. 130X (RT and 250 <sup>o</sup> F) .....	80
38. 90 Percent of Average Compression Failure Load. Top View. 130X (275 <sup>o</sup> F and 300 <sup>o</sup> F).....	81
39. 95 Percent of Average Compression Failure Load. Top View. 130X (RT and 250 <sup>o</sup> F).....	82
40. 95 Percent of Average Compression Failure Load. Top View. 130X (275 <sup>o</sup> F and 300 <sup>o</sup> F).....	83
41. 90 Percent of Average Compression Failure Load. In-hole View. 32X (RT and 250 <sup>o</sup> F) .....	85
42. 95 Percent of Average Compression Failure Load. In-hole View. 32X (275 <sup>o</sup> F and 300 <sup>o</sup> F) .....	86
43. 95 Percent of Average Compression Load. In-hole View. Lamina Separation.....	87
44. 95 Percent of Average Compression Failure Load. In-hole View. 32X (RT and 250 <sup>o</sup> F) .....	88
45. 95 Percent of Average Compression Load. In-hole View. 32X (275 <sup>o</sup> F and 300 <sup>o</sup> F).....	89

List of Figures (cont.)

Figure	Page
46. 90 Percent of Average compression Failure Load. In-hole View of Crippled 0° Fibers Within the Laminate. 6500X (RT and 250°F) .....	91
47. 90 Percent of Average Compression Failure Load. In-hole View of Crippled 0° Fibers Within the Laminate. 6500X (275°F and 300°F).....	92
48. Complete Failure of Compression Specimen With Breaking of Specimen at Room Temperature. Top View (RT and 250°F). . . .	94
49. Compression Failure Specimen. In-hole View. 32X(RT and 250°F).	96
50. Compression Failure Specimen. In-hole View. 32X(275°F and 300°F)	97
51. Compression Failure Specimen. In-hole View. Crippled 0° Fibers with Inter-laminar Matrix Deformation. 260X .....	98
52. Compression Failure Specimen, In-hole View. 0° Fibers Interlaminar Surface, Room Temperature..	100
53. Compression Failure Specimen, In-hole View. 0° Fibers Cripple Surface, 250°F.....	101
54. Compression Failure Specimen, In-hole View, 0° Crippled Fibers, 275°F.....	102
55. Compression Failure Specimen, In-hole View, 0° Crippled Fibers, 300°F.....	103
56. Compression Failure Specimen, In-hole View, 0° Crippled Fibers, 6500X (RT and 250°F) .....	105
57. Compression Failure Specimen, In-hole View, 0° Crippled Fibers, 6500X (275°F and 300°F) .....	106
58. Compression Failure Specimen, In-hole view, 0° Crippled Fibers, Inter-laminar Failure, 275°F.....	107
59. Compression Failure Specimen, In-hole View, 0° Crippled Fibers, Inter-laminar Failure, 300°F.....	109
60. Compression Failure Specimen, Top view. 130X (RT and 250°F) .....	110

List of Figures (cont.)

Figure	Page
61. Compression Failure Specimen, Top View. 130X(275 <sup>o</sup> F & 300 <sup>o</sup> F) .	111
62. Compression Failure Specimen, Top View, RT, Intra-laminar Fracture.....	113
63. Compression Failure Specimen, Top View, 275 <sup>o</sup> F, Crippled Fiber Ends.....	114
64. Compression Failure Specimen, Top View, 300 <sup>o</sup> F, Crippled Fiber Compressed Ends.....	115
65. Compression Failure specimen, Top View, 300 <sup>o</sup> F Crippled Fiber Compressed End, 6500X.....	116
66. Strain Results, 0.2" Diameter Cut Out, Tension, RT.....	120
67. Strain Results, 0.2" Diameter Cut Out, Tension, 275 <sup>o</sup> F.....	121
68. Strain Results, 0.2" Diameter Cut Out, Tension, 300 <sup>o</sup> F.....	122
69. Tension Specimen, 0 <sup>o</sup> Fibers, Top View, Near Hole 260X (RT and 250 <sup>o</sup> F) .....	124
70. Tension Specimen, 0 <sup>o</sup> Fibers, Top View, Near Hole. 260X (275 <sup>o</sup> F and 300 <sup>o</sup> F).....	125
71. Tension Specimen, 0 <sup>o</sup> Fibers, Top View, Near Hole, Matrix. 1300X (RT and 250 <sup>o</sup> F).....	126
72. Tension Specimen, 0 <sup>o</sup> Fibers, Top View, Near Hole, Matrix. 1300X (275 <sup>o</sup> F and 300 <sup>o</sup> F).....	127
73. Tension Specimen, 0 <sup>o</sup> Fibers, Top View, Away from Hole. 260X (RT and 250 <sup>o</sup> F) .....	129
74. Tension Specimen, 0 <sup>o</sup> Fibers, Top View, Away From Hole. 260X (275 <sup>o</sup> F and 300 <sup>o</sup> F) .....	130
75. Tension Specimen, 0 <sup>o</sup> Fibers, Top View Away From Hole, Matrix. 1300X (RT and 250 <sup>o</sup> F)....	131
76. Tension Specimen, 0 <sup>o</sup> Fibers, Top View, Away From Hole, Matrix. 1300X (275 <sup>o</sup> F and 300 <sup>o</sup> F).....	132

List of Figures (cont.)

Figures	Page
77. Tension Specimen, 0° Fibers, 250°F, Top View 3250X (Near hole and away from hole. . . . .)	134
78. Tension Specimen, 0° Fibers, 275°F, Top View 3250X (Near hole and away from hole. . . . .)	135
79. Tension Specimen, 0° Fibers, 300°F, Top View 3250X (Near hole and away from hole. . . . .)	136
80. Tension Specimen, 0° Fibers, Front View, Near Hole, 650X (RT and 250°F). . . . .	138
81. Tension Specimen, 0° Fibers, Front View, Near Hole. 650X (275°F and 300°F). . . . .	139
82. Tension Specimen, 0° Fibers, Front View, Near Hole, RT (1300X and 3250X). . . . .	141
83. Tension Specimen, 0° Fibers, Front View, Near Hole, 250°F, (1300X and 3250X). . . . .	142
84. Tension Specimen, 0° Fibers, Front View, Near Hole, 275°F, (1300X and 6500X). . . . .	143
85. Tension Specimen, 0° Fibers, Front View, Near Hole, 300°F, (1300X and 3250X). . . . .	144
86. Tension Specimen, 0° Fibers, Front View, Away From Hole, 650X (RT and 250°F). . . . .	145
87. Tension Specimen, 0° Fibers, Front View, Away From Hole. 275°F (650X). . . . .	146
88. Tension Specimen, 90° Fibers, Front View, Near Hole. 650X (RT and 250°F). . . . .	148
89. Tension Specimen, 90° Fibers, Front View, Near Hole. 650X (275°F and 300°F). . . . .	149
90. Tension Specimen, 90° Fibers, Front View Near Hole, 1300X (RT and 250°F). . . . .	151
91. Tension Specimen, 90° Fibers, Front View, Near Hole, 1300X (275°F and 300°F). . . . .	152

List of Figures (cont.)

Figures	Page
92. Tension Specimen, 90 <sup>o</sup> Fibers, Front View, Away From Hole. 650X (RT and 250 <sup>o</sup> F) .....	153
93. Tension Specimen, 90 <sup>o</sup> Fibers, Front View, Away From Hole. 650X (275 <sup>o</sup> F and 300 <sup>o</sup> F).....	154
94. Tension Specimen, 90 <sup>o</sup> Fibers, Front View, Away From Hole, Matrix. 1300X (RT and 250 <sup>o</sup> F)....	155
95. Tension Specimen, 90 <sup>o</sup> Fibers, Front View, Away From Hole, Matrix. 1300X (275 <sup>o</sup> F & 300 <sup>o</sup> F)...	156
96. Tension Specimen, Low Magnification. 20X.....	158
97. Tension Specimen, 45 <sup>o</sup> , Front View, Away From Hole, 250 <sup>o</sup> F.....	160
98. Tension Specimen, 45 <sup>o</sup> Fibers, Front View, Away From Hole, 250 <sup>o</sup> F, 1300X.....	161
99. Tension Specimen, 45 <sup>o</sup> Fibers, Front View, Away From Hole, 275 <sup>o</sup> F.....	163
100. Tension Specimen, 45 <sup>o</sup> Fibers, Front View, Away From Hole, 275 <sup>o</sup> F (High Magnification).....	164
101. Tension Specimen, 45 <sup>o</sup> Fibers, Front View, Matrix Plasticity.....	165
102. Tension Specimen, 45 <sup>o</sup> Fibers, Front View, Matrix Degradation.....	166



List of Tables

Table	Page
I. Number of Tests to Failure for APC-2.....	34
II. Number of Tests to 90% Average Failure Load.....	35
III. Values of Characteristic Length ' $d_0$ ' for Composite Laminates.....	53
IV. Values of Characteristic Length, $a_0$ , for Composite Laminates.....	58
V. Values of Notch Sensitivity Factor, C, and Exponential Parameter, m, for Composite Laminates.....	59

### List of Symbols

- $a_0$  Distance (inches) from the edge of the hole to the point where the average stress reaches the critical value, associated with Whitney's average stress failure criterion.
- $C$  Notch sensitivity factor, parameter associated with Pipe's three parameter model for failure prediction.
- $d_0$  Distance (inches) from the edge of the hole to point where the finite stress reaches the critical value, associated with Whitney's point stress failure criterion.
- $h$  Thickness of lamiate
- $K_T$  Stress concentration factor for finite width.
- $K_T^{\infty}$  Stress concentration factor for infinite width plate.
- $m$  Exponential parameter associated with Pipe's technique of failure analysis.
- $N_y$  Resultant force in global y-direction (lb/in).
- $R$  Radius of cut out or hole (in.).
- $R_0$  Reference radius (usually taken as unity).
- $\sigma_N$  Notched strength of finite width laminate.

List of Symbols (cont.)

$\sigma_N^0$  Notched Strength of infinite width laminate.

$\sigma_0$  Unnotched strength of a laminate.

Abstract

Thermoplastics have been developed to improve fracture toughness compared to the widely used thermosetting polymers such as epoxy systems. A semi-crystalline thermoplastic, poly-ether-ether-ketone(PEEK), matrix has been developed with significant toughness improvement over thermosets. A review of literature resulted in very little information related to the Aromatic Polymer Composite-2 (APC-2) which is formed from graphite fibers (60% volume) and PEEK. The experimental study reported herein was conducted to investigate the high temperature strength (tension and compression) of APC-2 laminates with holes. The experimental data was then used to determine parameters necessary to predict failure stress trends for the average stress failure criterion, point stress failure criterion, and a three parameter model failure criterion. The comparison of experimental and predicted failure strengths are depicted graphically. The failure modes of APC-2 are also studied utilizing the scanning electron microscope.

Comparison of Notch Strength Between Gr/PEEK  
(APC-1 and APC-2) and Gr/Epoxy Composite  
Material at Elevated Temperature

I. Introduction

Designers have always faced complicated decisions on what is the best material for a final product. During the age of metals, decisions were tough enough. The designer had to choose between several metals, heat treatments, alloy combinations, and yet retain the most profitable design possible. Metals were well studied and understood. Prediction of fracture loads and fatigue life cycles were possible for these isotropic materials even at elevated temperatures. However, as progress was made in strength-to-weight ratios, a new concept of design materials was introduced--composite materials.

Composite material consisted of extremely strong fibers surrounded by a weaker, yet much more ductile resin matrix. The composite material was no longer isotropic and traditional methods of failure loads no longer worked. The seemingly endless choices of material combinations (fibers and matrices) and material lay-up sequences (ply combinations), made the designer's choice grow unbounded, but he lacked the tools for proper design. He not only had an infinite choice of materials, he had no method of analysis that was general enough to use routinely.

The more that is known about specific combinations of fiber and matrix material and the comparison between failure prediction methods and experimental failure data using these specific fiber-matrix combinations, the easier the designer's task becomes. Notched specimens were used in this study because this type of discontinuity is one of the most critical in composite design.

Keeping these needs in mind, an experimental study was undertaken to analyze the failure of a composite material which consisted of a recently developed matrix, poly-ether-ether-ketone(PEEK). The PEEK matrix material has been found to have better fracture toughness than the more brittle epoxy matrices [1,2]. Since fracture toughness is an important characteristic in damage tolerance, crack growth, and impact damage, this new material seems desirable for aircraft designers.

Experiments were conducted at the USAF Material Laboratory, Wright-Patterson Air Force Base, Ohio. The experiments used quasi-isotropic laminates of Aromatic Polymer Composite-2 (APC-2), consisting of AS-4 graphite fibers and PEEK matrix. Tension and compression tests were carried out at room temperature, 250<sup>o</sup>F, 275<sup>o</sup>F, and 300<sup>o</sup>F for unnotched specimens and specimens with 0.1", 0.2", 0.4" and 0.6" diameter holes cut through the specimens. These temperatures were chosen with the knowledge that the glass transition temperature (T<sub>g</sub>) was approximately 275<sup>o</sup>F

to 290°F. The results of the experimental data are compared to three separate failure prediction criteria.

A recent experimental study by Malik [3] used Gr/Ep and APC-1. The results of Malik's work are used in this study for comparison purposes.

A study of failure characteristics should include an examination of the specific failure modes within the given material. The failed specimens from this experiment were examined utilizing a scanning electron microscope to determine the fracture failure mechanisms characteristic of APC-2.

#### A. Background

##### 1. Strength Predictions

There are many difficulties in determining strength reductions for composite laminates. The infinite number of possible ply lay ups (stacking sequence), a large variety of fiber and matrix combinations, uncertain failure criteria, the specific application geometry (i.e. thickness of the laminate, notch size, thickness-to-hole size ratio, and width-to-hole size ratio), and the environmental conditions around the composite must be considered. Currently, there are several techniques available for prediction of strength reduction in composite laminates: a finite element method [4,5], a fracture mechanics approach [5,6], a modified isotropic plate theory [7,8] and an isotropic plate approach [9]. However, designers are continually

searching for methods sufficiently general for routine applications.

Classical approaches to solving the composite notch strength reduction problem do not work, primarily because the stress concentration factors (SCF) for composites are not successfully characterized as in metals. The anomalies are believed to come from differences in methodology [6,7,10,11]. Metal SCF's are based on the conditions at a point on the hole boundary while the strength of the composite laminate appears related to the in-plane elastic stress region adjacent to the hole boundary [6,7,10]. Therefore, stress concentration factor alone is not a sufficient measure of strength for composite laminates containing circular cut-outs. The measure must be based on a more complete description of the stresses around the cutout.

One method employs the linear elastic fracture mechanic (LEFM) model. The fracture mechanic models proposed by Waddoups, et. al, [12] and Tirosh [13] have a theoretical intense energy region of dimension 'a' which contains a Griffith crack adjacent to the notch. This characteristic dimension is assumed to be a material property and remains constant for all values of notch radii. Thus, the model becomes the same as the linear elastic fracture mechanics (LEFM) method for a circular hole with two symmetrical cracks of length 'a'. The LEFM model contains two undetermined parameters: (1) the unknown 'a',



characteristic of the material and (2) the unnotched strength of the laminate,  $\sigma_0$ . Once having determined these for a notch size, this model allows prediction of the strength of same material laminates for any other notch size. However, composites do not show single cracks of dimension 'a', as do metals. Rather, composites tend to form several failure directions based on lay-up, direction and sequence. Also, composites demonstrate a relationship between the unnotched strength and the fracture toughness [14].

Whitney and Nuismer [10] developed two methods for predicting notched laminate strength as an alternative to the LEFM model for hole size diameters less than one inch. Their criterion result in the prediction of discontinuity size effects without applying the principles of LEFM. The first approach, point stress method, assumed that failure occurs when the stress over some distance ' $d_0$ ', away from the discontinuity is equal to or greater than the strength of the unnotched material. The second approach, average stress method, assumed that failure occurs when the average stress over some distance, ' $a_0$ ', equals the unnotched laminate strength. This approach allows for physical redistribution of local stress concentrations. Both methods were tested experimentally by the authors and experimental results confirmed applications to specific laminates and materials. The authors looked for a value of ' $d_0$ ' and ' $a_0$ '

which could be compared from one material laminate to the next material [11], but were unable to define one. Because these methods weren't exact and showed deviations between experiment and theory, others attempted to improve on the methods.

Karlak presented a criteria that ' $d_0$ ' had a square root dependence on hole sizes [15]. A characteristic factor,  $k_0$ , defining the relationship between ' $d_0$ ' and the hole diameter was introduced. Although Karlak was able to better fit failure results from Whitney and Kim [16] with his criteria than with the point stress method, he could not assign a physical significance to the square root dependency. He stated that the particular exponential fit may have been a peculiarity of quasi-isotropic laminates, or more likely, related to the ratio of the hole size to laminate thickness. More work needed to be done to improve failure prediction criteria.

Pipes, Wetherhold and Gillispie introduced a three parameter model to enhance failure prediction [17]. The three parameter model was dependant on (1) the strength of the composite laminate without holes, (2) a notch sensitivity factor ' $C$ ', and (3) an exponential factor ' $m$ '. This three parameter model is an enhancement of Whitney's two parameter model.

Much experimental work has been done and comparisons made with the failure prediction methods previously

discussed. The point stress and average stress have been studied at room temperature for tension and compression by several authors [3,10,11,18,19,20]. The three parameter model was tested by Malik and Pipes [3, 17]. Only the work of Malik compared experimental data to failure predictions at elevated temperatures.

Analysis of the fracture surface of failed specimen is important in order to determine what factors influence the fracture process. Microstructural features identify failure modes which can be removed by redesign of the material to increase the strength of the material. Nuismer and Labor noticed a specimen failed in tension perpendicular to load path for a short distance and then dynamic failure occurred with multi-directional failure taking place [18]. This short distance compared favorably to the average stress criteria failure for their experimental specimen.

## 2. Material Choice

In continuous fiber reinforced plastics, it is the fiber which determines the basic property profile. The function of the resin is to allow the fiber to develop its full potential by transferring the load from one fiber to another and by providing a support to prevent the fiber from buckling. The best possible load achievement is accomplished when fibers are completely wetted by matrix. It is important that the matrix continue to provide fiber support during service conditions. When a polyaromatic

matrix, such as polyetheretherketone (PEEK), is placed in a continuous fiber composite, the resultant laminates are known as aromatic polymer composites (APC).

The material chosen for this study, APC-2, is an improved laminate over the previously introduced APC-1. The principle change from APC-1 is the substitution of Hercules AS-4 graphite fibers into APC-2 in lieu of the Courtauld XAS graphite fibers in APC-1. This change was made to give a better bond between the PEEK matrix and the graphite fibers.

PEEK is a thermoplastic material and can be converted into a range of component shapes and sizes by the full spectrum of fabrication technologies [21]. Micro-composites are formed using PEEK and short glass or carbon fibers in preparing injection molding materials. A further area of technology where PEEK is used is the macro-composite role. In this role, PEEK is used with continuous fibers to form a continuous fiber reinforced composite.

As a composite material, PEEK provides the widest mechanical property spectrum achieved by a thermoplastic [21]: (1) with a modulus in the range of 3 to 150  $\text{GNm}^{-2}$  at 23<sup>0</sup>C and (2) with strength in the range 100 to 2,000  $\text{MNm}^{-2}$  at 23<sup>0</sup>C. Each engineering application imposes requirements on properties, which in turn dictate the compositional form for PEEK matrix. The study of APC properties is important to the aerospace community.

Donaldson compared unidirectional APC-1 directly to unidirectional graphite/epoxy [22]. He found APC-1 to be significantly tougher than graphite/epoxy for mode I and II fractures as well as various combinations of modes I and II. Using a scanning electron microscope, he observed significant differences between the two composite laminates' fracture surfaces. APC-1 microphotographs indicated much more plastic deformation than graphite/epoxy, clearly demonstrating the toughness superiority of APC-1 over graphite epoxy.

Hartness found that carbon fiber/PEEK system was superior to carbon fiber/epoxy system where interlaminar fracture toughness was measured and that the PEEK material was superior in strength and toughness [23].

In a comparative study of fatigue properties between carbon cloth impregnated with PEEK and carbon cloth impregnated with epoxy [24], Hartness and Kim found the PEEK composite system has superior fatigue properties over the graphite composite system.

Malik compared notched strength of quasi-isotropic APC-1 to quasi-isotropic graphite/epoxy for varying temperatures [3]. He noted adverse matrix-to-fiber interface degradation led to reductions in strength at elevated temperatures for APC-1.

As seen, little study has been completed for APC-1. The newer APC-2 is studied even less than APC-1,

however. The Materials Property Group at Imperial Chemical Industries (which manufactures APC) has presented studies [25,26] that demonstrate APC-2 has relatively high inter-laminar toughness and the extent of damage from low energy impact is lower for APC-2 than for carbon fiber/epoxy system. The need for a detailed fracture analysis and strength capability of APC-2 is evident.

#### B. Purpose of This Study

In support of the overall effort to understand various composite laminates and to increase the base of knowledge so designers can better choose materials, in particular in areas of discontinuities, this thesis is presented and has the primary purposes of: (1) studying the effect of temperature and stress concentrations on the fracture behavior of composite laminates with the same fiber system (graphite), but different matrix resin with unique properties in each resin (one laminate system is AS-4 graphite fibers in epoxy matrix, the second laminate system is XAS graphite fibers in PEEK matrix (APC-1) and the third laminate system is AS-4 graphite fibers in PEEK matrix (APC-2)); (2) studying the fracture surface characterization near the cut outs and away from the cut outs of the laminate systems at room temperature and elevated temperature; and (3) comparing the results of three laminate systems to common denominators.

This thesis will use the theory developed in the following sections to carry out analysis and use experimental APC-2

data to compare results. Results from previous work for APC-1 and Gr/Ep [3] will be compared to results obtained in this experimental study. Only quasi-isotropic laminates with  $[0/+45/-45/90]_{2S}$  directions will be examined for all three systems. The APC-2 specimens have been tested at room temperature,  $250^{\circ}\text{F}$ ,  $275^{\circ}\text{F}$ , and  $300^{\circ}\text{F}$ . The APC-1 and Gr/Ep specimen were tested at room temperature,  $250^{\circ}\text{F}$ , and  $300^{\circ}\text{F}$ . Each of the three systems tested consisted of an unnotched specimen as well as 0.1", 0.2", 0.4" and 0.6" diameter holes drilled through the specimen respectively. Scanning electron microphotographs are presented to demonstrate the fracture failure mechanisms.

## II Theory

### A. Failure Prediction

Designers must be able to predict the load carrying capabilities and strain-displacement actions of the materials they expect to use. To solve this problem and also consider practical characteristics of design, researchers have expended considerable effort into the understanding of laminated, continuous fiber reinforced, polymer matrix composites containing through-the-thickness circular cut outs. Three of the more general techniques are of practical interest for predicting the notch strength of laminated composites. One approach uses the concept of stress at a point, a fixed distance ahead of the hole [10], the second approach considers the average stress at some fixed distance ahead of the hole [10], while the third approach, a three parameter model introduced by Pipes [27], takes into consideration the notch sensitivity of the material as well.

Whitney and Nuismer [10] introduced two methods of predicting failure of composite laminates with holes less than 1.0". Consider the isotropic material equation comparing the ratio of the normal stress  $\sigma_y$ , along the x-axis to the uniform, applied tensile stress  $\bar{\sigma}$ , applied parallel to the y-axis [28]:

$$\sigma_y/\bar{\sigma} = 1 + \frac{1}{2} \left( \frac{R}{X} \right)^2 + \frac{3}{2} \left( \frac{R}{X} \right)^4 \quad (1)$$



When the normalized stress is plotted as a function of distance ahead of the hole, X-R, as shown in Fig. 1, it can be seen that the stress concentration is much more localized for the smaller radius holes. If a larger volume of material is subjected to high stress, the likelihood of having a sufficiently large flaw for failure is greater, resulting in a lower average strength for the laminate. Additionally, the smaller radius holes have more capability to redistribute the stress, resulting in a higher average failure strength than a plate with a larger hole. Since the brittle failure of a body under a given stress field is usually attributed to inherent flaws of sufficient dimensions being distributed throughout the body [11], the concept of determining the strength of a brittle composite material from maximum stress at a single point seems suspect, even more so if the maximum stress is very localized. With this in mind, two methods of failure prediction presented by Whitney and Nuismer require closer examination.

For a balanced, symmetric construction containing an elliptical hole with major and minor axis parallel to the x and y material axes respectively, the infinite width plate with a remote uniaxial stress is depicted in Fig. 2. The far field stress resultant, for laminate of thickness h, is denoted by  $N_y^{\infty}$ , yielding the average stress

$$\sigma_y^{\infty} = N_y^{\infty} / h \quad \text{Constant} \quad (2)$$

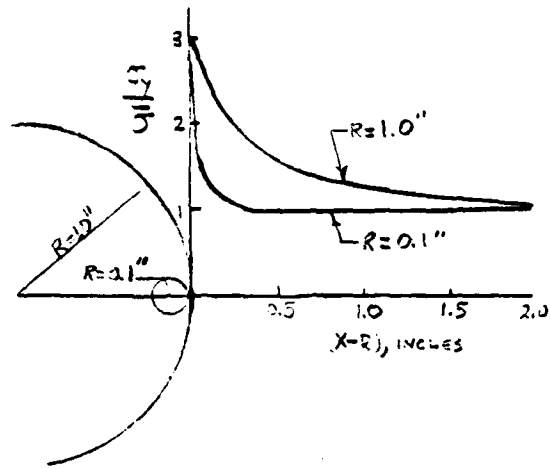


Fig. 1 Stress Distribution for a hole in an infinite isotropic plate.

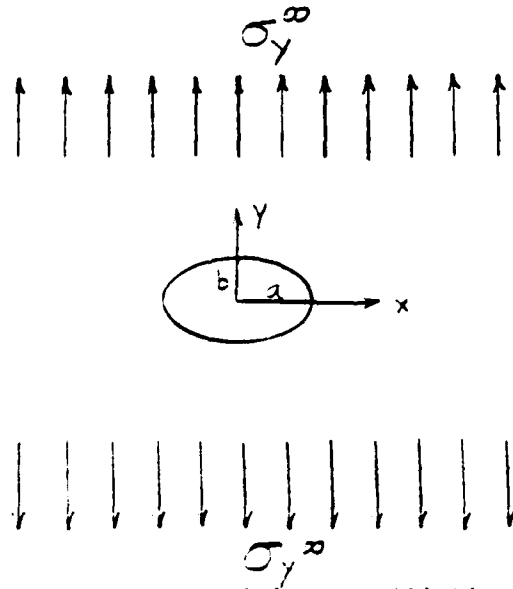


Fig. 2 Infinite Plate containing an elliptical hole under remote uniform tension.

In the presence of an elliptical hole, the effective normal stress along the major axis is of particular interest. The normal stress is then given by

$$\sigma_y(x,0) = N_y(x,0) / h \quad (3)$$

The stress field in the vicinity of a circular hole of radius, R, in an orthotropic laminate under uniaxial loading,  $N_y$ , can be determined by the solution of an elliptical hole as the special case where  $a=b=R$ . The effective normal stress,  $\sigma_y(x,0)$ , is given by [11]

$$\sigma_y(x,0) = \frac{\sigma_y^\infty}{2} \left\{ 2 + \left(\frac{R}{X}\right)^2 + 3\left(\frac{R}{X}\right)^4 - (K_T^\infty - 3) \left[ 5\left(\frac{R}{X}\right)^6 - 7\left(\frac{R}{X}\right)^8 \right] \right\} \quad (4)$$

for  $X \geq R$

Where  $K_T^\infty$  is the orthotropic stress concentration factor for an infinite width plate denoted in terms of effective elastic moduli

$$K_T^\infty = 1 + \sqrt{2 \left( \sqrt{\frac{E_{11}}{E_{22}}} - \nu_{12} \right) + \frac{E_{11}}{G_{12}}} \quad (5)$$

This equation is found to provide excellent approximation to the exact orthotropic plate solution [7], and for the isotropic case ( $K_T^\infty=3$ ) the expression is exact.

#### Whitney's Point Stress Criteria

The point stress failure criteria approach assumes that failure occurs when the stress over some distance away from the discontinuity is equal to or greater than the strength of the unnotched material [10]. It further assumes

that this characteristic distance, ' $d_0$ ', is a material property independent of laminate geometry and stress distribution. From Fig. 3, it can be written

$$\sigma_y(x,0) \Big|_{x=R+d_0} = \sigma_0 \quad (6)$$

This dimension represents the distance over which the material must be critically stressed in order to find a sufficient flaw size to initiate failure and is analogous to the approach used for predicting the plastic zone found in metals [29]. For the case of a circular hole in an isotropic plate, these assumptions in conjunction with equation (1) lead to the stress failure criterion

$$\sigma_N / \sigma_0 = 2 / (2 + z_1^2 + 3 z_1^4) \quad (7)$$

where  $\sigma_N$  is the laminate notched strength,  $\sigma_0$  is the unnotched laminate strength and

$$z_1 = \frac{R}{R + d_0} \quad (8)$$

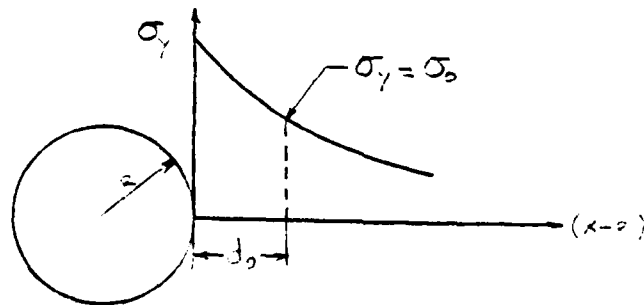


Fig. 3 Point stress failure criteria

It can be seen that for large values of  $R$ , equation (7) reduces to the SCF criteria for isotropic materials, that is  $\sigma_0/\sigma_N^{\infty}=3$ ; while for small values of  $R$ , equation (7) reduces to  $\sigma_0/\sigma_N^{\infty}=1$ , as expected. Although written for an isotropic material, equation (4) can be extended to include any laminate of symmetric construction by using the orthotropic solution for a hole in an infinite plate and thus becomes [10,30]

$$\frac{\sigma_N^{\infty}}{\sigma_0} = 2 / [(2 + z_1^2 + 3z_1^4) - (K_T^{\infty} - 3)(5z_1^6 - 7z_1^8)] \quad (9)$$

Here  $\sigma_N^{\infty}$  is the notched strength of an infinite width laminate; that is, the applied stress  $\sigma_y(x,0)$  at failure. Equation (9) reduces to the classical stress concentration result for very large holes (i.e. as  $R \rightarrow \infty$ ,  $z_1 \rightarrow 1$ ) and for very small holes (i.e. as  $R \rightarrow 0$ ,  $z_1 \rightarrow 0$ ).

#### Whitney's Average Stress Criteria

A second method of predicting failure loads in composites is called the average stress method [10]. This method assumes failure to occur when the average stress over some distance, ' $a_0$ ', equals the unnotched laminate strength (Fig. 4). As with the point stress method, this critical distance is assumed to be a material property independent of laminate construction and stress distribution. The physical argument for this approach is given by the assumption that the material has the ability to redistribute

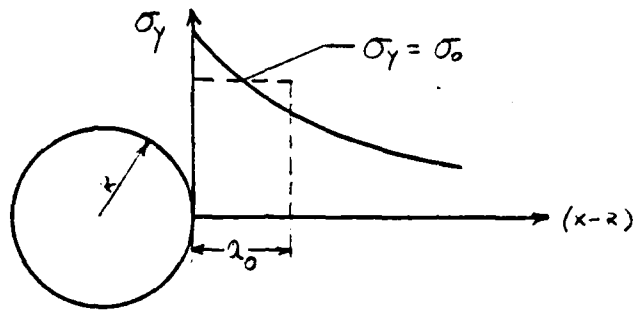


Fig. 4 Average stress failure criteria

local stress concentrations. Thus, 'a<sub>0</sub>', could be considered as a first order approximation to the distance ahead of the discontinuity across which failure has taken place. The average stress criterion takes the form of

$$\bar{\sigma}_0 = \frac{1}{a_0} \int_R^{R+a_0} \sigma_y(x,0) dx . \quad (10)$$

By substituting equation (1) into equation (10) and then performing the integration, the stress failure criterion for an isotropic plate is found

$$\frac{\bar{\sigma}_0}{\sigma_c} = \frac{2(1 - z_2)}{2 - z_2^2 - z_2^{-2}} \quad (11)$$

where

$$z_2 = \frac{R}{R + a_0} \quad (12)$$

As before, for large radius holes, the strength reduction predicts the SCF and for small values of radius, no strength reduction is predicted. For the case of notched strength of an infinite width laminate, integrating equation (10) to the ratio of the notched strength of an infinite width laminate to unnotched strength is given as

$$\frac{\sigma_N^0}{\sigma_0} = 2(1 - z_2) / [(2 - z_2^2 - z_2^4) + (K_T^0 - 3)(z_2^6 - z_2^8)] \quad (13)$$

These two methods of failure strength prediction use only two parameters to determine the predictions, (1) a characteristic length and (2) the unnotched strength of the material. Both methods assumed the characteristic lengths to be constant for all holes sizes which is contrary to experimental observations of other researchers [3,11,15]. Recall Karlak [15] first proposed that ' $d_0$ ' had a square root dependency on the notch radius, but was not sufficiently satisfied with the exponential parameter.

#### Pipes' Three Parameter Model

Pipes, Gillispie, and Wetherhold [17,27] proposed that the material notch sensitivity,  $C$ , be considered along with an exponential parameter,  $m$ . Thus, this method has three material parameters: (i) the unnotched material strength

$\sigma_0$ , (2) the material notch sensitivity,  $C$ , and (3) the exponential parameter,  $m$ . This method yields the relationship

$$\sigma_0 = \left(\frac{R}{R_0}\right)^m / C \quad (14)$$

Where  $R_0$  is a reference radius. Combining equation (14) with equations (8) and (9) makes it possible to write an equation for prediction of notched strength as a function of notch radius where the parameters  $m$ ,  $C$ , and  $\sigma_0$  are known.

$$\frac{\sigma_N^\infty}{\sigma_0} = 2 \left\{ 2 + L^2 + 3 L^4 - (K_T^\infty - 3)[5 L^6 - 7 L^8] \right\}^{-1} \quad (15)$$

Where

$$L = \left( 1 + R^{m-1} R_0^{-m} C^{-1} \right)^{-1} \quad (16)$$

Physically, as the notch sensitivity increases there is a reduction in strength for a given notch radius. For complete notch insensitivity ( $C=0$ ), unnotched strength is equal to notch strength for all radii. For infinite notch sensitivity ( $C=\infty$ ), notched strength/unnotched strength is equal to  $1/K_T^\infty$ . The exponential parameter,  $m$ , acts to change the slope of the notch sensitivity. This parameter should be  $0 \leq m \leq 1$  for admissible material systems. The upper value,  $m=1$ , results in a relation which is independent of notch size [12,27] while the lower bound,  $m=0$ ,



reduces to the two parameter model [11, 12, 27]. This three parameter model gives very good approximations to failure load predictions [3,17,27].

For constant values of  $K_T^{\infty}$ , it is possible to superimpose the notched strength relation uniquely defined by the parameters  $m$  and  $C$  to a second relation defined by  $m^*$  and  $C^*$  [17]. It is possible to construct notched strength as a function of notch radius for all such laminate configurations or materials by measuring the relation for a single laminate or material and measuring sufficient data (typically three points) for a new material or laminate in order to establish shift parameters. These shift parameters,  $m^*$  and  $C^*$ , are used to find the radius shift parameter,  $R^*$ . This allows superposition of notched strength to a single master curve for all materials and laminates of common stress concentration factor,  $K_T^{\infty}$ . Notched strength data for quasi-isotropic laminates of all composite materials may be superimposed to form a single master relation since  $K_T^{\infty}=3$  for all quasi-isotropic laminates.

Pipes found the necessary and sufficient condition for the superposition to be

$$L^* = L \quad (17)$$

and

$$R^*{}^{m^*-1} R_0^{-m^*} C^{*-1} = R_0^{m-1} C^{-1} \quad (18)$$

For the case where  $K_T^{\infty}=3$ , a master curve can be drawn to relate materials of different orthotropy provided  $m^*$  and  $C^*$  do not vary. Thus, the master curve has  $K_T^{\infty}=3$ ,  $m^*$  equal to a constant, and  $C^*$  equal to a second constant. Many materials demonstrate that  $C=10$  and  $m=0.5$  are intermediate values. For this special case and  $R_0=1$ ", it is possible to determine  $R^*$  in terms of  $\sigma_N^{\infty}/\sigma_N$  (let  $\sigma_N^{\infty}/\sigma_0=S$ ) and the parameters 'm' and 'C'.

$$R^* = \frac{1}{C^{m-1}} \left\{ \left[ \frac{-1 + \sqrt{1 + 24\left(\frac{1-S}{S}\right)}}{6} \right]^{-1/2} - 1 \right\}^{\frac{1}{m-1}} \quad (19)$$

This allows the strength data for any material laminate system to be superimposed to a common master curve of equal orthotropy ( $K_T^{\infty}=3$ ).

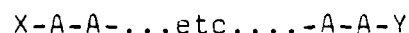
#### B. Material Analysis

Although macroscopic failure predictions, such as those discussed in the previous section, are acceptable to designers for general purposes, it is often significant for the designer to be more intimate with the specific "weaknesses" of a given material. For instance, a particular matrix may resist water absorption more efficiently than a second matrix. The effects of temperature variations and cut outs are other parameters the designer must have available. The choice of materials is an important decision and the more information available for a designer, the more efficient the end product becomes. In this

section, the nature of polymers, in general, are explained, followed by specific information about the polymer, PEEK. A discussion of fiber and matrix independent and dependent actions will be addressed to complete this section.

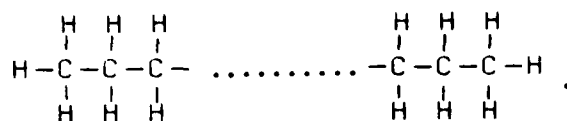
As mentioned previously, the stresses within laminates have been studied often. Still the state of stress at a specific location within any composite can be very complex. The effects of non-linear matrix materials, inter-laminar stresses, and intra-laminar stresses are not constant throughout a composite. The specific composition of the matrix must be known for better understanding of the failure mechanisms and the expected strength of a composite. As polymers are manufactured into chain molecules, the following discussion is offered to help understand the nature of polymers and more specifically, the PEEK matrix material used in this experimental study.

Polymers are formed from long chain molecules. To form a long-chain molecule, each unit or monomer of the chain must be able to link itself to neighbors on each side [32]. This unit, usually repeated many times (e.g. 100-10,000) along the chain, can be a single atom, as in sulphur and selenium, or a molecule, as in asbestos, silicones and organic polymers. Single linear polymers have the form



where A is the repeated structural unit and X and Y are

monovalent terminal units. An example is polyethylene, a long-chain paraffin,



Here, A is CH<sub>2</sub> and X=Y=H. The carbon atoms are shown as a straight line, but in reality form a zigzag sequence.

The units in the chain need not be all identical. Innumerable variations are possible. In copolymers, two different units A and B occur randomly along the chain. In blocked copolymers they form an ordered sequence.

The exceptional deformability of the rubber molecule is due to the spiral nature of the carbon chain. In some materials, the carbon chain is a zigzag, not a spiral and the molecule is less deformable. In recent years ways have been found for synthesizing isostatic polymers, i.e. of controlling the relative orientation of the monomers along the chain.

Structural units of higher valency in the main chain provide side chains by which the main chain can be linked to others, so forming a network polymer. These densely cross-linked polymers are described as thermosetting, because once formed, they do not soften on heating but remain linked together in a hard, rigid form until temperatures are reached at which they disintegrate chemically. Dissolved in organic solvents or combined with drying oils,

they form varnishes, lacquers, and adhesives. When aged in air and especially when cured by heating, they polymerize.

Polymers can exist in various mechanical states: fluid, rubbery, gel, glassy and crystalline. Linear polymers without cross-links, such as rubber latex, are viscous fluids. They consist of long, convoluted molecules tangled together like a mass of earthworms, and they flow by the sliding of molecular segments over one another. This is a thermally activated process, and the viscosity varies rapidly with temperature. At low viscosities ( $<1000$  poises) the flow is Newtonian, but not at high viscosities. Such materials are thermoplastic polymers. Above their glass transition temperature they are soft, deformable and, if not cross-linked, fluid. Below their  $T_g$ , they are typical glasses. By increasing the density of the cross-links, a continuous range of properties can be produced; soft elastic to vulcanite.

The rate of chain straightening or crumpling depends on viscosity, because it involves the sliding segments of chains past one another. The strain for a continuous stress develops as shown in Fig. 5 [32]. The total deformation is contributed by "true" elasticity (straining of the nearest neighbor), high elasticity and viscous flows, the latter being suppressed in the more highly cross-linked materials. On unloading, the true elasticity is recovered instantly but the high elasticity recovers more gradually because of the viscous drag on the chains, giving delayed elasticity or elastic "after-effect".

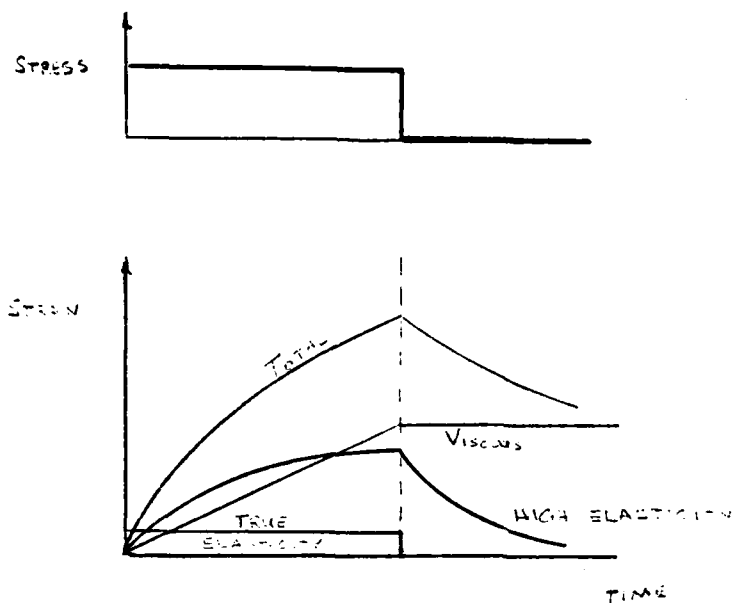


Fig. 5 Deformation of a thermoplastic polymer

Some polymers crystallize. Polymers, of hydrocarbon chains less than about 100 units long, crystallize almost completely on cooling. Those with longer chains (100-10,000 units) crystallize partly. In the crystalline regions, about  $100 \text{ \AA}$  across, the chains are parallel, whereas in the non-crystalline regions they are tangled. The chains form crystallites by folding back and forth in straight lengths, about  $100 \text{ \AA}$  long. A single molecular chain may extend through both crystalline and non-crystalline regions.

Glassy polymers are softened and made less brittle by the addition of plasticizers, substances of low

molecular weight that lower the  $T_g$ . Brittleness is then reduced at the expense of rigidity.

Kamur and Anderson depict the repeat unit of PEEK as that shown in Fig. 6a [33]. The orthorhombic unit cell of PEEK has values of  $a$ ,  $b$  and  $c$  which are reported to be in the range of  $7.75 - 7.78\text{\AA}$ ,  $5.89 - 5.92\text{\AA}$  and  $9.88 - 10.06\text{\AA}$  respectively. The unit cell contains two chains, each with two-thirds of a repeat unit. PEEK enters the non-crystalline state by quenching from the melt temperature and turns to semi-crystalline polymer by heat treatment above the  $T_g$ .

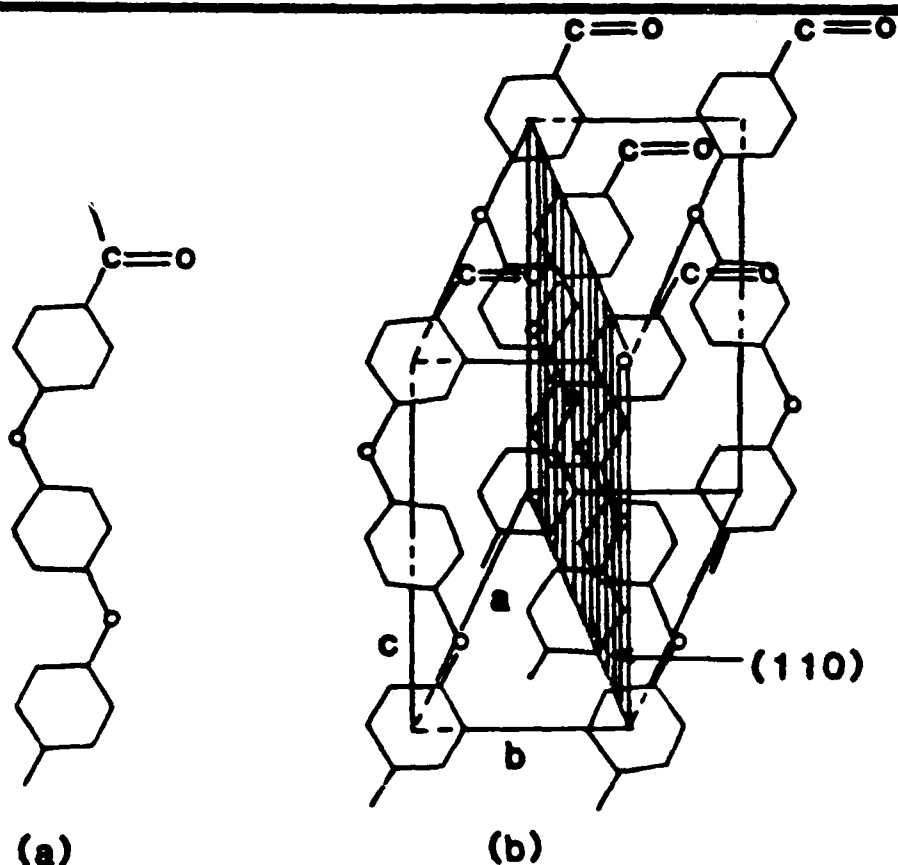


Fig. 6. PEEK cell structure. (a) Repeat unit of PEEK  
(b) Unit cell of PEEK

The PEEK matrix in APC-2 surrounds the AS-4 graphite fibers and forms microscopic bonds with the fibers. The combination of PEEK and AS-4 fibers form a lamina when continuous fibers are laid side-by-side in a single direction.

A lamina is a flat arrangement of unidirectional fibers or woven fibers in a matrix. Two typical laminae are shown in Figure 7 [34] along with the principal material axes. The fibers are the principal reinforcing or load-carrying agents. The fibers are typically strong and stiff. the function of the matrix is to support and protect the fibers and to provide a means of distributing load among and transmitting load between fibers. The latter function is especially important if a fiber breaks as in Fig. 8[34]. Load from one side of a broken fiber is transferred to the matrix and subsequently to the other side of the broken fiber as well as adjacent fibers. The mechanism for the load transfer is the shearing stress developed in the matrix. The shearing stress resists the pulling out of the broken fiber.

The major purpose of lamination or ply build-up is to tailor the directional dependence of strength and stiffness of a material to match the loading environment of the structural element. Laminates are uniquely suited to this objective since the principal material directions of each layer can be oriented to need. Symmetric laminates with balanced laminae (same number of positive angle plies as



negative angle plies) in addition to  $0^\circ$  and  $90^\circ$  orientations are considered quasi-isotropic for plane stress conditions. The  $[0/+45/-45/90]_{2S}$  lay up of this study provide quasi-isotropic properties to fibers.

To complete the failure analysis cycle, from the molecular chain build-up of the matrix to the testing of the composite, a scanning electron microscope provides an excellent means to evaluate the fracture surfaces of the failed specimen. The scanning electron microscope can be used to evaluate the fibers, for method of fracture and matrix-to-fiber bonding, as well as to analyze the matrix for ductility, temperature degradation, and adherence of matrix to fibers. Matrix deformations, such as hackles in brittle matrix materials, provide information about stress fields. These deformations must be evaluated for complete failure analysis. The term "hackle" is used to identify fracture by tearing, that results from inter-laminar shear. Although hackles have different shapes and sizes, they do have some common characteristics. Individual hackles are flake-like in appearance and they overlap on top of one another similar to the shingles on the roof of a house. Hackles usually lie between adjacent parallel fibers and are oriented approximately normal to the fiber axes. It has been observed [2], for brittle failures, that the angle of the hackles is an indication of the amount of shear stress experienced by the matrix. A flat hackle indicates more

shear stress in the failure mechanism than a vertical hackle. For a shear mode failure (mode II), the hackles appear flat and for an opening tensile failure (mode I), the hackles appear vertical. The formation of "hackles" is a much debated topic when thermoplastic fracture modes are discussed. Thermoplastics, such as PEEK, do not exhibit the regularity of hackle formations during fracture as do the more brittle epoxy systems. There are hackle-like formations in thermoplastics but they are not well defined compared to epoxy hackle formations. The term "hackle", as used in this study, refers to flake-like fracture surfaces, even though the "hackles" are not regular in formation.

Miller and Wingert [35] defined fiber-matrix interactions as similar to adhesive-bonded joints. Fracture between the fiber and the adjacent matrix is termed "adhesive" fracture. Fracture that occurs in the matrix adjacent to the fibers is called "cohesive". Clean, pulled-out fibers indicate an adhesive fracture process for pullout. However, when thin matrix adheres to the fiber, a partially cohesive fracture failure occurs. This type of terminology will be used subsequently as the author observes the failure mechanisms within this study.

### III Experimental Procedure

Experimental tests must be performed to determine the intrinsic strength properties and characterization of any composite system. This experimental program was developed to provide data for: (1) analyzing and evaluating the strength reduction of APC-2 for various hole sizes within a given specimen, (2) analyzing and evaluating the effect of elevated temperature on the strength properties, (3) study the failure mechanisms at 90 and 95 percent of average failure load and (4) determine, if possible, the specific failure mechanisms on the microstructural level using scanning electron microscope techniques.

The material used in this study was purchased from the manufacturer and, because of this, the specific details of laminate construction are not known. However, published information concerning general construction procedures is presented. The information is from Imperial Chemical Industries, ICI, literature.

APC-2 sheets are fabricated by consolidating multiple layers of unidirectional pre-impregnated tapes above the melting point of the polymer and then cooling to allow the polymer to crystallize and rigidize the structure. APC-2 composites have a complex hierarchy of structures. Within APC-2, the largest sub-units are the stacked 125  $\mu\text{m}$  plies of unidirectional impregnated tapes. The carbon fibers within each pre-preg layer are about 7  $\mu\text{m}$  diameter and

typically occupy 60 percent of the volume. The gaps occupied by the matrix between the fibers are in the same size range as the fibers, that is 1 to 10  $\mu\text{m}$ [31]. Composite fabrication involves stacking layers of APC-2 prepreg between press platens, heating to 720<sup>o</sup>F under low pressure, applying a consolidating pressure and cooling rapidly.

The laying up of prepreg prior to pressing is carried out cold. The lay up is symmetrical about the centerline and off-axis angles are balanced, plus and minus, to prevent warping due to differential thermal contractions on cooling.

The material used in this study was received in 16 inch square panels from the manufacturer. The panels were quasi-isotropic laminates of  $[0/+45/-45/90]_{2S}$  fiber directions, 16 plies thick.

The notch effect was examined by considering circular holes of 0.1", 0.2", 0.4" and 0.6" diameters drilled through specimen centers.

Temperature effects were studied by performing tests at room temperature, 250<sup>o</sup>F, 275<sup>o</sup>F, and 300<sup>o</sup>F, keeping in mind the glass transition temperature,  $T_g$ , of 290<sup>o</sup>F[23].

The absolute minimum number of test specimens necessary to produce meaningful results was considered to be three due to the statistical failure nature of composites. The ultimate strength was therefore based on three ostensibly identical tests. At least one specimen from each test condition for 0.2" diameter notched specimen was strain gaged

away from the hole, called the far field gage, to measure strain-to-failure for the laminate. One set of specimens were strain gaged at the side of the notch. This measurement is termed side-of-hole data. Additionally, specimens were gaged at the top of the hole and the results from this gage are named "top-of-hole" data. These gage locations are depicted in a photograph in the next section. One specimen each for 0.2" at RT, 250<sup>o</sup>F, 275<sup>o</sup>F, and 300<sup>o</sup>F was investigated at 90 and 95 percent of average failure load. This portion of the experiment attempted to demonstrate the pre-catastrophic failure modes of APC-2. The number of test specimens and conditions are shown in Table 1. It should be noted the same number of specimens were tested at 95% average failure load as were tested at 90% average failure load shown in Table 2.

Table 1 Number of Tests to Failure for APC-2

<u>Temp</u>	<u>Loading</u>	<u>Unnotched</u>	<u>Hole diameter (inches)</u>				<u>Total</u>
			<u>0.1</u>	<u>0.2</u>	<u>0.4</u>	<u>0.6</u>	
RT	Tension	3	3	3	3	3	15
	Compression	3	3	3	3	3	15
250 <sup>o</sup> F	Tension	3	3	3	3	3	15
	Compression	3	3	3	3	3	15
275 <sup>o</sup> F	Tension	3	3	3	3	3	15
	Compression	3	3	3	3	3	15
300 <sup>o</sup> F	Tension	3	3	3	3	3	15
	Compression	3	3	3	3	3	15
Total		24	24	24	24	24	120

Table 2 Number of Tests to 90% and 95% Average Failure Load

<u>Temp</u>	<u>Loading</u>	<u>Hole Diameter (inches)</u>	
		<u>0.2</u>	<u>0.6</u>
RT	Compression	1	1
	Tension	1	1
250 <sup>0</sup> F	Compression	1	1
275 <sup>0</sup> F	Compression	1	1
	Tension	1	1
300 <sup>0</sup> F	Compression	1	1
	Tension	1	1

A. Material Preparation and Test Procedure

All specimens were flat rectangular plates cut from the 16 inch square panels using conventional fabrication techniques and were inspected by x-ray techniques to ensure freedom from defects. The typical specimen is shown in Fig. 9. The end tab material was 1/16 inch thick glass epoxy bonded to the APC-2 specimen using a general purpose epoxy. The specimens were then heat treated for one hour at 200<sup>0</sup>F to ensure complete bonding. A bridgeport milling machine was used to drill the 0.1", 0.2", 0.4", and 0.6" diameter holes, minimizing runouts. Dog bone specimens for compression testing of unnotched specimens were machined on a router equipped with an abrasive cylinder.

The tensile tests were accomplished on an Instron Model 1115 at a constant cross head displacement rate of 0.01 in./min. The test results are presented in Table 3.

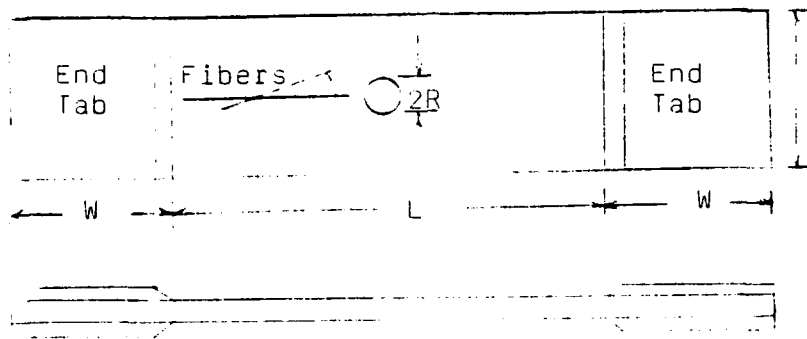


Fig. 9 Typical Geometry of Notched Specimen

problems at elevated temperatures, specimens were heated in a cylindrical chamber using an adjustable hot air gun. Specimens were equipped with thermocouples and allowed to stabilize for 10 minutes thermally prior to testing at the elevated temperatures. The temperature test equipment is shown in Fig. 10.

The compression tests were performed on an MTS model 312.31 with a 35,000 pound capacity using a constant cross head displacement rate of 0.03 inches per minute. The specimens were placed in an anti-buckling fixture, consisting of two aluminum plates surrounding the entire specimen length, under a displacement mode as shown in Fig. 11. The compression specimens were thermally tested in the same

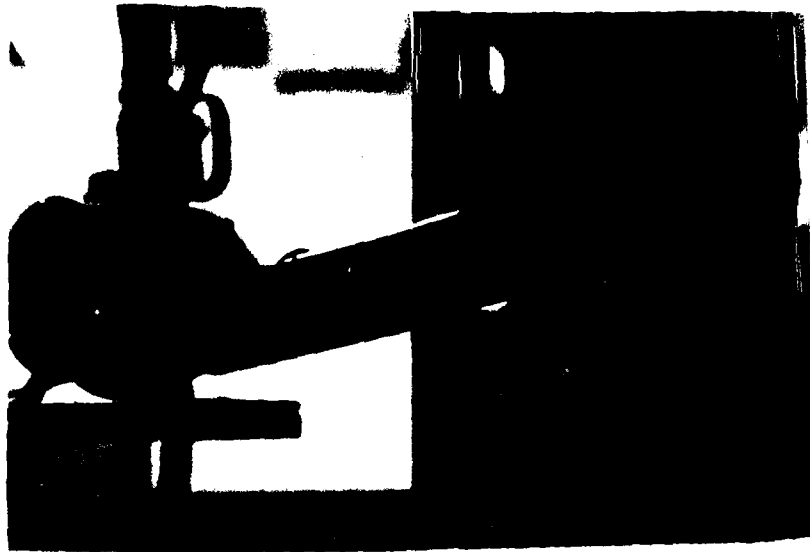


Fig. 10. Test Equipment Heat System Set-up.

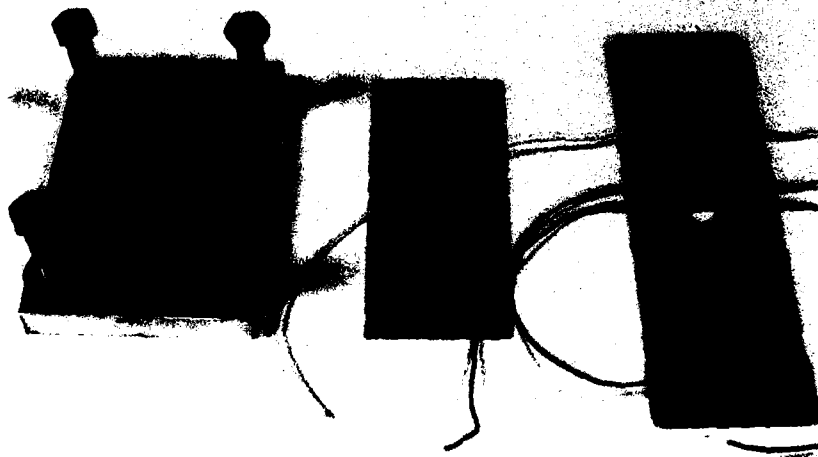


Fig. 11. Compression Test Specimen and Anti-buckling Support.



manner as the tensile specimens previously addressed. No tab adhesion problems occurred during the compression or tensile tests.

Failed tension specimens are shown in Fig. 12, while failed compression specimens are shown in Fig. 13.

#### B. Microscopic Analysis

Scanning electron microscope photomicrographs were taken using an International Services Inc. model Alpha-9 to characterize the fracture surfaces and investigate the specific failure modes of the laminates. After the specimens were tested, they were cut for mounting, taking care not to damage the fracture surfaces. Specimens were mounted on aluminum pedestals and a gold coating applied to enhance viewing of the specimen.

Specimens were viewed in the vicinity of the hole to determine failure mechanisms and then viewed at least one radius away from the hole and this region compared to the failure modes in the vicinity of the hole. Care was taken not to examine the outer edge of specimen where edge conditions might effect the failure modes. The  $0^{\circ}$ ,  $90^{\circ}$ , and  $45^{\circ}$  plies were examined in a lamina location consistent throughout the viewing (i.e. the two  $90^{\circ}$  lamina were examined for all specimen, the  $0^{\circ}$  plies inside the laminate were examined for all specimens. Various magnifications were used ranging from 20X to 6500X. The results of this experiment and the scanning are presented and discussed in the next section.



Fig. 12. Failed APC-2 Tension Specimens

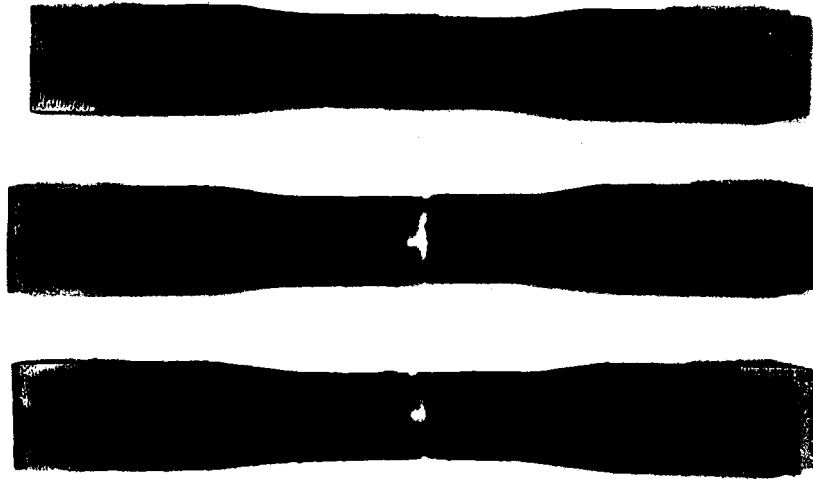


Fig. 13. Failed APC-2 Compression Specimens

#### IV Results and Discussion

The prediction of failure strengths for composite laminates is of prime concern to designers. Designers must be able to predict the strength of a material during the design phase to ensure structural integrity as well as provide the most cost effective material available. Additionally, the first step in prediction of strength reduction for impact damaged composite materials is to develop well defined prediction techniques for shapes such as holes, which can be analyzed mathematically. Failure prediction techniques for composites have been explored by several investigators [7,11,15,18,19,20,36], with little effort directed to elevated temperature predictions.

In this experimental investigation, a comparison of three methods of failure strength prediction are evaluated. The point stress method assumes failure to occur when the normal stress in front of the hole at some fixed distance,  $d_0$ , first reaches the unnotched strength,  $\sigma_0$ , of the material. The average stress method assumes failure to occur when the average stress at some fixed distance,  $a_0$ , equals the unnotched strength. The third method is a three parameter model and depends on the unnotched strength,  $\sigma_0$ , the notch sensitivity factor,  $C$ , and the exponential parameter,  $m$ .

Thorough evaluation of failure strengths of a composite must include a micro-structure failure analysis. The use of

scanning electron microscope techniques permits detailed inspection of each laminate fracture surface.

The spectrum of this investigation is very broad and because of this it is fitting to divide this section into two parts. First, the strength analysis and failure strength prediction methods will be presented for APC-2 and, where applicable, comparisons made with results from Malik's work for APC-1 and Gr/Ep. The last section is devoted to the results of the microscopic evaluation and comparative analysis with other results and stress-strain data gathered from this study.

#### A. Strength and Failure Strength Predictions

As mentioned earlier, three ostensibly identical tests were performed for each particular hole size and temperature. This number is considered to be the absolute minimum number necessary to produce meaningful results due to the statistical nature of composite material.

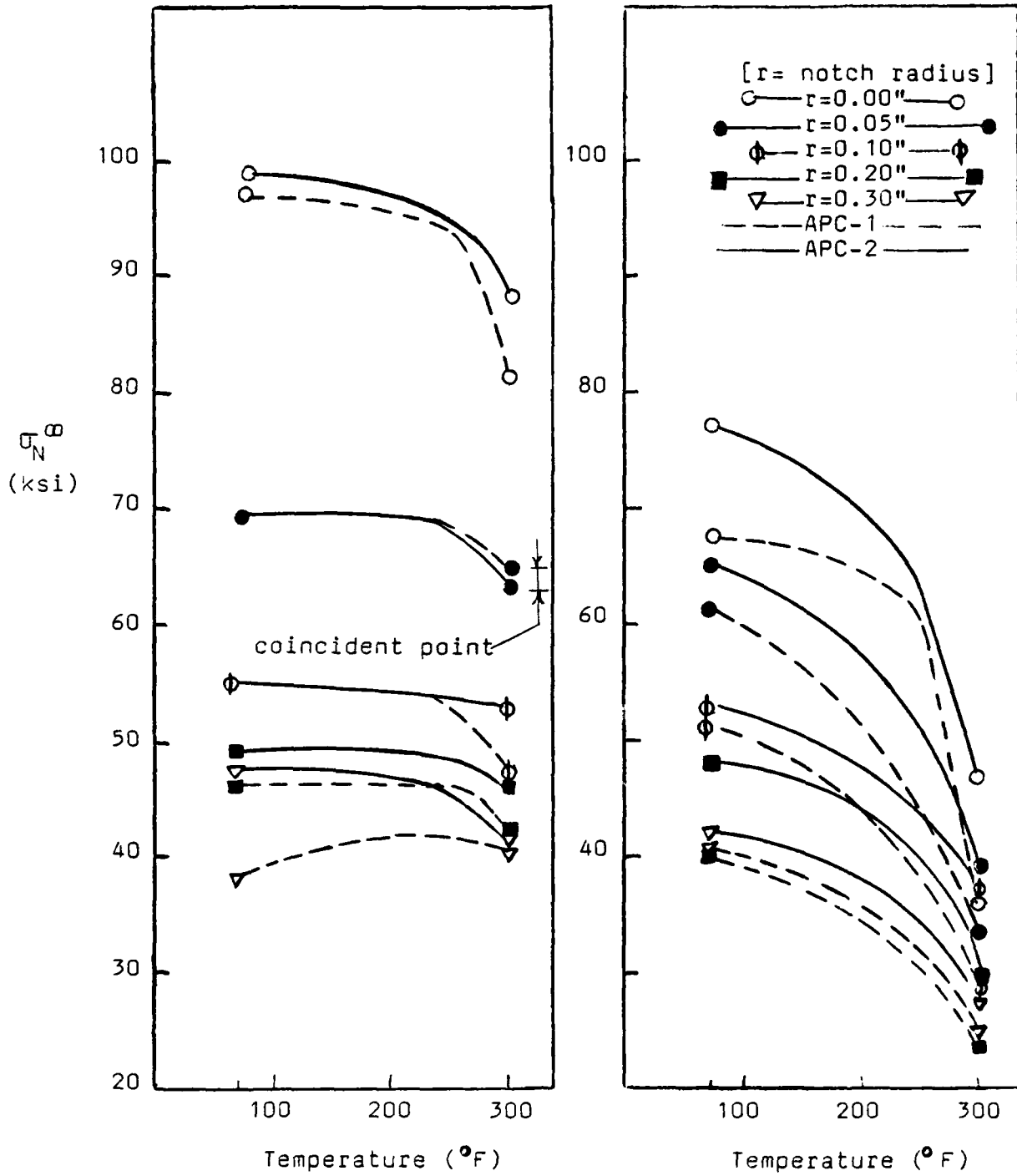
From the failure load of an unnotched specimen, the failure stress,  $\sigma_o$ , was computed. Similarly, the gross failure stress,  $\sigma_N$ , of the notched specimen was obtained from the failure load of that specimen. The values were then adjusted for all laminates by multiplying  $\sigma_N$  by the isotropic finite width correction factor,  $K_T/K_T^{\infty}$  for holes to obtain the notched, infinite width plate failure stress,  $\sigma_N^{\infty}$ . The finite width correction factor is given by

$$\frac{K_T}{K_T^\infty} = \frac{2 + (1 - 2R/W)^3}{3(1 - 2R/W)},$$

where  $W$  is the finite width of the specimen and  $R$  is the hole radius [11]. Whitney found that a finite element program solution using a hole diameter to width ratio of  $1/3$  compared well with corrected notch strength. The infinite width failure stress for each notched specimen was normalized by dividing by the unnotched strength to form the ratio  $\sigma_N^\infty / \sigma_0$ .

The results of the tension tests for APC-2 are shown as solid line entries in Fig. 14a and Fig. 15a. The APC-2 results shown are identical, but presented in two separate figures for comparison purposes which will be discussed later. From these figures, the effect of notch cut-out dimension can be clearly observed. As the notch size increases, the APC-2 laminate strength decreases. This is true for all temperatures tested.

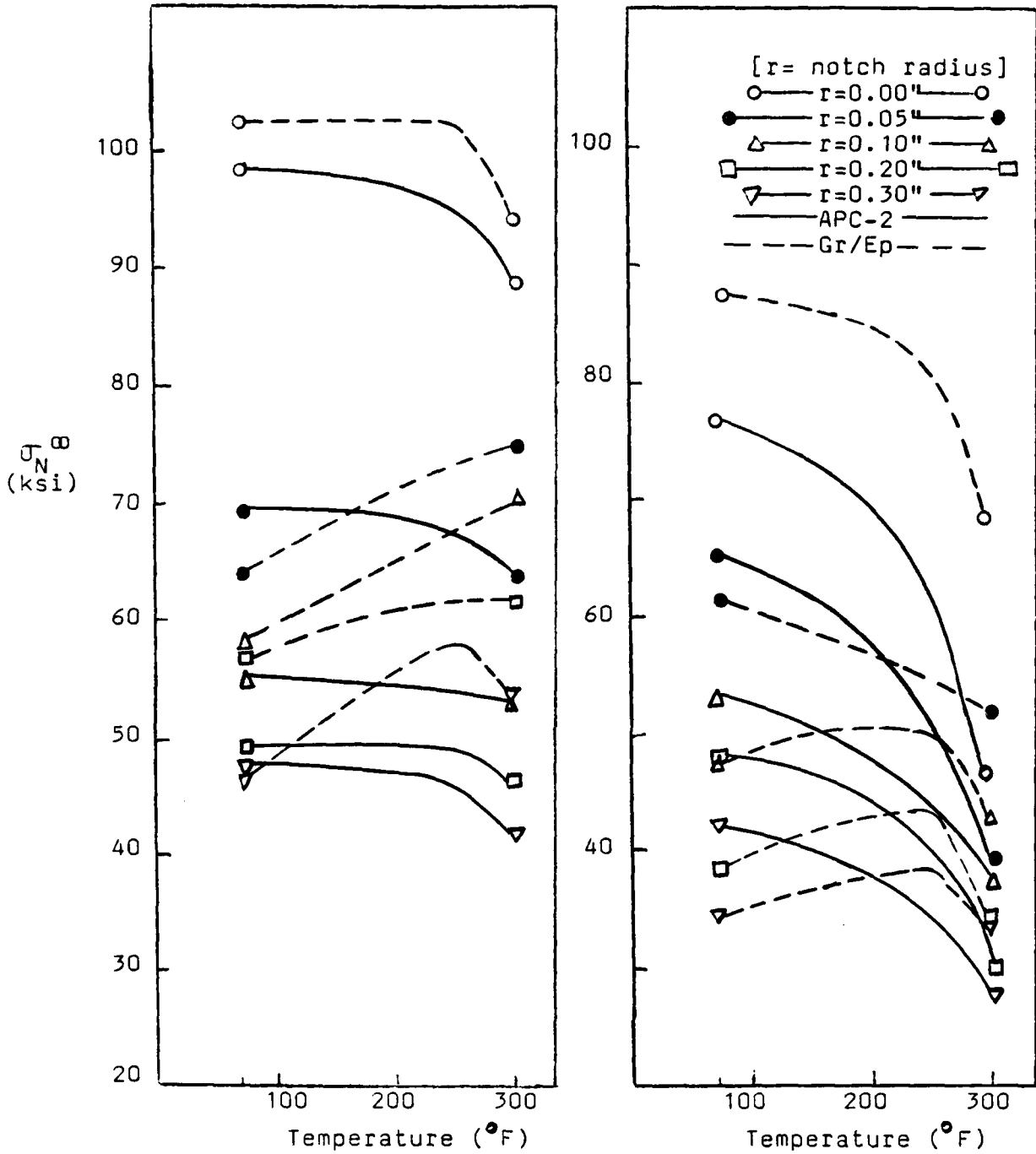
In Fig. 14a APC-2 is compared directly to APC-1 results from Malik. Recalling that APC-2 has a 3-4 percent fiber volume increase over APC-1, the relative similarity between the two systems is not surprising. The unnotched strength of APC-2 is slightly increased over APC-1 for all temperature ranges. For radii less than 0.2" and temperature below



(a.) TENSION

(b.) COMPRESSION

Figure 14. Strength for Notched and Unnotched Specimen Varying Temperature



(a.) TENSION

(b.) COMPRESSION

Figure 15. Strength for Notched and Unnotched Specimen Varying Temperature

250<sup>0</sup>F, the two systems are quite similar in strength. However, with radius of cut outs of 0.1" and larger, there is a larger decrease in the strength of APC-1 compared to APC-2 for temperatures of 250<sup>0</sup>F to 300<sup>0</sup>F. For the two larger radii, 0.2" and 0.3", APC-1 strength is reduced from APC-2 for all temperatures including room temperature. The smaller radii strengths indicate that APC-1 might have sufficient load distribution characteristics to retain comparable strength with APC-2, while the larger radii specimens indicate that redistribution of stress concentration is not accomplished as efficiently in APC-1 as in APC-2 (recall load distribution theory associated with Fig. 1).

The comparison of tension results for APC-2 and Gr/Ep is shown in Fig. 15a. The sixty percent fiber volume APC-2 is not as strong as the sixty-seven percent fiber volume Gr/Ep. Malik presented two reasons for the increase in strength of Gr/EP for increasing temperature [3]. First, the matrix volume of Gr/Ep is less than APC-2 and APC-1. As the matrix is much more sensitive to temperature increase than the fibers, the expected decrease in strength is found. Secondly, the epoxy, a brittle thermoset, becomes more ductile in these temperature ranges, making better use of the matrix ability to transfer more loading to the fibers.

The compression data for APC-2 is shown in Fig. 14b and Fig. 15b. As before, the two presentations are identical

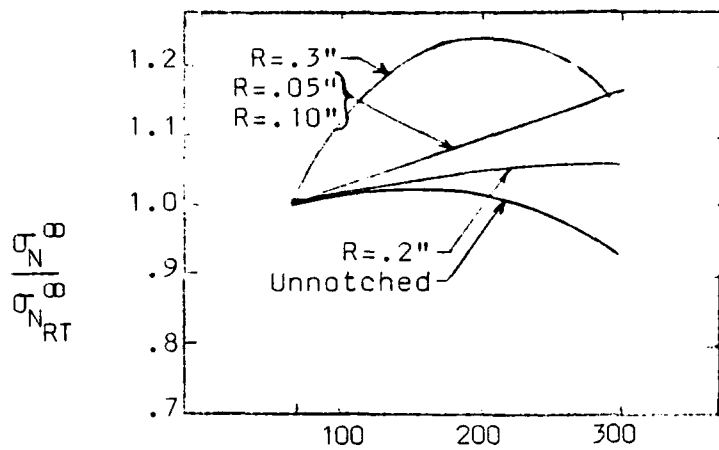


for APC-2. APC-2 shows a significant decrease in the compression strength for elevated temperatures for all unnotched and notched specimens. Decreases over 30 percent can be seen from RT test results to 300<sup>0</sup>F test results.

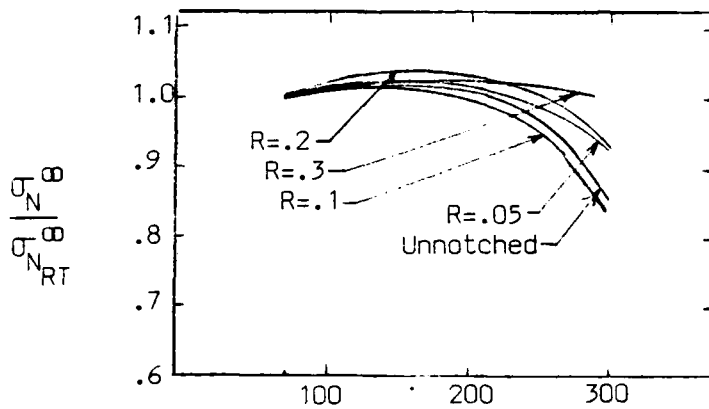
APC-2 is stronger in compression than APC-1 for all test conditions and test temperatures, as shown in Fig. 14b. Both systems show the same relative degradation for notch and temperature effects.

Gr/Ep in Fig. 15b demonstrates a higher unnotched strength than APC-2 for all temperatures. APC-2 demonstrates higher compressive strength than Gr/Ep for all notch sizes at room temperature. However, as test temperatures increase, the Gr/Ep system demonstrates higher compressive strength than APC-2. This again demonstrates that the brittle epoxy system becomes more ductile and capable of transferring loading to the fibers. Recall that the epoxy matrix has a higher T<sub>g</sub> than PEEK.

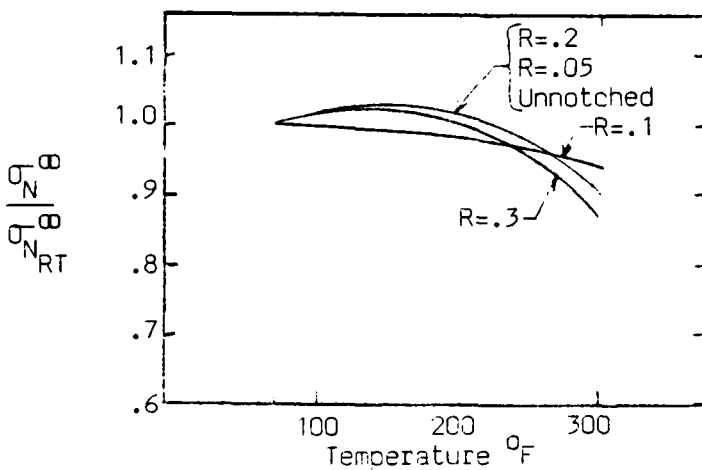
The retention of room temperature tensile strength for the three composite systems is depicted in Fig. 16. It is noticed that the Gr/Ep system demonstrates a large sensitivity to notch size for elevated temperature, but notched specimens retain room temperature strengths. APC-1 does not demonstrate sensitivity to notch size until temperatures approach PEEK's T<sub>g</sub>. APC-2 demonstrates less sensitivity to notch size than APC-1 and Gr/Ep. This is primarily due to the fact that the matrix is more ductile and capable of



(a.) Gr/Ep



(b.) APC-1



(c.) APC-2

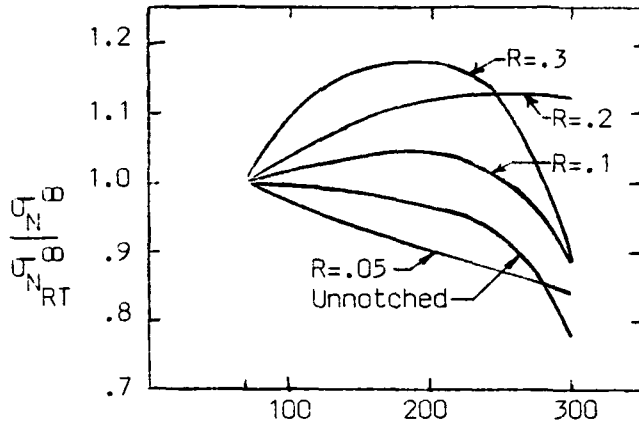
**Fig.16** Tensile Failure Stress Normalized with Room Temperature Strength for Various Hole Diameters

distributing stress concentrations throughout the fibers. This phenomena will be demonstrated by the microphotographs in the next section, showing the ductility of the matrix.

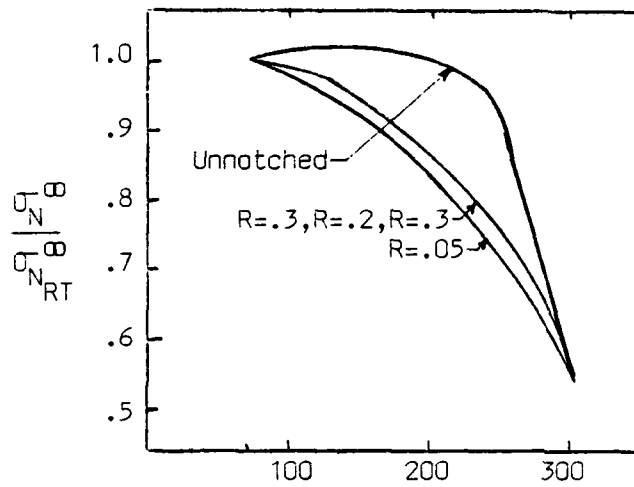
The compression failure stress normalized with room temperature is shown in Fig. 17. All three systems demonstrate a decline in strength with increase in temperature. The APC-2 system demonstrates less difference between notched strength and unnotched strength for the notch sizes tested, as compared to APC-1 and Gr/Ep laminate systems for compression loading.

Experimental failure data is an important key to proper use of failure prediction techniques. Experimental test results are the only true indicator for the accuracy of failure prediction techniques. Once the experimental data is evaluated, the task of comparing experimental results with theoretical predictions can be accomplished.

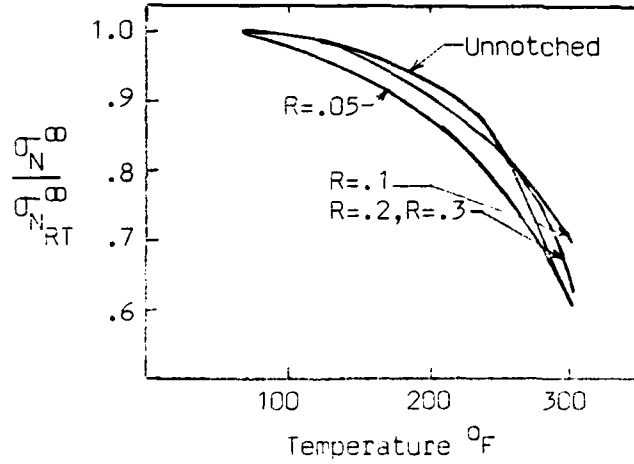
The first failure strength prediction method evaluated is the point stress method. Graphical comparisons between experimental failure strengths and Whitney's point stress method predictions are given in Fig. 18, Fig. 19 and Fig. 20 where  $\sigma_N^{\infty}/\sigma_0$  is plotted versus notch size. In these figures,  $\sigma_N^{\infty}$  is the gross failure stress of notched specimen multiplied by the finite width correction factor  $K_T/K_T^{\infty}$  and  $\sigma_0$  is the failure stress of the unnotched specimen. Small variation of the characteristic length,  $d_0$ , for the experimental temperature range is noticed for tension results in Fig. 19. Although compression data in Fig. 18 does not



(a.) Gr/Ep

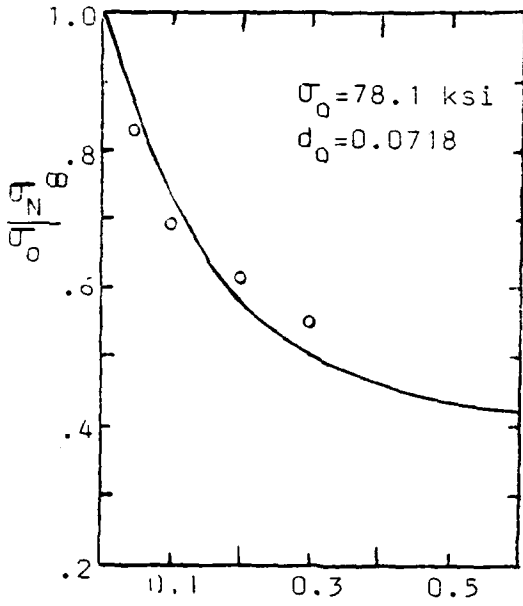


(b.) APC-1

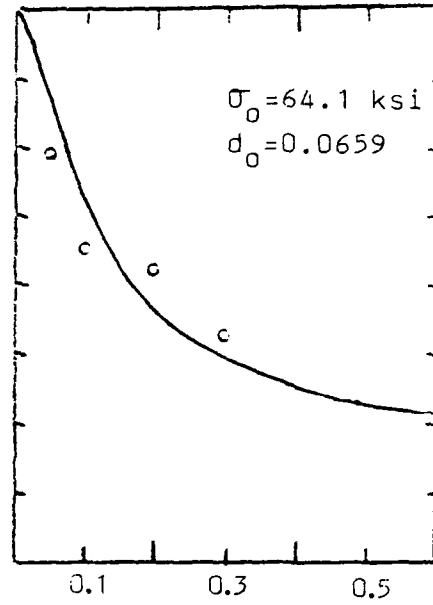


(c.) APC-2

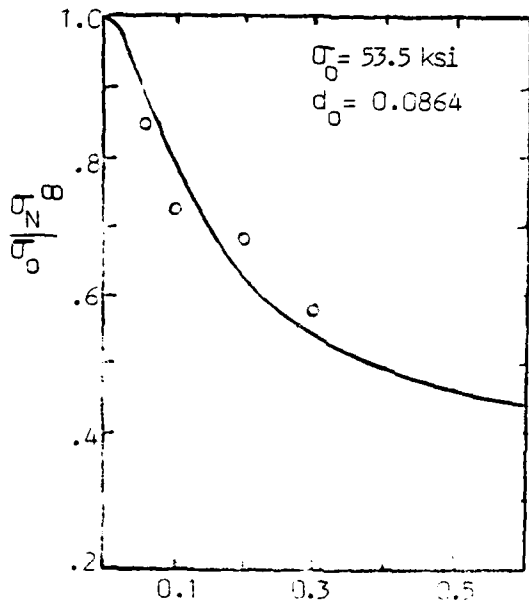
Fig. 17 Compression Failure Stress Normalized with Room Temperature Strength for Various Hole Diameters



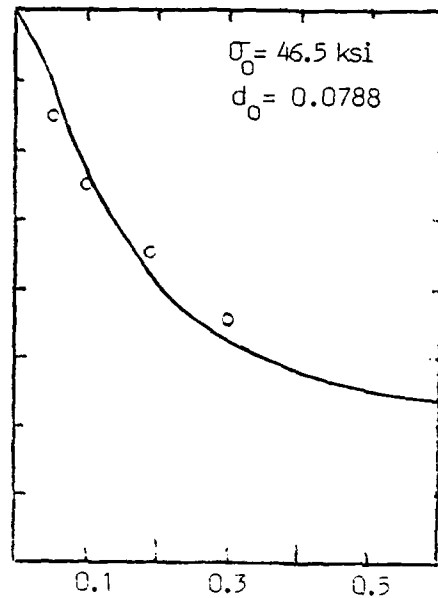
(a.) Room Temperature



(b.) 250°F

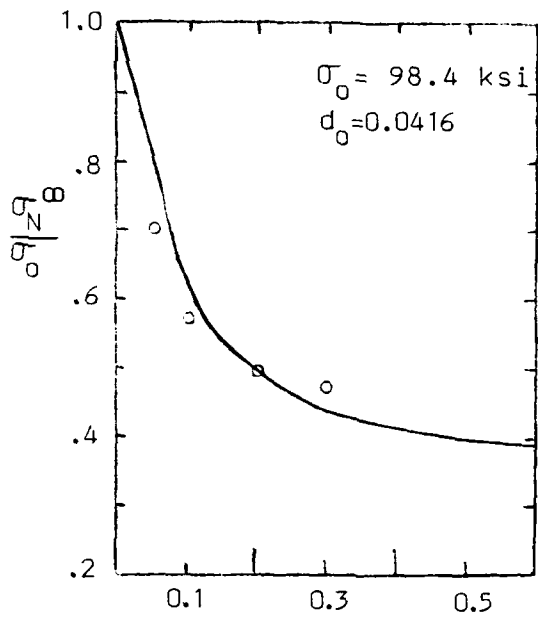


(c.) 275°F

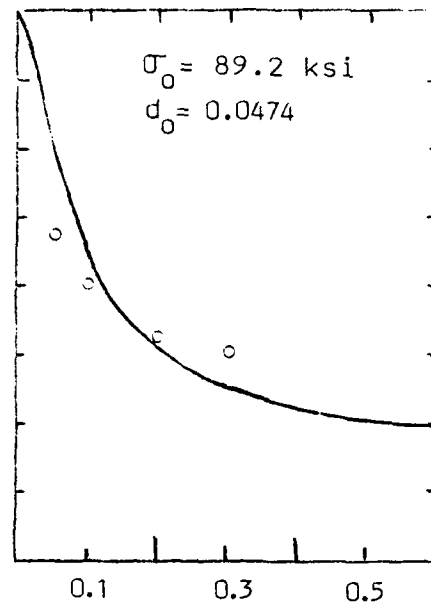


(d.) 300°F

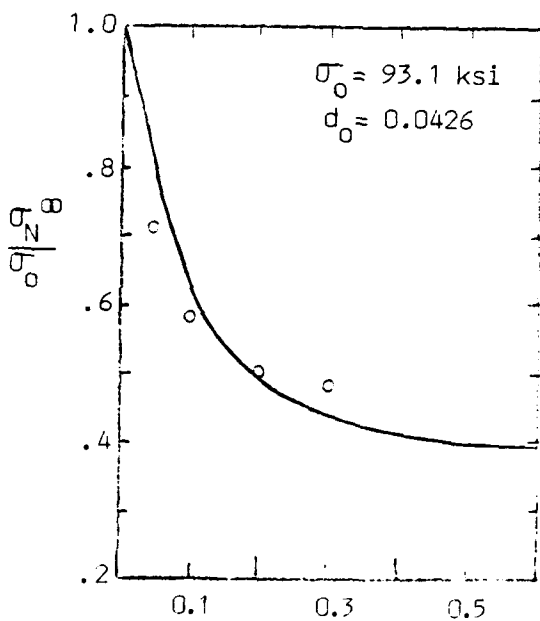
Fig. 18 Comparison of Predicted and Experimental Compression Stresses for APC-2 at Failure



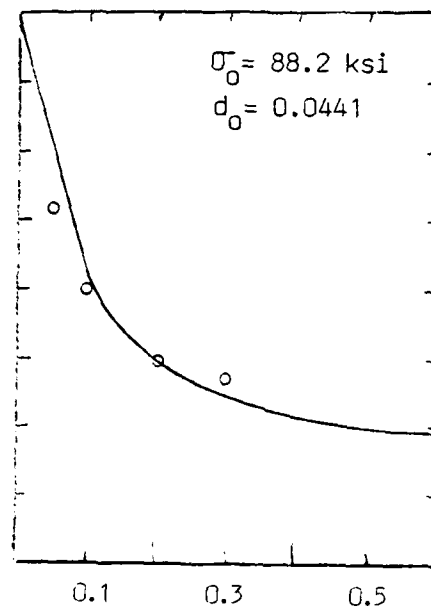
(a.) Room Temperature



(b.) 250°F

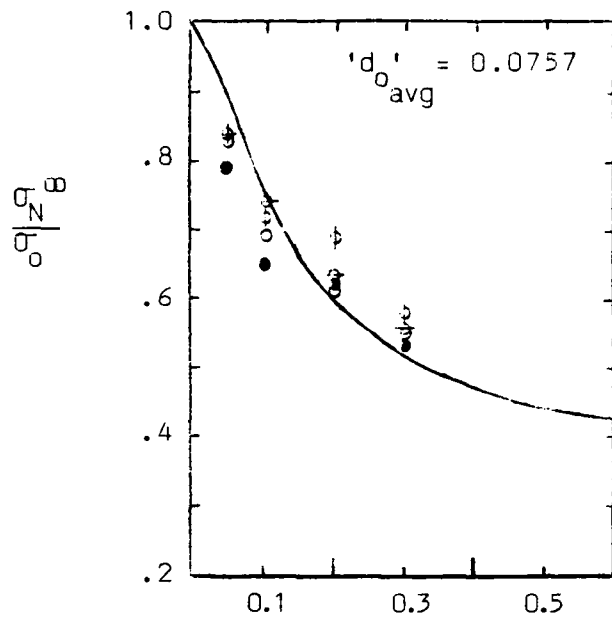


(c.) 275°F



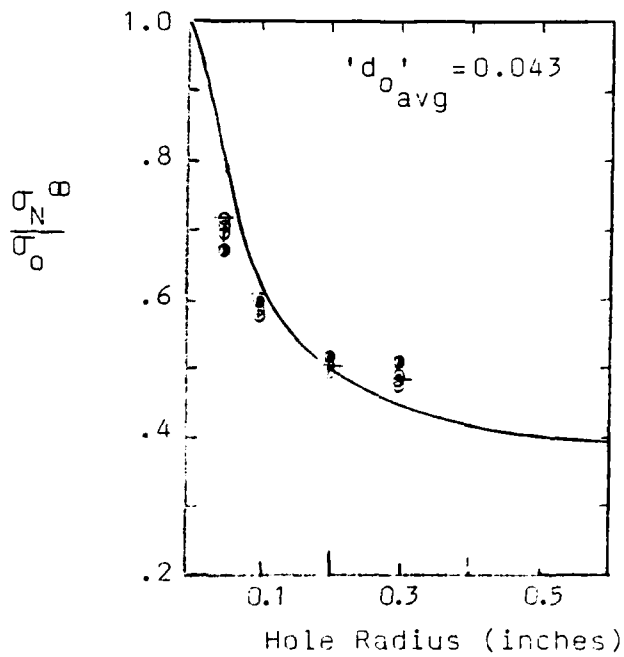
(d.) 300°F

Fig. 19 Comparison of Predicted and Experimental Tension Failure Stresses for APC-2



- = RT
- = 250°F
- ◻ = 275°F
- ◊ = 300°F

(a.) Compression



(b.) Tension

Fig. 20 Master ' $d_0$ ' Curve Comparison of Experimental and Predicted Failure Stresses

demonstrate the small variation of  $d_0$ , the variation in values is not as wide as the Gr/Ep and APC-1 data [3] in Table III. This indicates the value of  $d_0$  is not as notch sensitive for APC-2 as compared to APC-1 and Gr/Ep.

The comparison of predicted failure strength to experimental results is good for all temperature ranges in tension and compression. A master curve is presented in Fig. 20. The master curve is an attempt to find a characteristic length,  $d_0$ , for the APC-2 laminate system regardless of temperature. The master curve prediction gives a maximum difference between predicted values and experimental results of -13.2% in compression for the 0.1" diameter cut out specimen at 250°F and a -12.8% difference between predicted values and experimental data in tension for 0.05" diameter cut out at 250°F.

Table III. Values of Characteristic Length ' $d_0$ ' for Composite Laminates

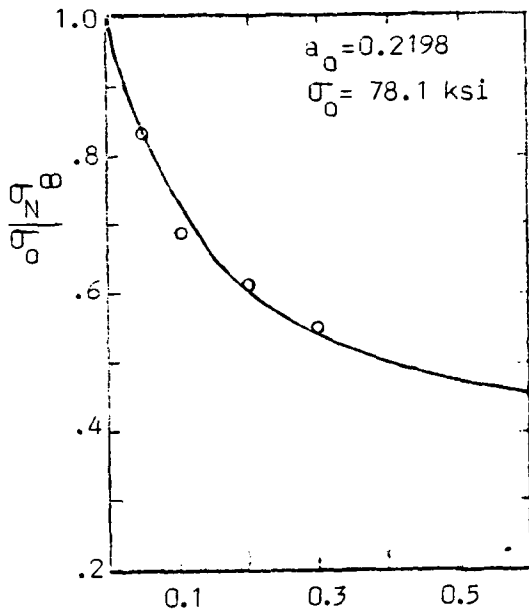
<u>Material</u> (Tension)	<u>RT</u>	<u>250°F</u>	<u>275°F</u>	<u>300°F</u>
Gr/Ep	.04	.06	--	.08
APC-1	.033	.04	--	.05
APC-2	.04	.05	.04	.04
(Compression)				
Gr/Ep	.03	.04	--	.04
APC-1	.10	.06	--	.12
APC-2	.07	.07	.09	.08



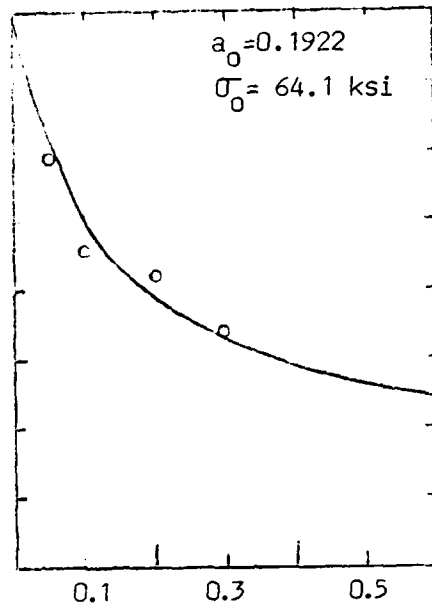
The second approach considered for evaluation is Whitney's average stress method. In this technique failure is assumed to occur when the average stress at some fixed distance,  $a_0$ , ahead of the hole reaches the unnotched strength,  $\sigma_0$ . Graphical comparisons of APC-2 experimental results and predicted values are presented in Fig. 21, Fig. 22 and Fig. 23 and show quite good comparisons. It is noted immediately the better "fit" for tension and compression data at all temperatures for the average stress method compared to the previously addressed point stress method. Previous authors have noticed the same comparative results concluding that the averaging process for each method must be the principal reason [3].

Examining Table IV, it is noted that APC-2 ' $a_0$ ' values demonstrate a smaller variation for tension and compression than APC-1 and Gr/Ep. This indicates that the  $a_0$  value for APC-2 is less sensitive to notch size than APC-1 and Gr/Ep. On the master curve in Fig. 23, the experimental data demonstrates less than 10 percent difference from the predicted values. These results affirm the results shown Fig. 16 and Fig. 17, where APC-2 was seen to be less sensitive to notch size than APC-1 and Gr/Ep.

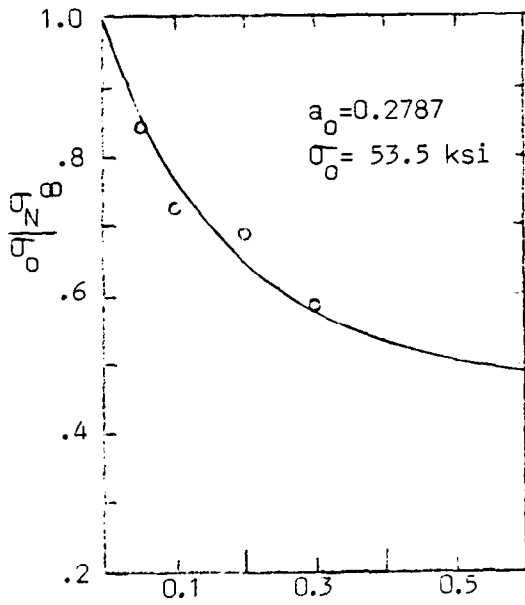
The third prediction method considered is Pipes' three parameter model which uses the unnotched strength,  $\sigma_0$ , the notch sensitivity factor, C, and the exponential parameter, m. In this model, the notch sensitivity and



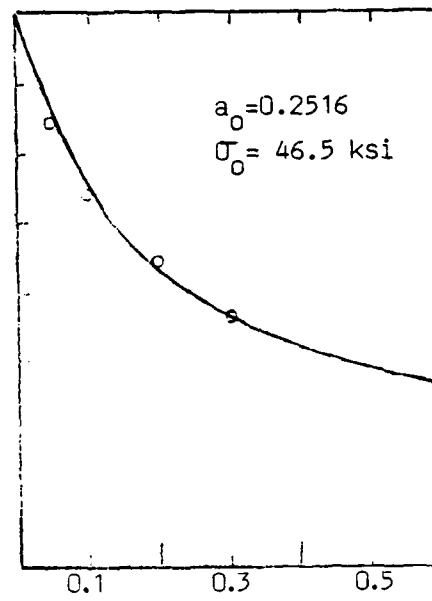
(a.) Room Temperature



(b.) 250°F

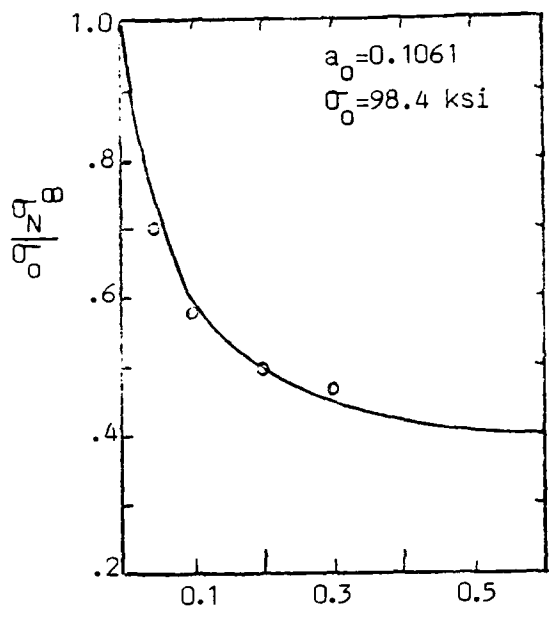


(c.) 275°F

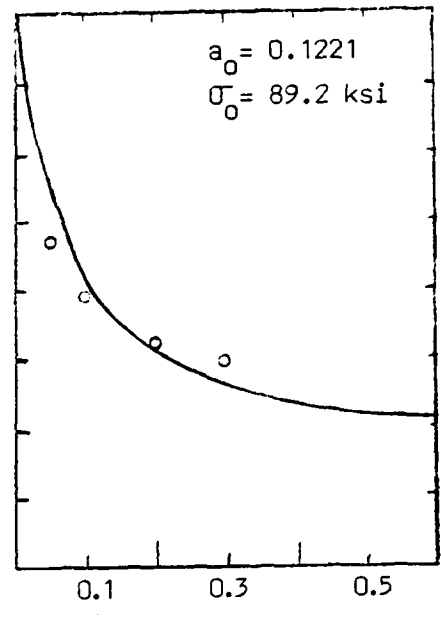


(d.) 300°F

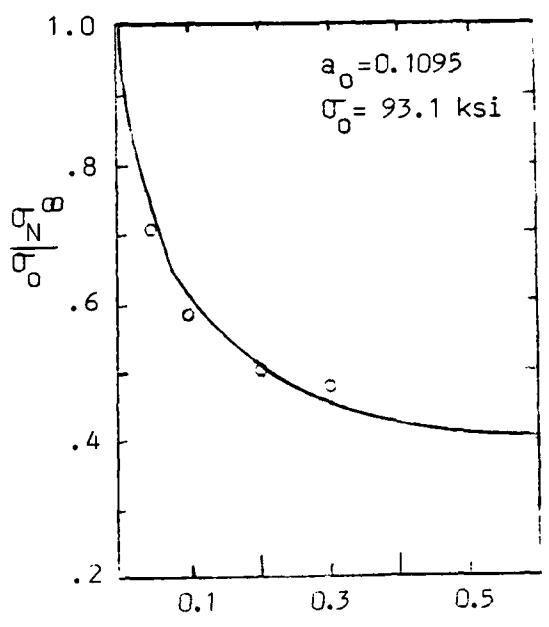
Fig. 21 Comparison of Predicted and Experimental Compression Failure Stresses for APC-2



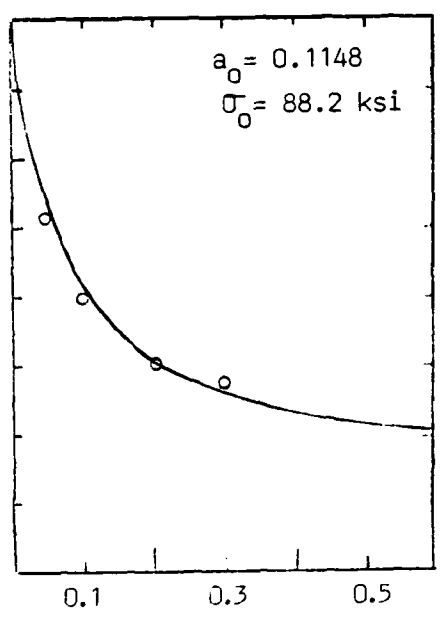
(a.) Room Temperature



(b.) 250°F

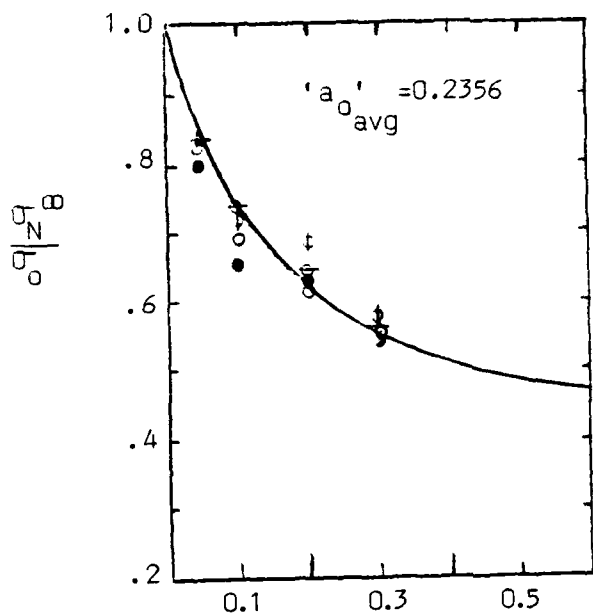


(c.) 275°F



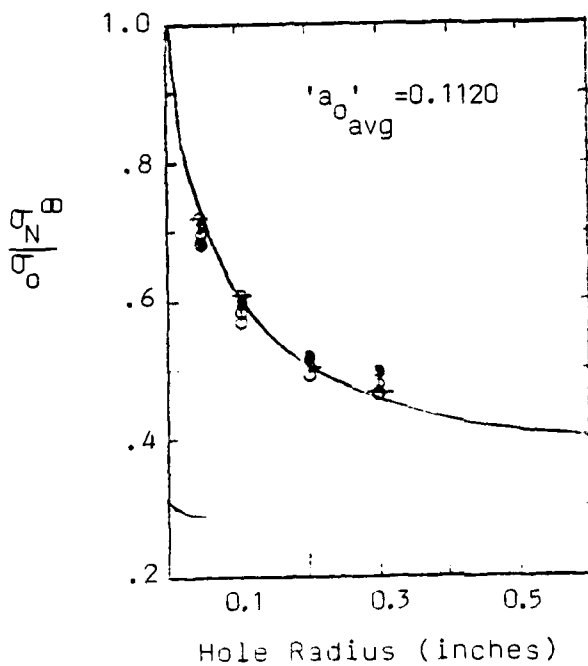
(d.) 300°F

Fig.22 Comparison of Predicted and Experimental Tension Failure Stresses for APC-2



○ = RT  
 ● = 250°F  
 ⊙ = 275°F  
 ⊗ = 300°F

(a.) Compression



(b.) Tension

Fig. 23 Master 'a<sub>0</sub>' Curve Comparison of Predicted and Experimental Failure Stresses

Table IV Values of Characteristic Length,  
 $a_0$ , for Composite Laminates

<u>Material</u> (Tension)	<u>RT</u>	<u>250<sup>o</sup>F</u>	<u>275<sup>o</sup>F</u>	<u>300<sup>o</sup>F</u>
Gr/Ep	.12	.17	--	.24
APC-1	.09	.13	--	.14
APC-2	.22	.19	.28	.25
(Compression)				
Gr/Ep	.07	.12	--	.12
APC-1	.36	.13	--	.43
APC-2	.11	.12	.11	.11

exponential parameter are assumed to be material constants. The values of C and m found in this experiment are compared to Gr/Ep and APC-1 in Table V. The average notch sensitivity for APC-2 in tension is less than APC-1 and Gr/Ep. The average notch sensitivity for APC-2 in compression is less than Gr/Ep and only slightly higher than APC-1.

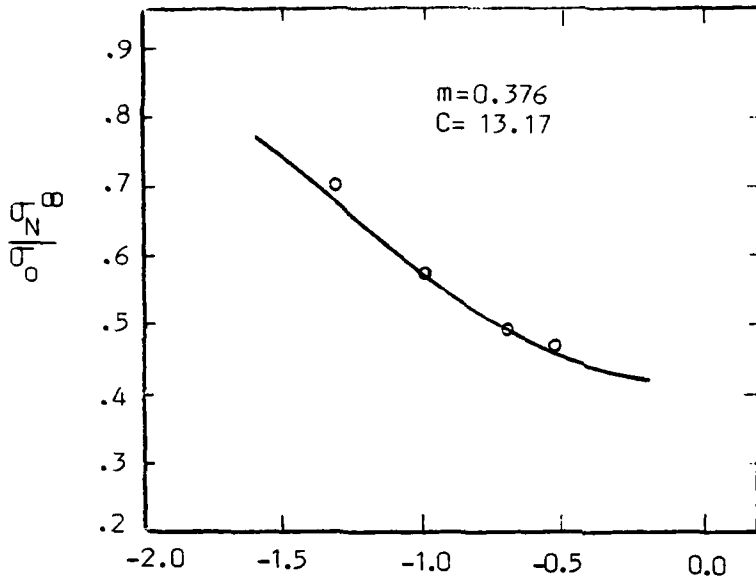
Comparisons of experimental and predicted three parameter method values for APC-2 are presented in Fig. 24 through Fig. 29. The comparative results are quite good, however, it is obvious that the notch sensitivity, C, and exponential factor, m, are not material constants when temperature varies. Fig. 28 is an attempt to use average values of C and m to plot results in a maximum of approximately 8 percent difference

between theory and experiment. The master curve using the  $C^* = 10$  and  $m^* = 0.5$  values is shown in Fig. 28, again demonstrating very good comparisons between predicted values and experimental data.

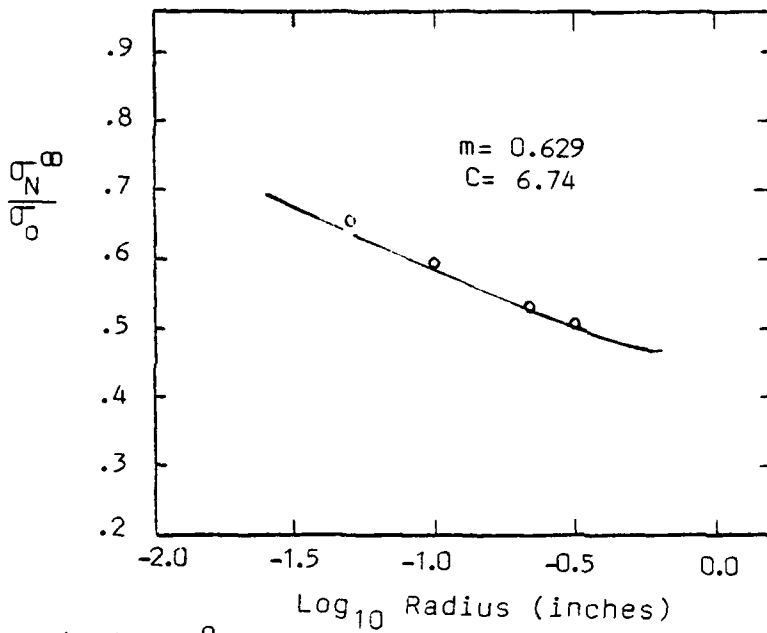
---

Table V. Values of Notch Sensitivity Factor, C, and Exponential Parameter, m, for Composite Laminates

Temp.	<u>Tension</u>					
	Gr/Ep		APC-1		APC-2	
	C	m	C	m	C	m
RT	8.85	.53	28.5	0.0	13.17	.376
250 <sup>o</sup> F	5.65	.63	11.24	.21	6.74	.629
275 <sup>o</sup> F	--	--	--	---	11.85	.376
300 <sup>o</sup> F	32.25	.44	11.36	.29	13.75	.275
Average	15.58	.53	17.03	.17	11.38	.414
	<u>Compression</u>					
RT	32.0	0.0	6.54	.23	8.57	.265
250 <sup>o</sup> F	9.17	0.46	8.07	.47	6.73	.446
275 <sup>o</sup> F	--	--	--	--	5.63	.396
300 <sup>o</sup> F	18.86	0.1	4.81	.32	6.63	.352
Average	20.01	.19	6.47	.34	6.79	.366

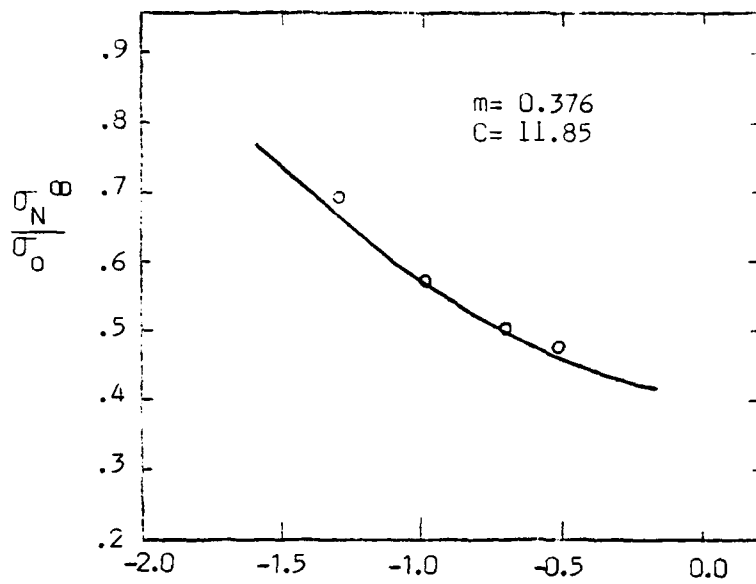


(a.) Room Temperature

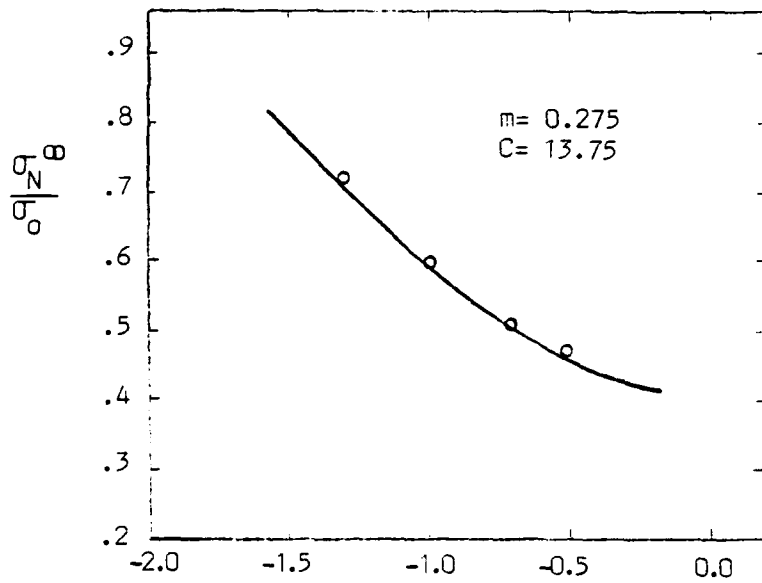


(b.) 250°F

Fig.24 Comparison of Predicted and Experimental Tension Failure Stresses for APC-2, Three Parameter Model



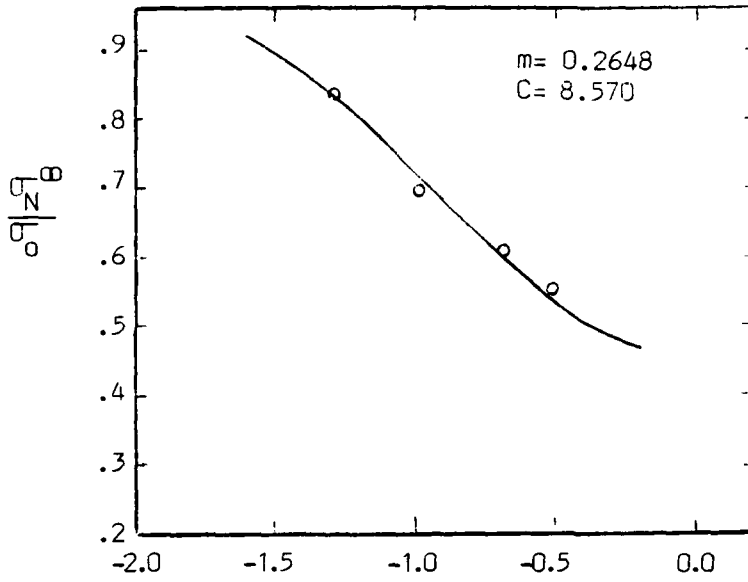
(a.) 275°F



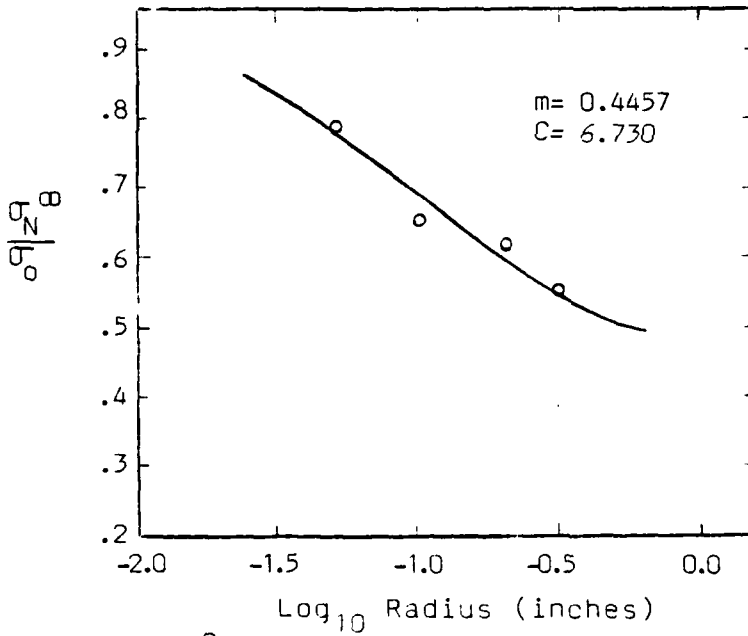
(b.) 300°F  $\text{Log}_{10}$  Radius (inches)

Fig. 25 Comparison of Predicted and Experimental Tension Failure Stresses for APC-2, Three Parameter Model



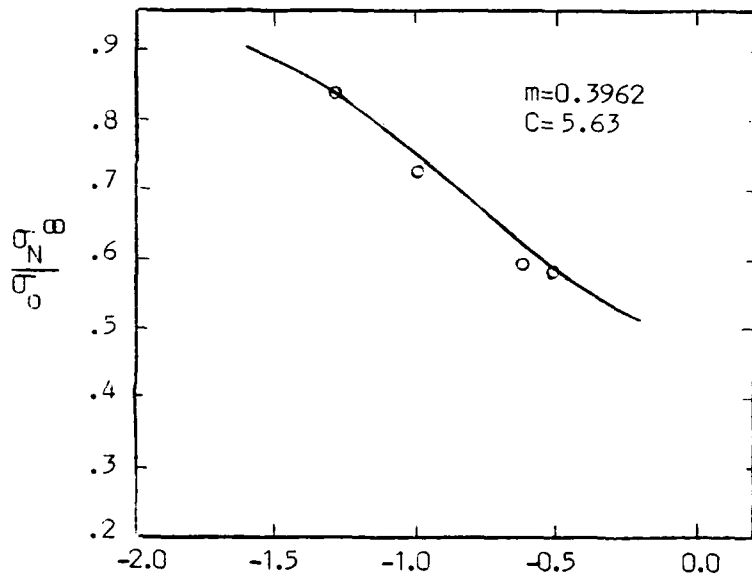


(a.) Room Temperature

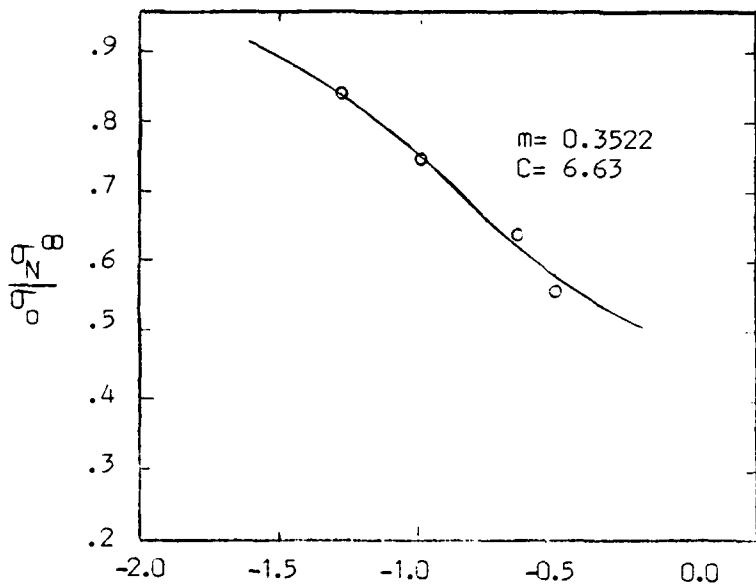


(b.) 250°F

Fig. 26 Comparison of Predicted and Experimental Compression Failure Stresses for APC-2, Three Parameter Model

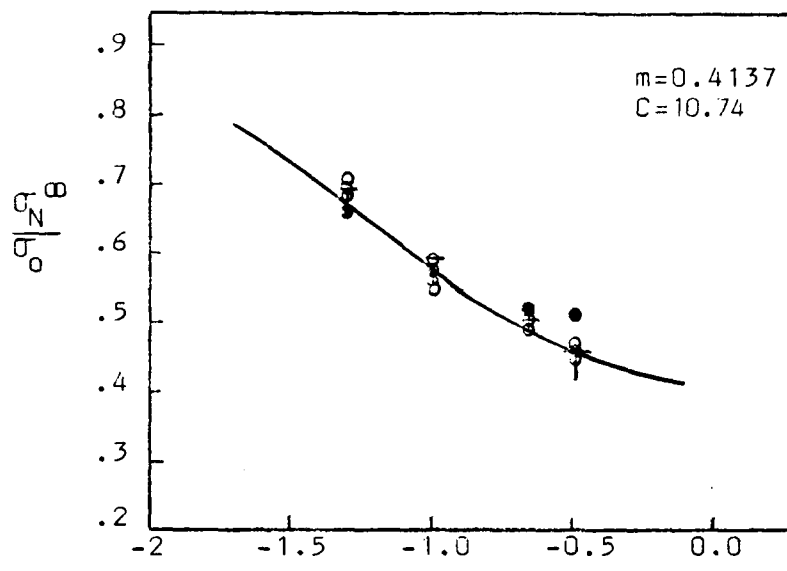


(a.) 275°F



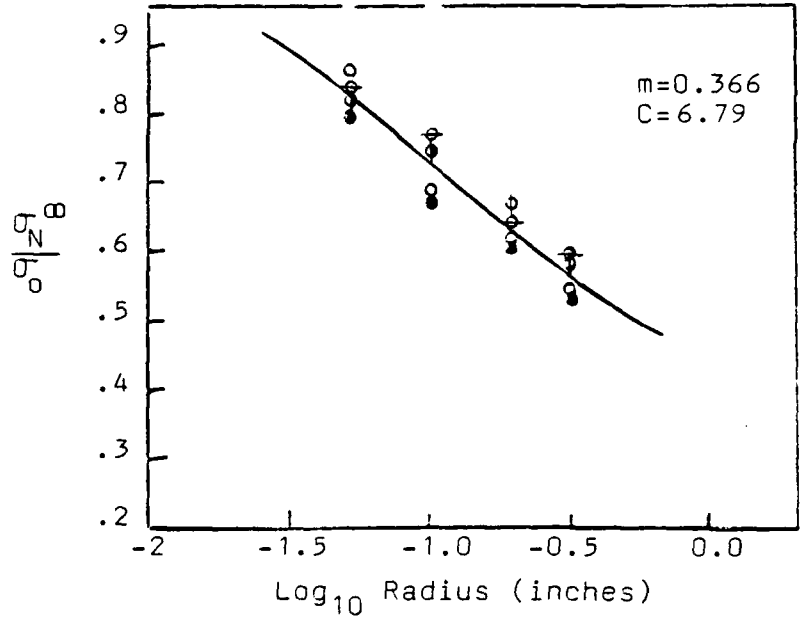
(b.) 300°F

Fig 7 Comparison of Predicted and Experimental Compression Failure Stresses for APC-2, Three Parameter Model



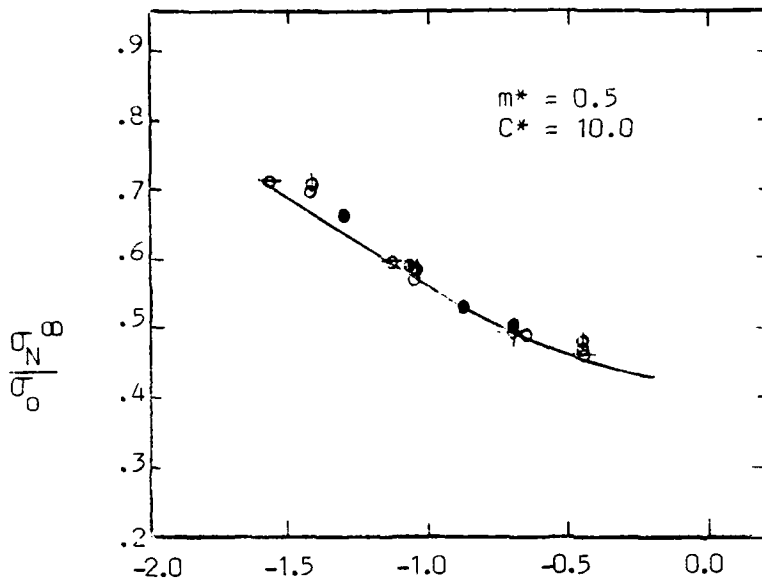
(a.) TENSION

- = R
- = 250 °F
- ⊥ = 275 °F
- ⊕ = 300 °F



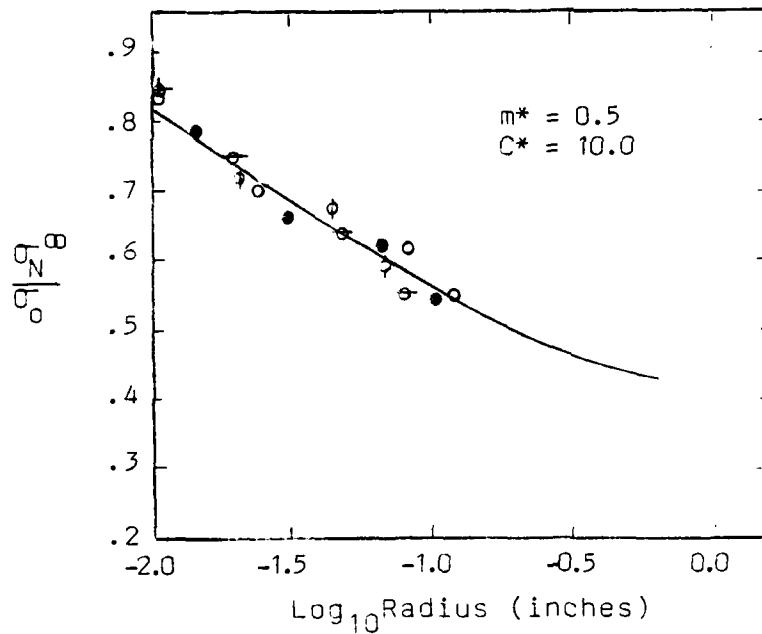
(b.) COMPRESSION

Figure 29 Comparison of Predicted and Experimental Failure Stresses for APC-2 Using Three Parameter Model



(a.) Tension

- = RT
- = 250°F
- ◐ = 275°F
- ◑ = 300°F



(b.) Compression

Fig. 2) Three Parameter Model Master Curve Comparison of Predicted and Experimental Failure Stresses for APC-2

## B. Microscopic Evaluation and Stress-Strain Results

The behavior of a composite material during fracture is a combined effort of matrix and fiber individual properties as well as their mutual interaction. Systematic evaluation of fracture surface characterizations yield information about the composite failure mode and the nature of matrix-fiber interaction. The comparison of composite properties with microstructural fractures provides a basis for complete failure analysis. Evidence to support the postulated effects of the fiber-matrix bond, the load distribution capability of the matrix, the toughness of the matrix, and the temperature degradation effects on the matrix can be obtained from fracture surface analysis.

Gr/Ep fracture surfaces have been looked at by several authors. In fact, ASTM STP 696, from which reference [35] was taken, has no less than seven articles on Gr/Ep failure mechanisms while ASTM STP 775 has at least five articles on Gr/Ep failure mechanisms. Accordingly, no Gr/Ep failed specimen photographic analysis is given in this study. However, comparison of APC-2 fracture mechanisms will be compared to Gr/Ep findings when applicable.

APC-1 is not as well-studied as Gr/Ep. However, some papers depicting APC-1 fracture surface photographs are available [3,21,22,25,26]. Thus, no photographic analysis of APC-1 is made in this paper. However, comparison of APC-2 fracture mechanisms will be compared to APC-1 findings when applicable.

Many brittle material systems are known to exhibit a linear stress-strain relation to fracture. The dominance of fibers in a composite system are primarily responsible for linearity in brittle systems. More ductile material systems demonstrate non-linearities for stress-strain data. In order to capture the nature of any non-linearities in APG-2 several specimens were strain gaged. These specimens were strain gaged with three gages as shown previously in Fig. 11. The far field gage measured total specimen strain while the top-of-hole and side-of-hole gages measured the effects of the cut outs on strain for the specimen.

The microscopic evaluations and stress strain results in this section are further subdivided into a compression sub-section and a tension sub-section with each sub-section containing stress-strain results and discussions and scanning electron microscope microphotographs and discussions. The compression section contains an additional sub-section discussing the 90 and 95 percent of average compression failure load test results. The 90 and 95 percent of average tension specimens did not show external visible signs of failure and, therefore, are not addressed separately in the tension sub-section.

#### 1. Compression Failure Analysis

To understand the compression microphotographs better, the compression analysis begins with the strain results.

These strain results indicate that non-linearities occur at various loadings depending on specimen test temperatures. To understand the failure process itself in compression, the next sub-section after strain results presents the 90 and 95 percent of average compression load specimen analysis. With the knowledge of the pre-failure patterns, the final sub-section of compression analysis deals with the completely failed surface analyses. The tension sub-section will follow the complete compression failure analysis.

(a) Compression Strain Results

Compression experimental strain results are depicted in Fig. 30-35 for 0.2" diameter specimens at the four test temperatures. The far-field strain data in Fig. 30 shows a non-linearity exists during compression loading at room temperature. The non-linearity is at approximately 77% of failure load or 3300 pounds. Examining strain gage results for this specimen, using the side-of-hole results, in Fig. 31, demonstrates that the non-linearity at 77% load is sufficient to cause failure of the side-of-hole strain gage. Examination of the 90 and 95 percent failure micro-photographs shows the out of plane fiber buckling which can cause the gage failure.

At 250<sup>0</sup>F, shown in Fig. 32, the far-field gage results demonstrate linear loading rate to failure, 3000 pounds. The side-of-hole gage result in Fig. 33 shows that there is

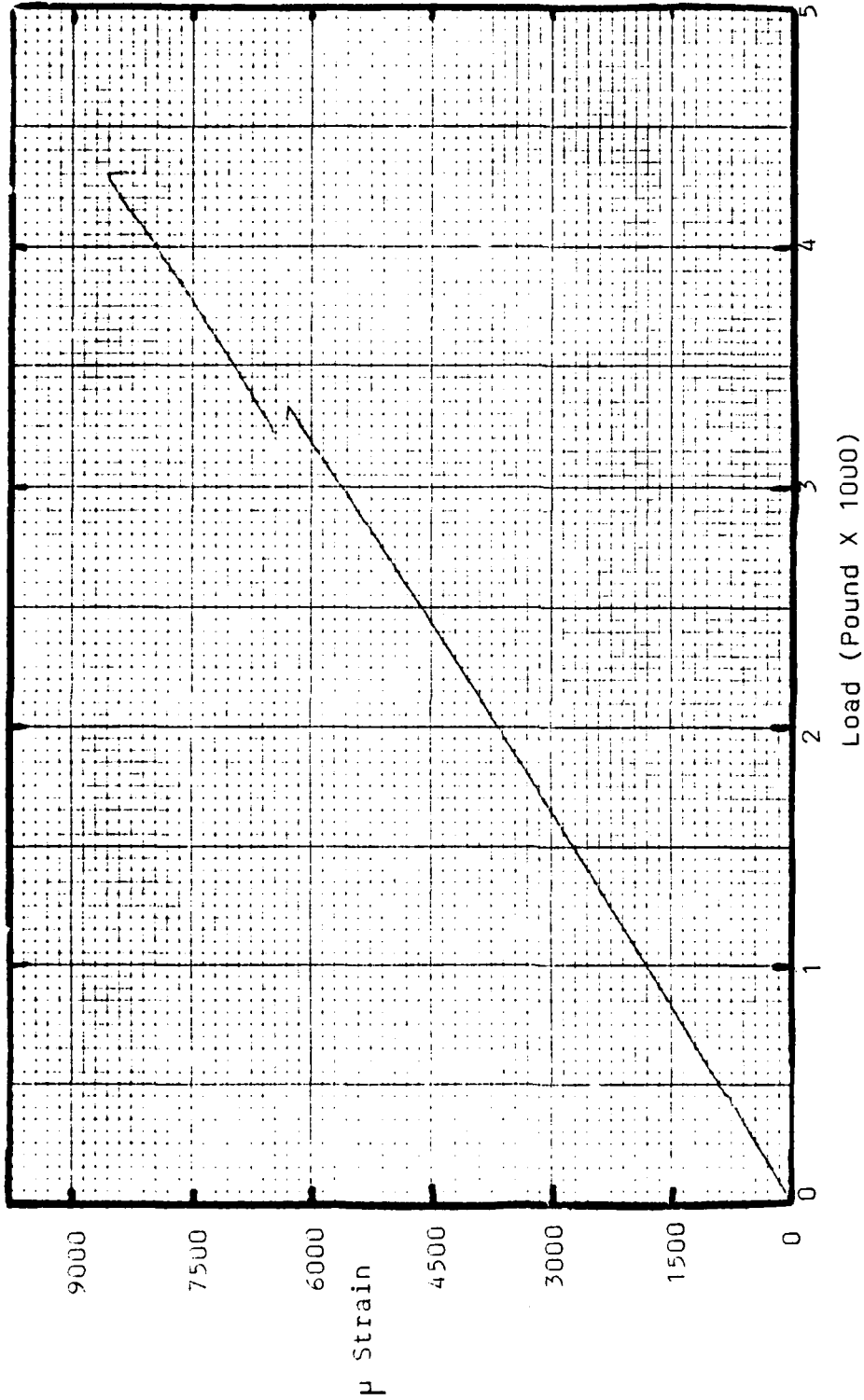


Fig. 30 Compression Specimen Far Field Strain-Load Data, 0.2" Diameter, Room Temperature



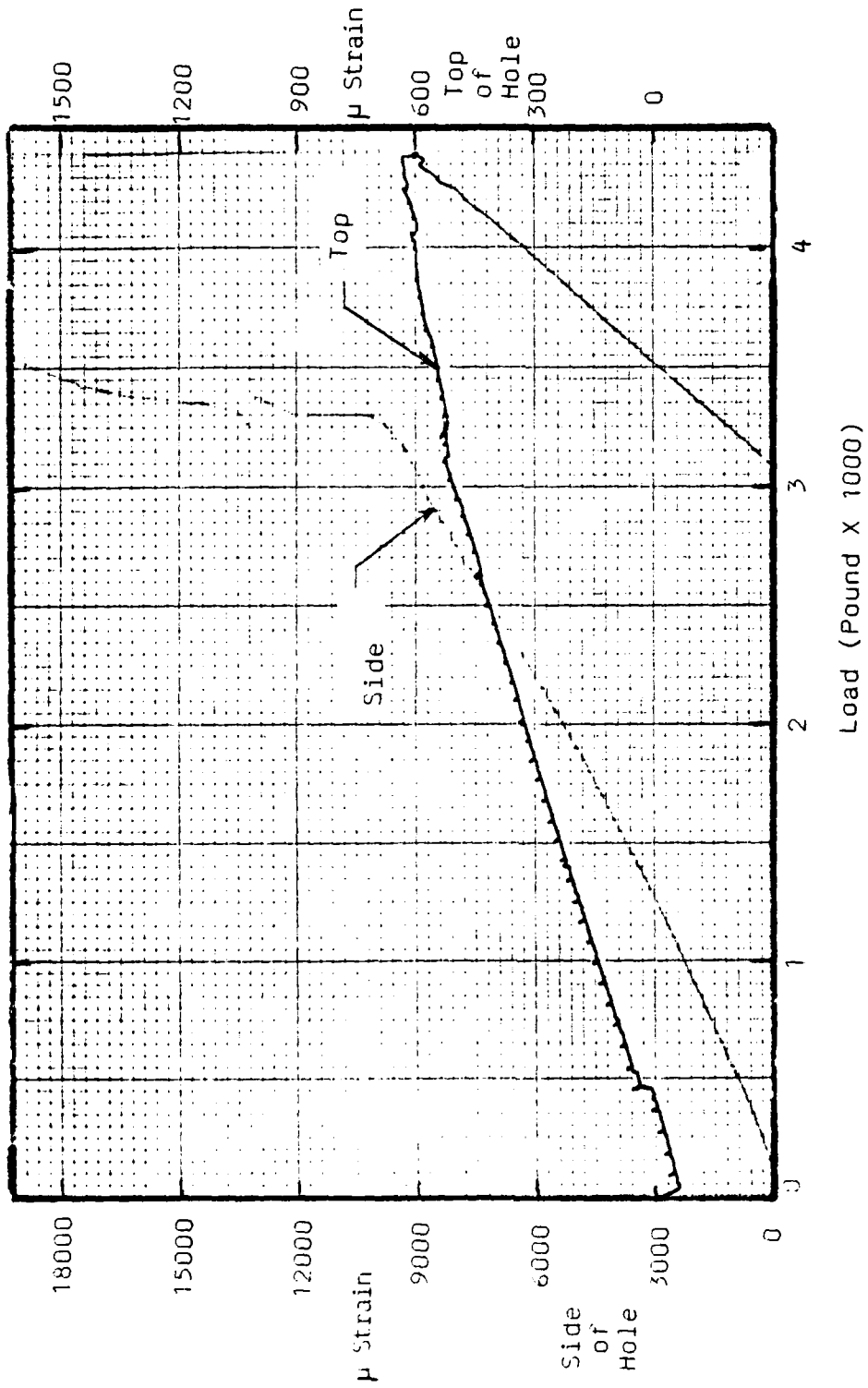


Fig. 31. Compression Specimen Strain-load Data, 0.2" Diameter, Room Temperature, Side of Hole Gage and Top of Hole Gage

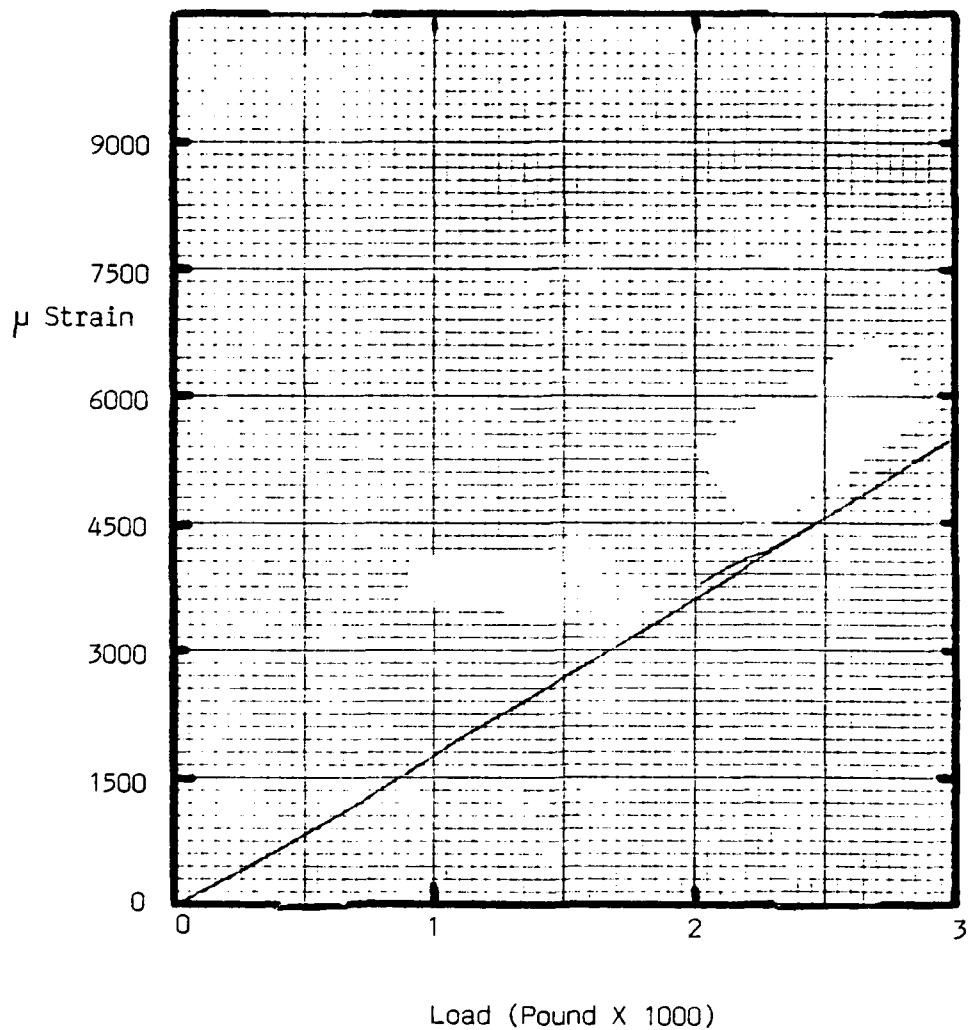


Fig. 32. Compression Specimen, Strain-Load Data, 0.2" Diameter 250°F, Far Field Strain Gage

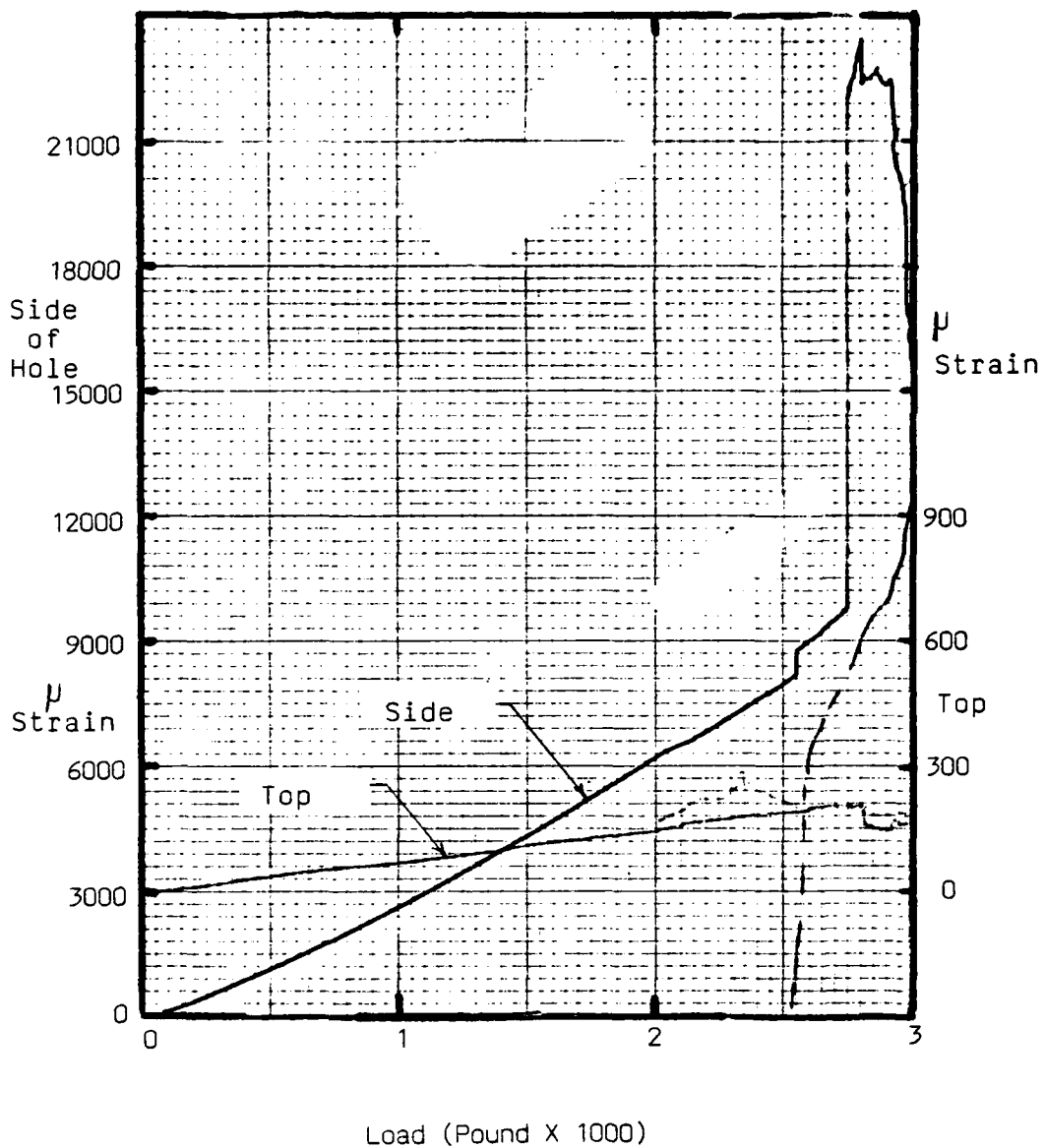


Fig. 33. Compression Specimen Strain-Load Data, 0.2" Diameter, 250°F, Side of Hole Gage and Top of Hole Gage.

significant non-linearity at the side of the notch and the non-linearity exists at 87 percent load, 2550 pounds.

At 275<sup>0</sup>F the non-linearity does not occur in the far-field results until 96 percent load, 2500 pounds, as seen in Fig. 34. The side-of-hole gage shows load non-linearity occurring at 1800 pounds, 72 percent of failure load.

The 300<sup>0</sup>F far field gage did not survive the temperature effects. The side-of-hole gage however, indicates non-linearity at approximately 74 percent of failure load, 1700 pounds in Fig. 35.

Overall, the far field results show that as temperature increases, the non-linearity in loading occurs at a lower load level. When fibers dominate the material properties, the reduction in actual load where non-linearity occurs can be caused by two separate mechanisms (or a combination of the two): (1) fiber degradation and (2) matrix degradation to the extent that the matrix fails to transfer loads to the fibers effectively and/or fails to retain the inherent properties of the matrix. Since the temperature ranges for this experiment are sufficiently lower than temperatures where graphite fiber degradation occurs and no symptoms of fiber degradation were observed in the microphotographs, the first cause for strength reduction may be eliminated. There are many instances where matrix degradation, the second cause for reduced strength, has occurred. Matrix

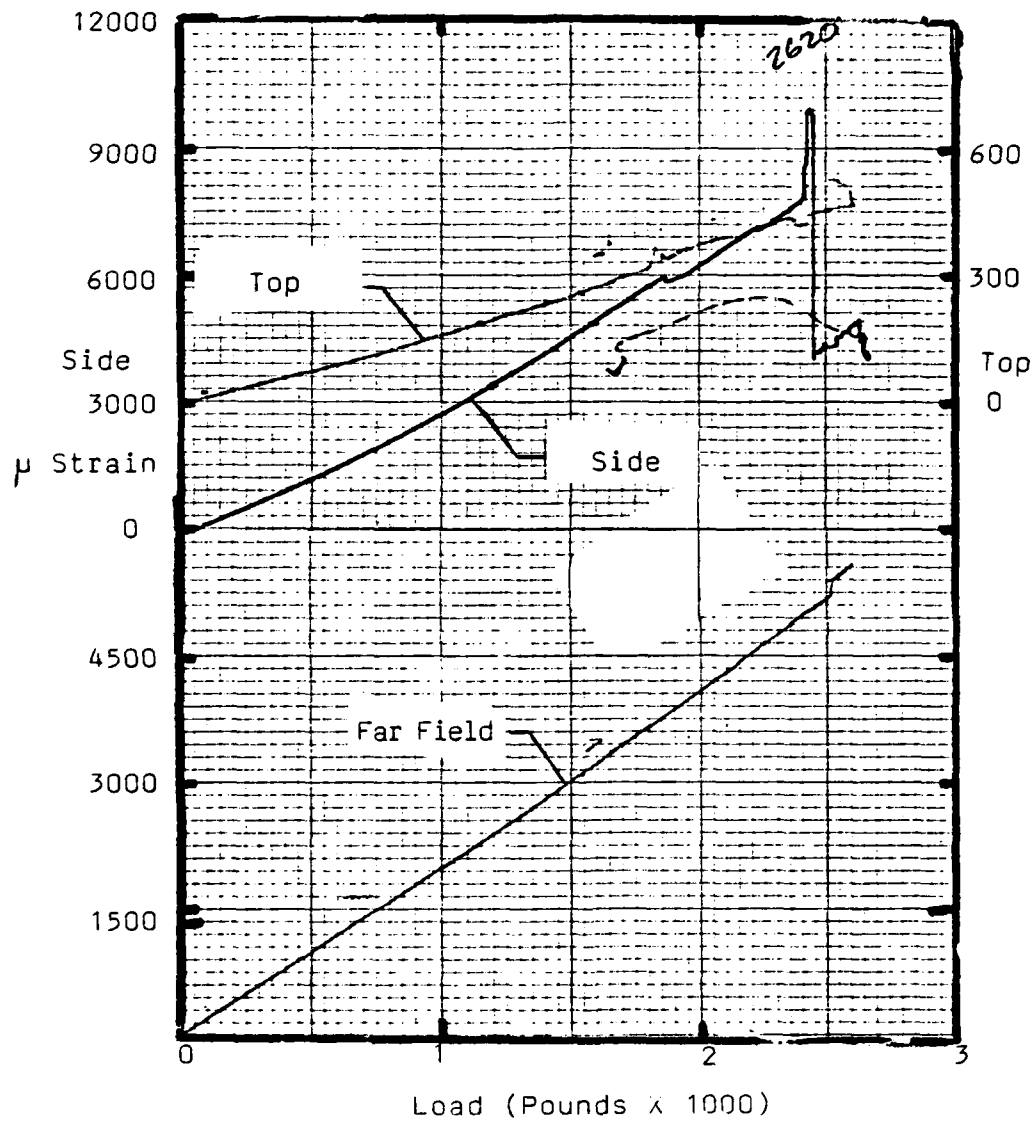


Fig. 34. Compression Specimen, Strain-load Data, 0.2" Diameter, 275<sup>o</sup>F, Far-Field Side of Hole, and Top of Hole gages.

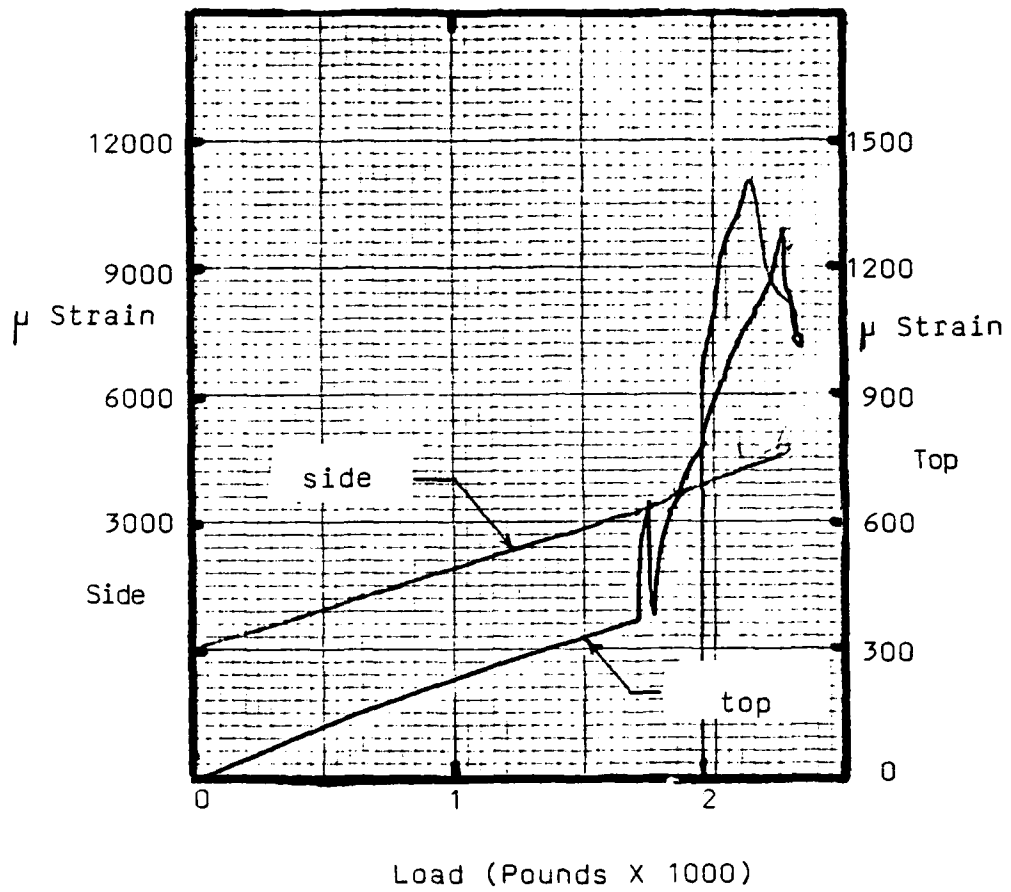
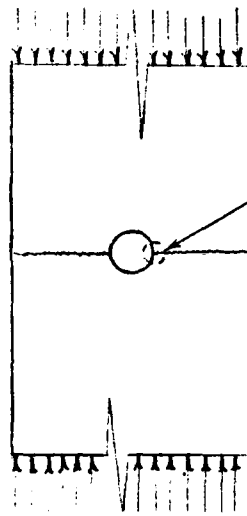
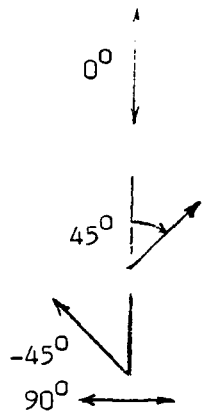


Fig. 35. Compression Specimen, Top of Hole and Side of Hole Strain-load Data, 300°F, 0.2" Diameter

degradation occurred between matrix and fiber, as well as, within the matrix itself. Examination of the scanning electron microscope microphotographs in the following section will demonstrate effectively the matrix degradations.

Before examining the scanning electron microphotographs for the compression failures, a few details must be provided so the reader will understand the location on the specimen where the photographs were taken. The compression microphotographs are generally divided into two primary categories. The first category is called the top view. In this view, the observer is looking at the flat width surface as shown in Fig. 36a, view A. In this viewing, specimens are studied at the top failure surface adjacent to the notch, perpendicular to the crack, and are termed "top view". View B of Fig. 36a shows a specimen cut lengthwise and viewed into the notch parallel to the crack, termed "in-hole". The tension microphotographs are divided into two primary categories with two lines-of-sight possible. The majority of tension microphotographs depict observations taken from the upper line-of sight in Fig. 36b with the primary categories being "near the hole" and "away from the hole". The remainder of tension specimens are viewed looking at the top surface fiber ends, that is the first ply  $0^0$  fibers as that shown in Fig. 36b lower line of sight. The microphotographs in this work are for the 0.2" diameter specimens. The compression microphotographs for specimens

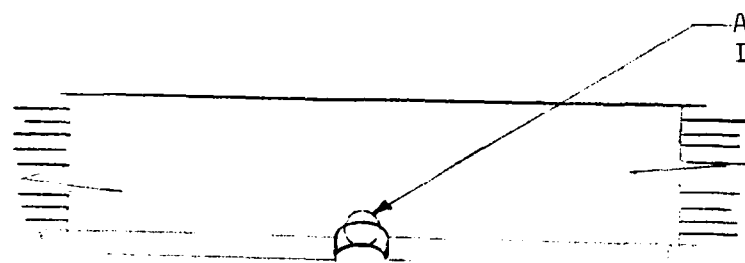
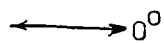
Original Direction of  
Fibers in Specimen



Area of Interest

View A, Top View

Original  
Direction of Fiber  
in Specimen



Area of  
Interest

Line of Eyesight

View B, In-hole View

Fig. 36a. Area of Study for Compression Specimen



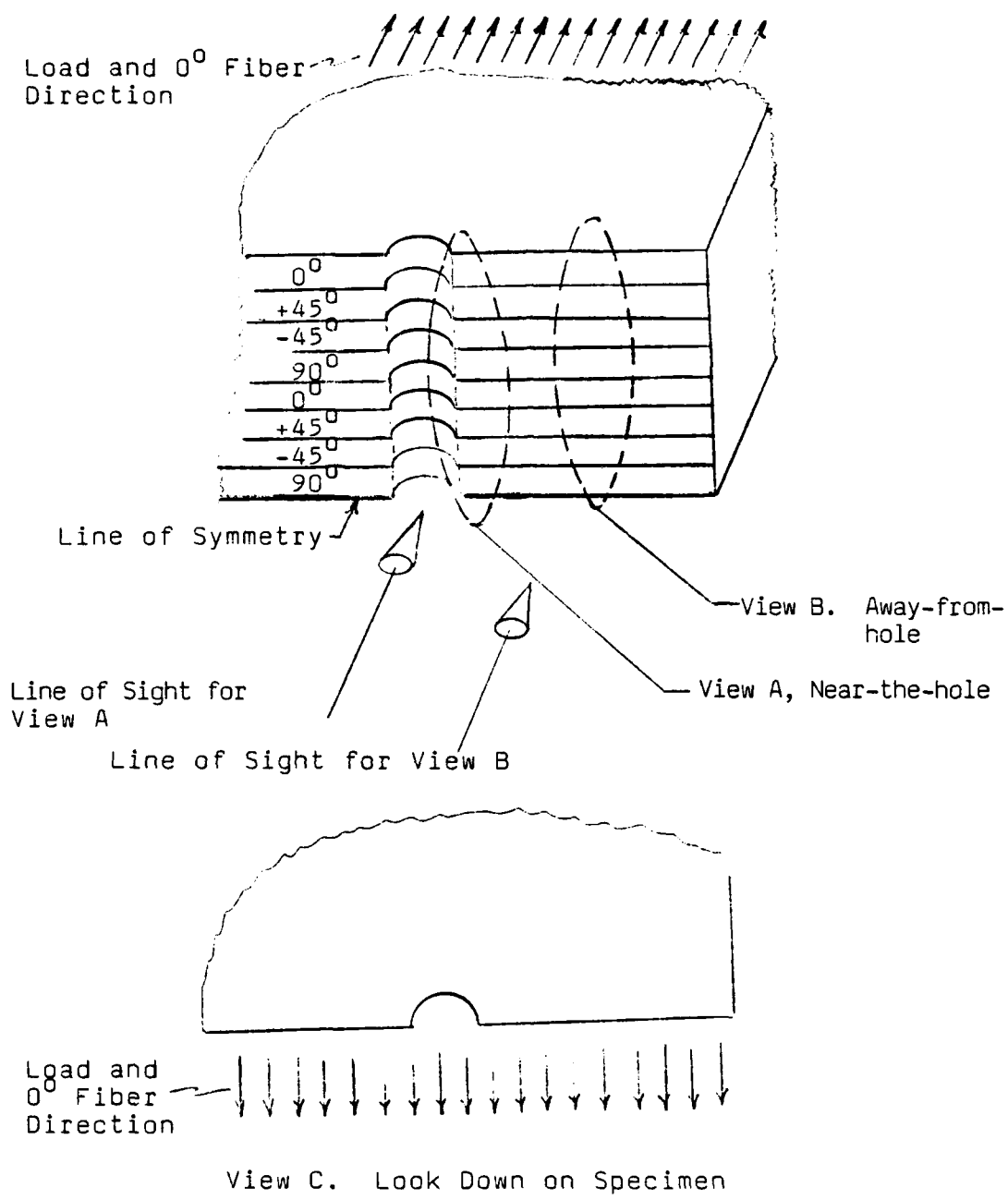


Fig. 36b. Area of Study for Tension Specimen

loaded to 90 and 95 percent of average compression load are presented and discussed in the next section, followed by complete compression failure specimen microphotographs. Following the compression sections, the tension strain results, and tension microphotographs are presented and discussed.

a. 90 and 95 Percent of Average Compression Failure Load Analysis

The first compression microphotographs, Fig. 37 and 38, are 90% of average compression failure load for the four test temperatures (i.e. Room temperature, 250<sup>0</sup>F, 275<sup>0</sup>F and 300<sup>0</sup>F). It is observed that laminates demonstrate more brittle behavior at the lower temperature. The matrix has provided better support at room temperature. The fibers have sustained a higher load at the lower temperatures. The fibers in the 300<sup>0</sup>F specimen, Fig. 38b, have had such low loading that very little fiber displacement has occurred.

Fig. 37b. demonstrates 0<sup>0</sup> fiber failure mechanism quite well. The hole is on the left side of the figure. Note the seeming exponential decay of fiber length that has crippled toward the hole. The more support the matrix gives to the fiber, the larger the length of fibers. That is, the room temperature specimen has crippled fibers near the hole in a larger area compared to the elevated temperatures.

The 95 percent of average compression failure load specimen are presented in Fig. 39 and 40. It can be seen that the fibers at room temperature and 250<sup>0</sup>F have failed





MICROCOPY RESOLUTION TEST CHART  
NATIONAL BUREAU OF STANDARDS-1963-A



(a) RT



(b) 250°F

Fig. 37. 90 Percent of Average Compression Failure Load. Top View, 130X (RT and 250°F)



(a) 275<sup>o</sup>F

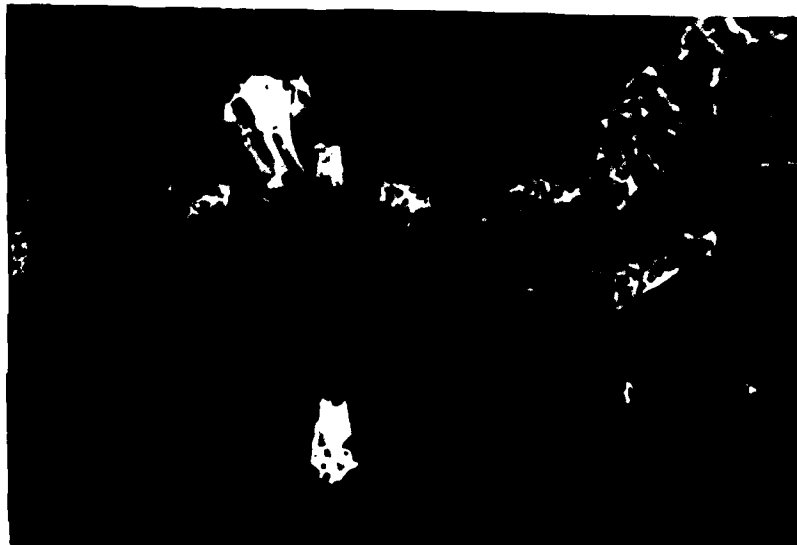


(b) 300<sup>o</sup>F

Fig. 38. 90 Percent of Average Compression Failure Load. Top View. 130X. (275<sup>o</sup>F and 300<sup>o</sup>F)

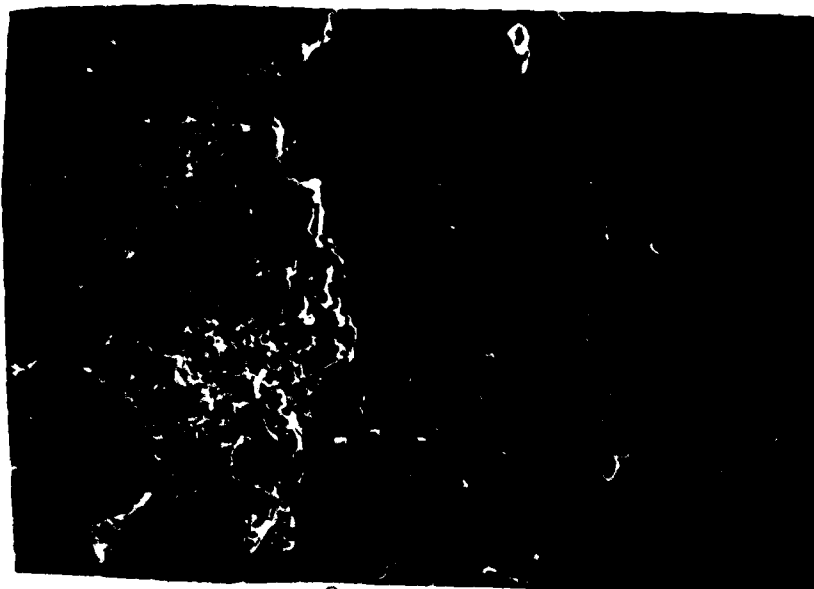


(a) RT

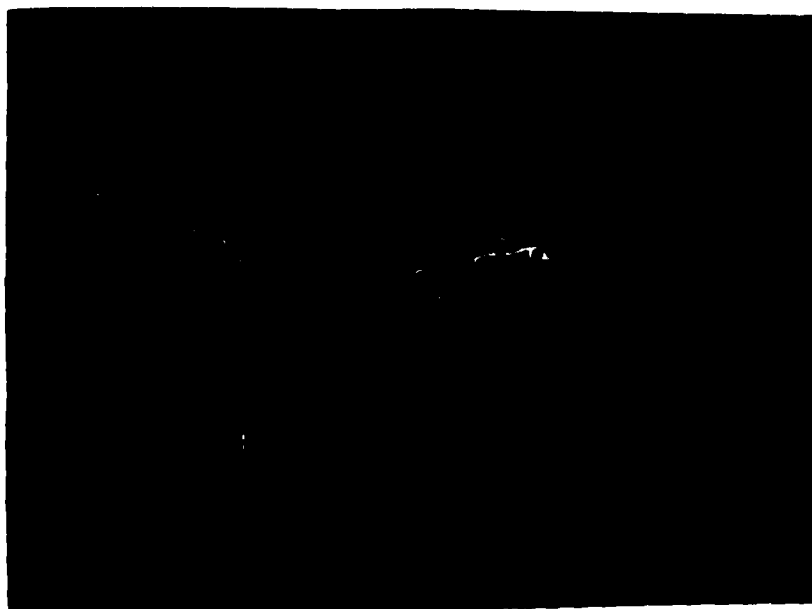


(b) 250°F

Fig. 39. 95 Percent of Average Compression Failure Load. Top View. 130X. (RT and 250°F)



(a) 275<sup>o</sup>F



(b) 300<sup>o</sup>F

Fig. 40. 95 Percent of Average Compression Failure Load. Top View. 130X. (275<sup>o</sup>F and 300<sup>o</sup>F).



in crippling toward the hole. The 275<sup>0</sup>F photograph, Fig. 40, shows some damage on the hole surface. This damage might act to cause severe local load redistribution, preventing fiber buckling. However, the start of fiber crippling is seen in the lower right quadrant of Fig. 40a.

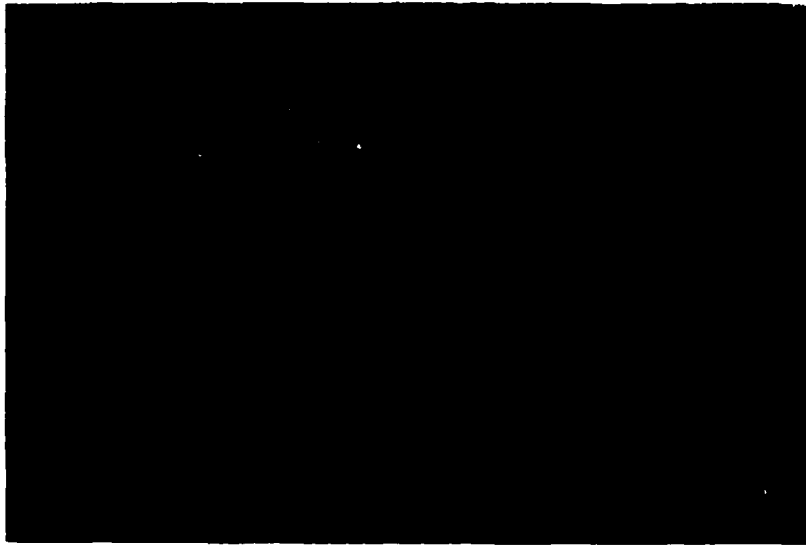
This damage is an anomaly and was not encountered elsewhere in this experiment.

The in-hole view of the 90 percent of compression failure load is presented in Fig. 41 and 42. The crippling of the 0<sup>0</sup> fibers into the hole can be seen in each microphotograph. The room temperature specimen indicates good matrix support of fibers. This is evident because much more fiber crippling has occurred for the lower temperature. The elevated temperature specimen indicate a decrease in matrix support. As temperature increases, less total compressive force is supported by the fiber-matrix composite.

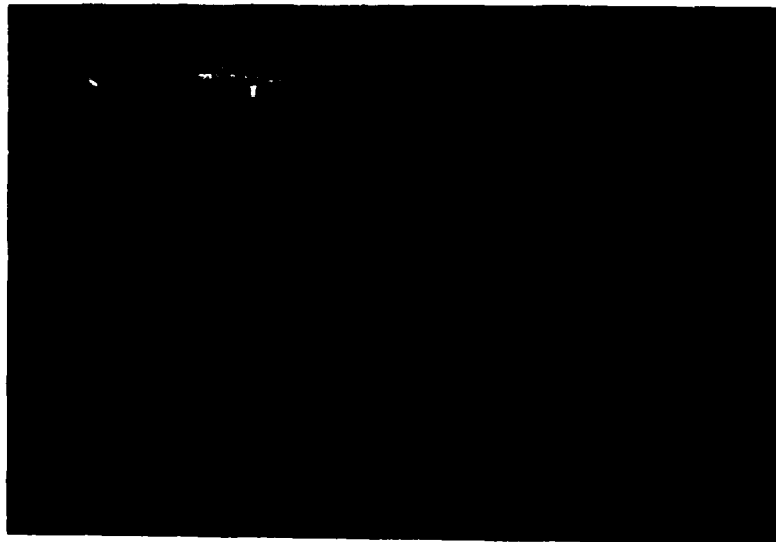
It is interesting to note that only the 0<sup>0</sup> fibers have crippled into the hole. This observation is consistent throughout the compression failure specimen.

The interaction of the various plies can be seen in each photograph also. The delamination process in its initial stages can be seen through the separation of laminae for a in-the-hole location in Fig. 43a. Note the ductility of the matrix as the laminae separate, seen in Fig. 43b.

The 95 percent of average compression failure load is depicted in Fig. 44-47. Again, the in-hole crippling of the



(a) RT

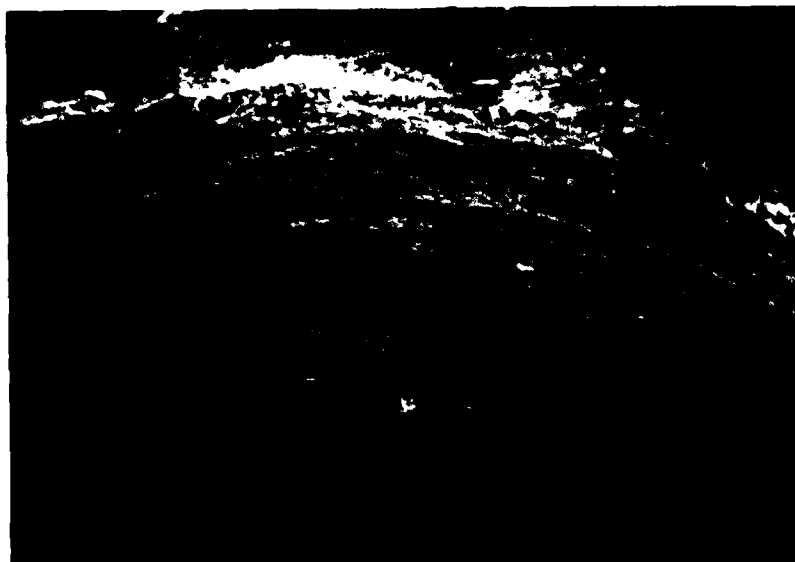


(b) 250°F

Fig. 41. 90 Percent of Average Compression Failure Load. In-hole View. 32X. (RT and 250°F)

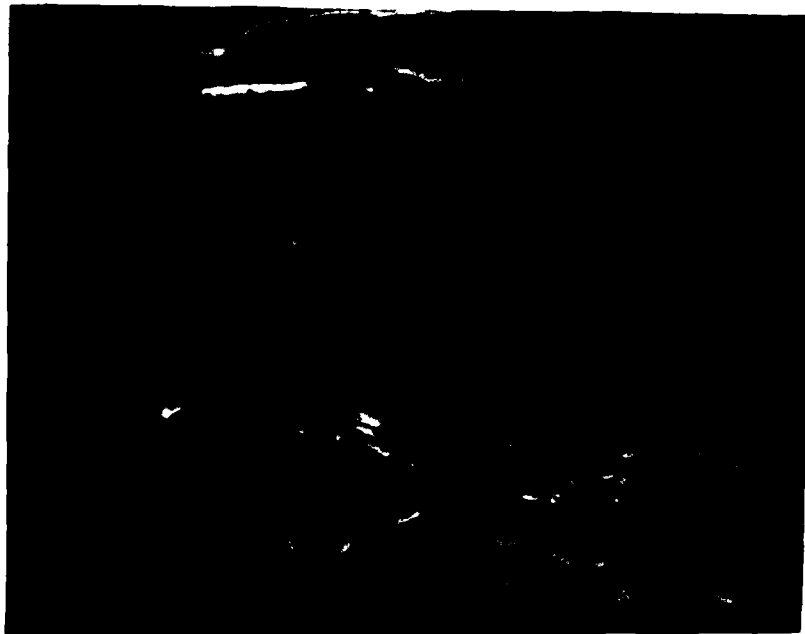


(a) 275<sup>0</sup>F

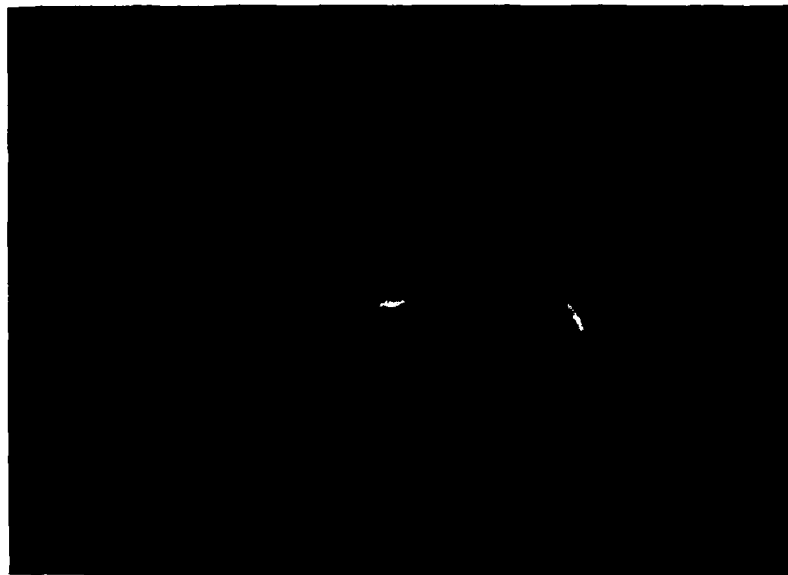


(b) 300<sup>0</sup>F

Fig. 42. 95 Percent of Average Compression Failure Load. In-hole View. 32X. (275<sup>0</sup>F and 300<sup>0</sup>F).



(a.) 1300X



(b.) 6500X

Fig. 43. 95 Percent of Average Compression Load. In-hole View. Lamina Separation.

the  $0^0$  fibers into the cut out is seen. Note the out of plane crippling of the top  $0^0$  lamina in Fig. 44 and 45. Not all of the crippling energy is expended to cripple the  $0^0$  fibers of the top lamina into the hole, some of this energy is expended to cripple out of plane. Microphotographs presented later in this work will demonstrate that the lamina itself is split, part of the top  $0^0$  lamina cripples into the cut out and part of the  $0^0$  lamina cripples out of plane. This use of energy in crippling out of plane is also shown by the larger amount of fibers crippled into the cut out within the laminate (the number five and twelve laminae) compared to the amount of fibers crippled into the cut out of the first and last laminae.

A closer view of the matrix is presented in Fig. 46 and 47. A thin film of matrix can be seen adhering to the fibers at room temperature. The matrix is more brittle at room temperature than elevated temperature, but the ductility of the thermoplastic PEEK can be seen quite easily. Although Miller did not study a compression loading [35], the Gr/Ep matrix shown in his work does not demonstrate the ductility of the matrix at room temperature that Fig. 46a depicts. The method of matrix failure at room temperature would be termed as partially cohesive because the matrix still adheres quite well to the fiber. Progressing through the temperature ranges in Fig. 46 and 47, one notices the matrix becomes more fluid, more

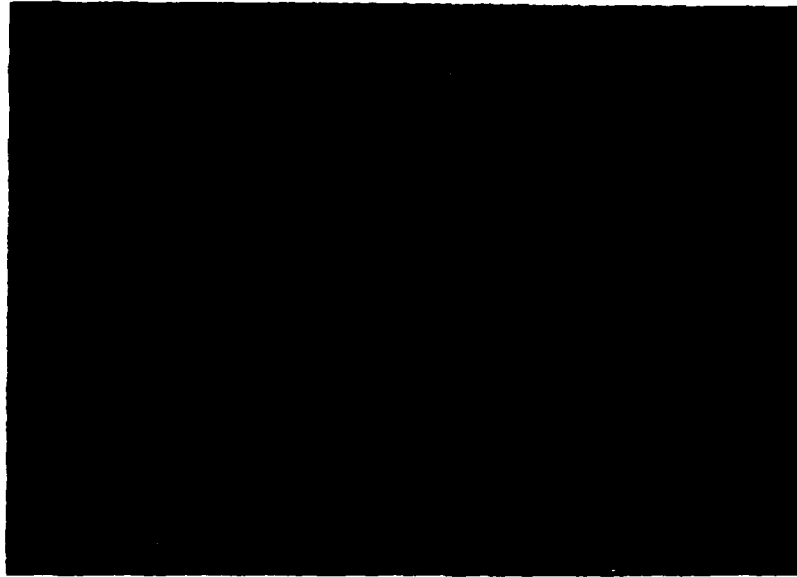


(a) RT

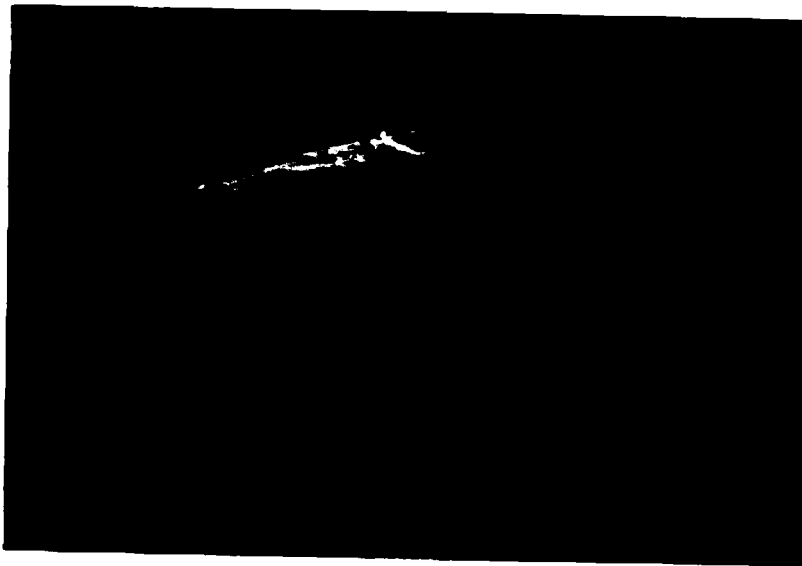


(b) 250<sup>o</sup>F

Fig. 44. 95 Percent of Average Compression Failure Load. In-hole View. 32X. (RT and 250<sup>o</sup>F).



(a) 275<sup>0</sup>F



(b) 300<sup>0</sup>F

Fig. 45. 95 Percent of Average Compression Load. In-hole View. 32X.  
(275<sup>0</sup>F and 300<sup>0</sup>F).



(a) RT



(b) 250°F

Fig. 46. 90 Percent of Average Compression Failure Load. In-hole View of Crippled 0° Fibers within the Laminate. 6500X. (RT and 250°F).





(a) 275<sup>o</sup>F



(b) 300<sup>o</sup>F

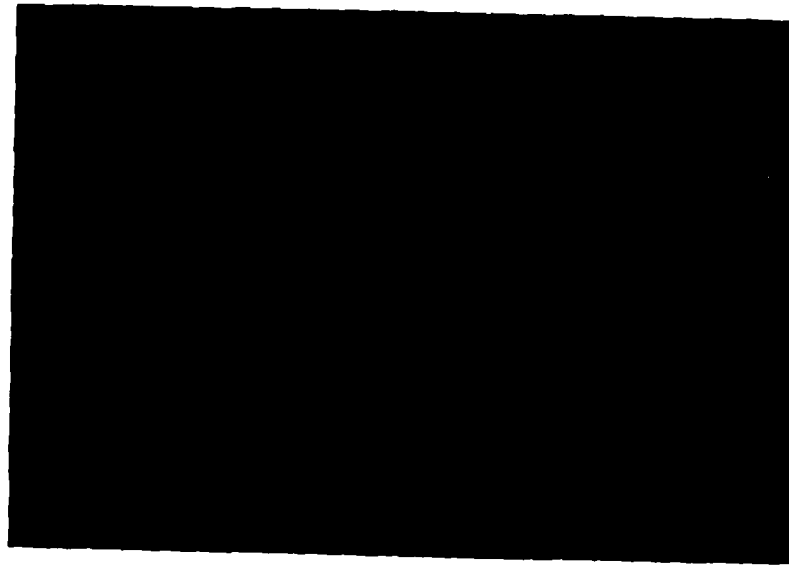
Fig. 47. 90 Percent of Average Compression Failure Load. In-hole View of Crippled 0<sup>o</sup> Fibers Within the Laminate. 6500X. (275<sup>o</sup>F and 300<sup>o</sup>F).

visco-elastic. In the 300<sup>0</sup>F microphotograph it can be seen that the matrix provides very little support to the fiber. The matrix is similar to a stiff fluid at this temperature.

It is interesting to note also the fiber failures. The fibers exhibit a mixed mode of bending, tension in part of the fracture face and compression the other, or a shear mode.

### C. Catastrophic Failure Analysis

When tested to failure, the compression specimens demonstrated a unique failure pattern. Compression specimens tested at room temperature broke into two separate pieces upon failure. Specimens tested at 250<sup>0</sup>F, 275<sup>0</sup>F, and 300<sup>0</sup>F did not fail in this manner (see Fig. 48). Each elevated temperature specimen remained in a "solid" piece. This failure pattern prevented through the thickness examination of the compression specimen. Instead, only the top view and in-hole view are capable of viewing without damaging the the fracture failure mechanisms themselves as one would attempt to examine through the thickness failure patterns. This failure pattern again supports the idea that the room temperature matrix supports the fibers more efficiently than elevated temperature matrix. The fiber-matrix resists more stresses or stores more energy to put it another way. Then, upon failure or release of the energy, the quantity of energy is sufficiently large to cause complete breakdown of the specimen.



(a) RT



(b) 250°F

Fig. 48. Complete Failure of Compression Specimen With Breaking of Specimen at Room Temperature. Top view. (RT and 250°F).

The in-hole views for compression failures are presented in Fig. 49 and 50. The crippling effect at failure can easily be seen for the  $0^0$  fibers. The room temperature failure shown in Fig. 49(a) shows that the  $0^0$  fibers have failed to such an extent, that they have turned perpendicular to the load direction and the original  $0^0$  direction. This figure also demonstrates the intra-laminar separation of the first and sixteenth plys. These plys demonstrate a separation of the lamina into separate directions, part of the  $0^0$  fibers in this lamina fail into the cut out and another part of the  $0^0$  fibers in this lamina fail out of plane. These failures demonstrate the complex nature of composite failures. Inter-laminar stresses and intra-laminar stresses are distributed in various manners throughout the specimen. The individual lamina can be seen acting somewhat independently in these figures (49 and 50). Examining Fig. 51, it is obvious that inter-laminar stresses cause the matrix deformation between the  $0^0$  crippled fibers and adjacent  $90^0$  fiber lamina.

Closer examination of the crippled  $0^0$  fibers is presented in Fig. 52 - 55 for the various experimental temperatures. It can be seen that the  $0^0$  fibers have failed from crippling modes: bending, shear and buckling stresses have contributed to individual fiber failures. Fig. 52 demonstrates excellent adhesive strength, the matrix has failed

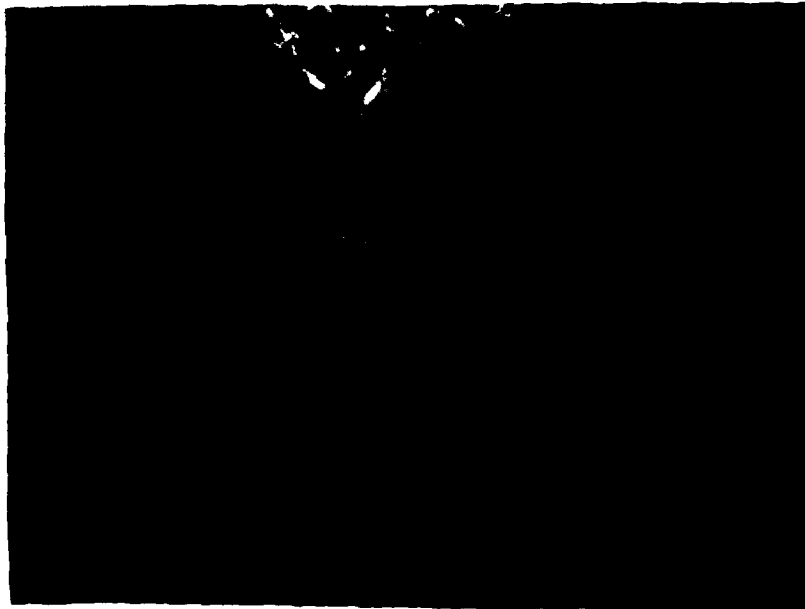


(a) RT

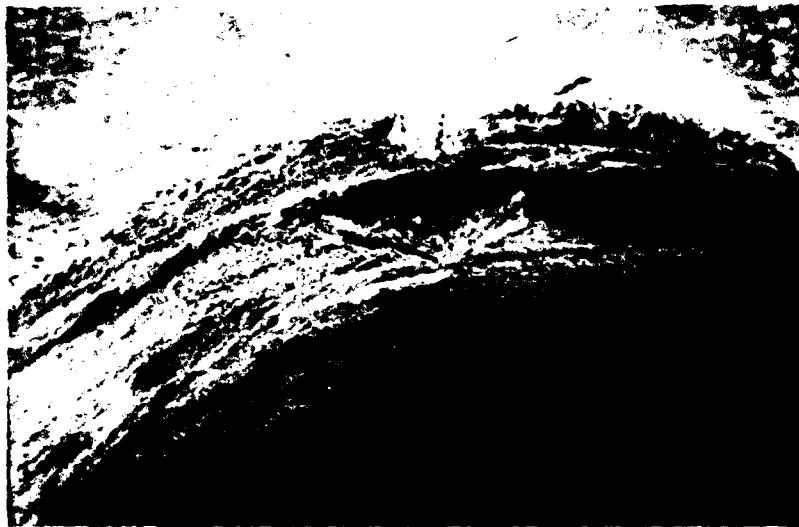


(b) 250<sup>o</sup>F

Fig. 49. Compression Failure Specimen. In-hole View. 32X. (275<sup>o</sup>F and 300<sup>o</sup>F).

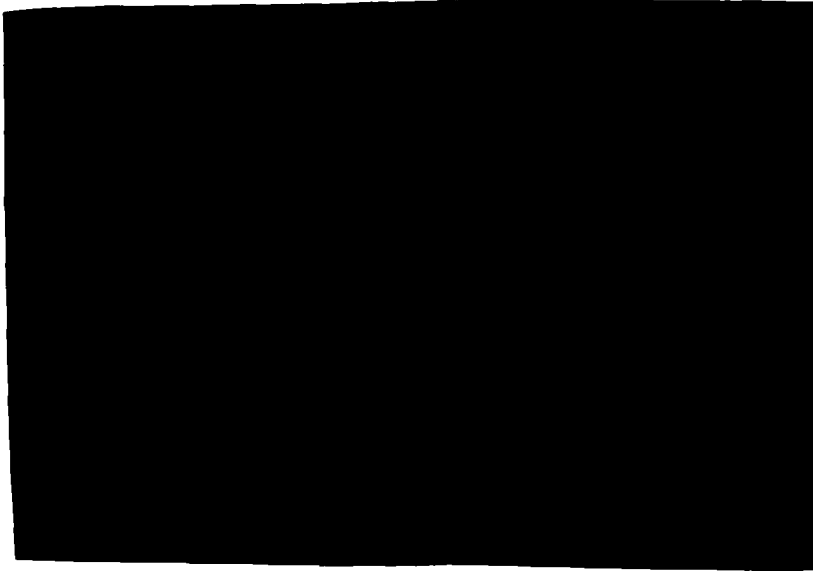


(a) 275<sup>o</sup>F

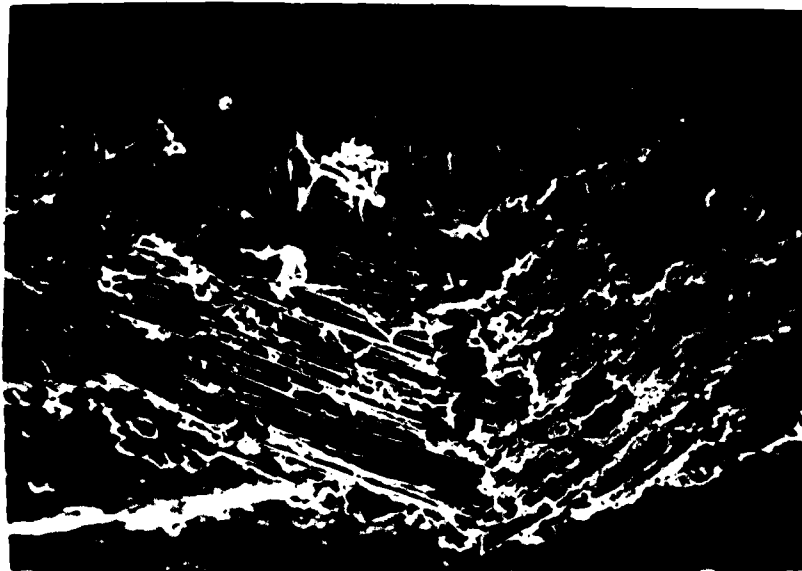


(b) 300<sup>o</sup>F

Fig. 50. Compression Failure Specimen. In-hole View. 32X. (275<sup>o</sup>F and 300<sup>o</sup>F).



(a) 250°F



(b) 300°F

Fig. 51. Compression Failure Specimen. In-hole View. Crippled 0° Fibers with Inter-lamina Matrix Deformation. 260X.

in at least partially cohesive mechanism. The matrix at room temperature is ductile, as observed between the fibers in the lower microphotograph of Fig. 52.

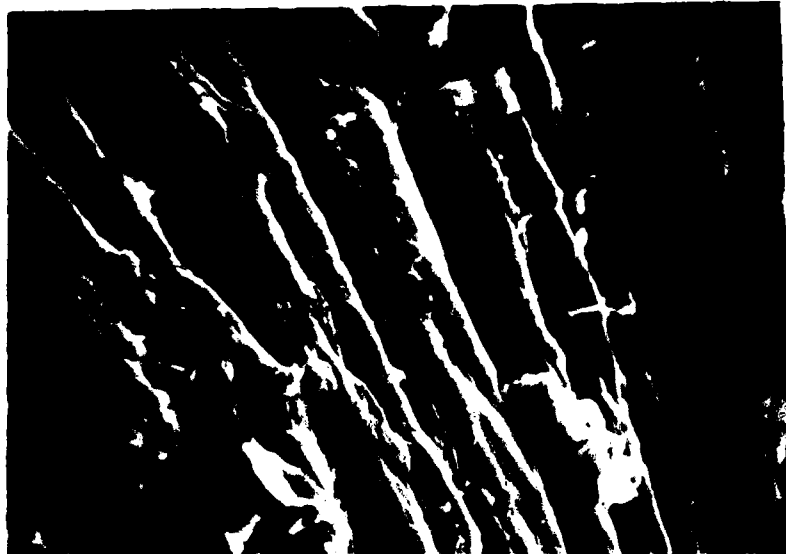
The 250<sup>0</sup>F test specimen in Fig. 53 show that the matrix is not as adhesive to the fiber when compared to the room temperature specimen. However, a complete adhesive failure mechanism is not seen at 250<sup>0</sup>F as some matrix still adheres to the fibers. The matrix at 250<sup>0</sup>F has some matrix still adhering to the fibers. The matrix at 250<sup>0</sup>F appears more ductile and more plastic than at room temperature.

The 275<sup>0</sup>F test specimen in Fig. 54 depict more cohesive failure than adhesive failure. The matrix can be seen adhering to the fiber but the toughness of the matrix seems to be deminishing. The shearing capability of the matrix appears to be much less compared to the room temperature microphotographs.

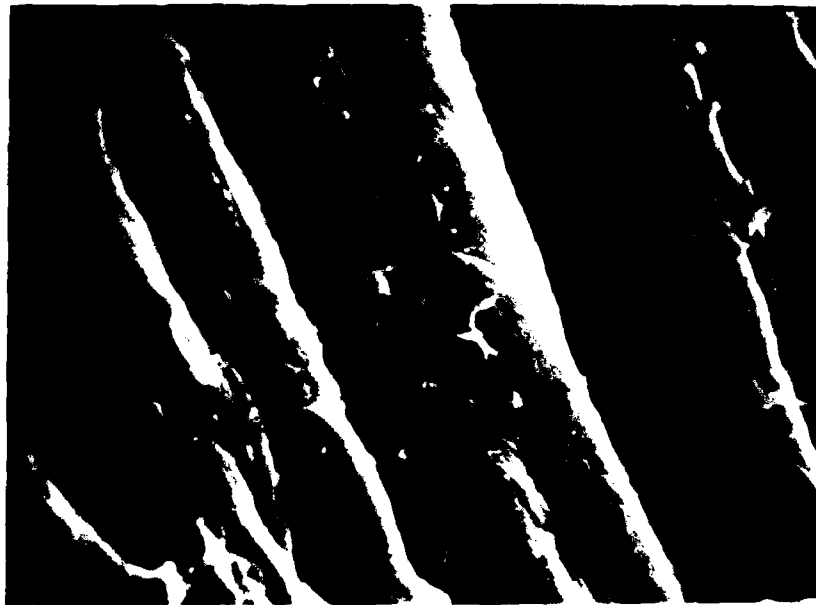
The 300<sup>0</sup>F test specimen in Fig. 55 demonstrate cohesive and adhesive failure. Matrix can be seen as a very thin film on some fibers while on other fibers the matrix appears very "fluid".

Very large magnification, 6500X, of compression specimen are presented in Fig. 56 and 57. These figures more graphically demonstrate the specific matrix-to-fiber bonding characteristics and are presented to amplify the discussion of matrix-to-fiber bond discussed for Fig. 52-55.



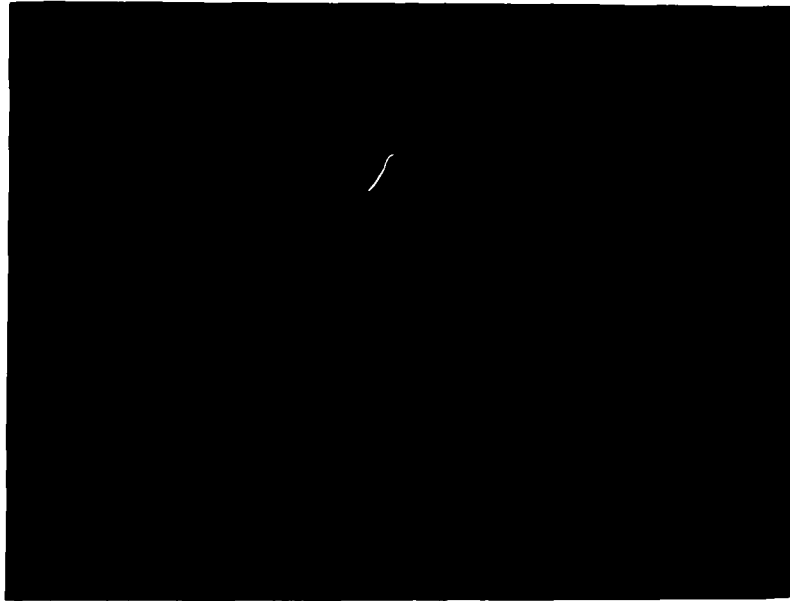


(a.) 1300X



(b.) 3250X

Fig. 52. Compression Failure Specimen, In-hole View.  $0^{\circ}$  Fibers Interlaminar Surface, Room Temperature.

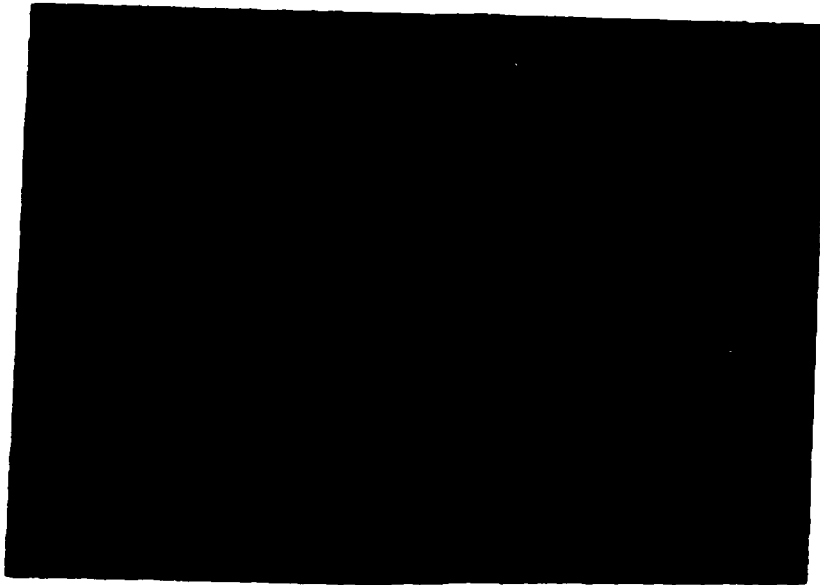


(a.) 1300X

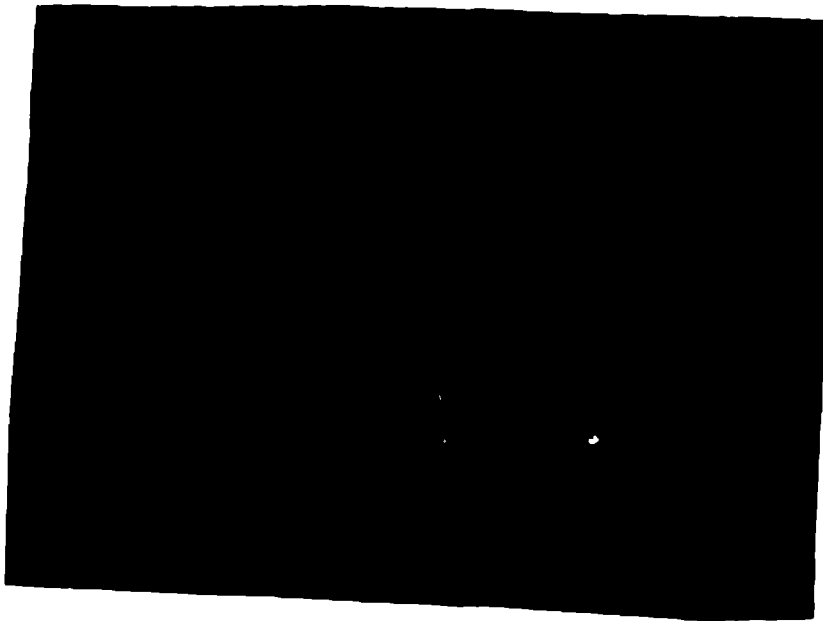


(b.) 3250X

Fig. 53. Compression Failure Specimen, In-hole View. 0° Fibers Cripple Surface, 250°F.

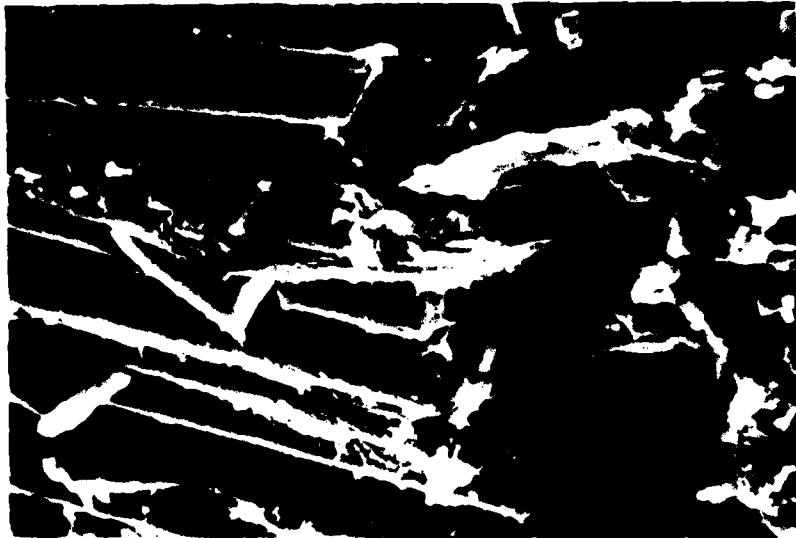


(a.) 1300X

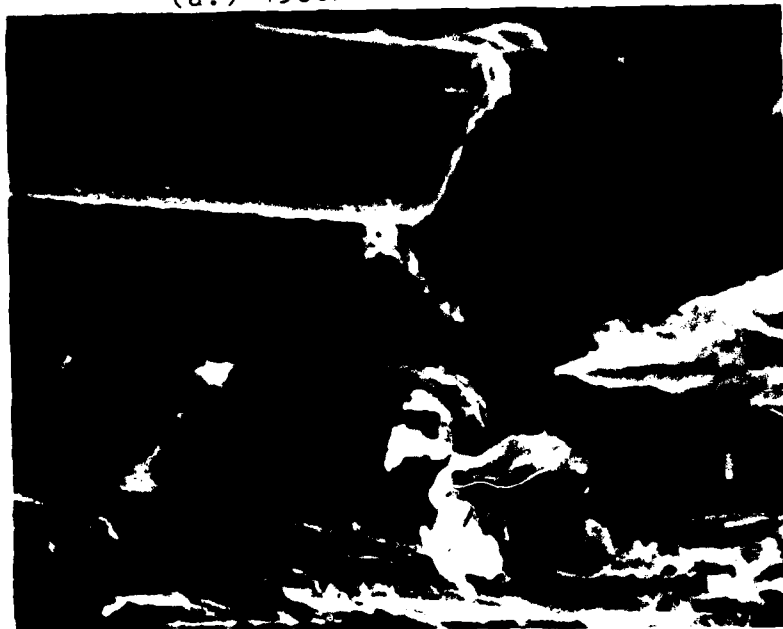


(b.) 3250X

Fig. 54. Compression Failure Specimen, In-hole View,  $0^\circ$  Crippled Fibers,  $275^\circ\text{F}$ .



(a.) 1300X



(b.) 3250X

Fig. 55. Compression Failure Specimen, In-hole View,  $0^\circ$  Crippled Fibers,  $300^\circ\text{F}$ .

The room temperature specimen matrix (Fig. 56a) shows shear, (hackles) failures. The matrix is ductile yet capable of distributing and resisting stress. The separation of fibers in a mode I fracture demonstrates the ductility of PEEK. Contrast the larger deformation of matrix in the 250<sup>o</sup>F specimen of Fig. 56 with the room temperature. Although the matrix deforms more, that is the matrix is more plastic, the matrix is not as cohesive as room temperature. In the 250<sup>o</sup>F specimen, the fiber fracture surface should be noted also. The bending failure of the fiber can be seen with the lower portion of the picture the tension loaded side, and the upper portion has been compressively loaded.

Inter-lamina matrix deformation for the crippled 0<sup>o</sup> fibers is amplified in Fig. 58 and 59. Reviewing Fig. 52 for the inter-lamina of the room temperature, the inter-lamina matrix deformation between the crippled 0<sup>o</sup> fibers and the 90<sup>o</sup> lamina directly adjacent show the degradation of matrix at elevated temperatures. At elevated temperatures, the matrix "flows" more and provides less capability to transfer loading or provide fiber support as it becomes more "fluid". Not only does the matrix provide less support for the fibers at elevated temperatures, the matrix also provides less inter-lamina strength also. This loss of support for the fibers and reduction of inter-lamina strength easily account for the overall reduction of strength for



(a) RT

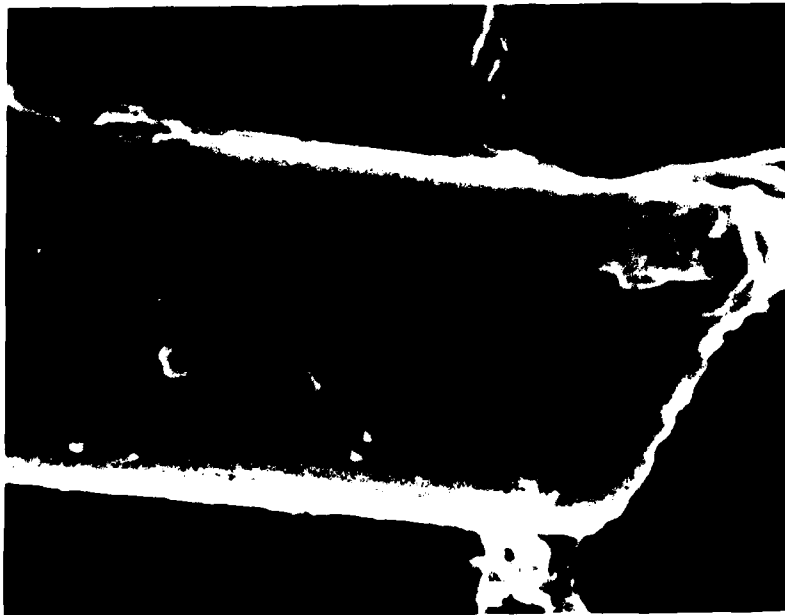


(b) 250<sup>o</sup>F

Fig. 56. Compression Failure Specimen, In-hole View, 0<sup>o</sup> Crippled Fibers, 6500X. (RT and 250<sup>o</sup>F).



(a) 275<sup>o</sup>F

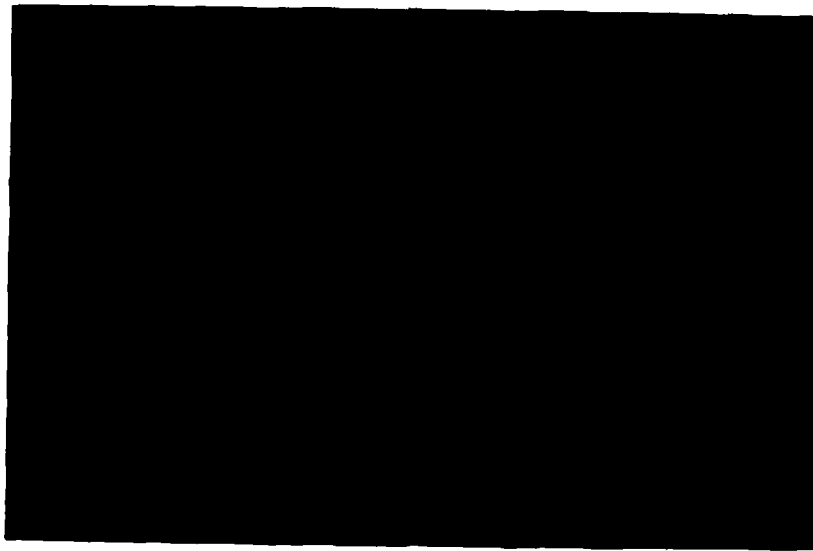


(b) 300<sup>o</sup>F

Fig. 57. Compression Failure Specimen, In-hole View, 0<sup>o</sup> Crippled Fibers, 6500X. (275<sup>o</sup>F and 300<sup>o</sup>F).



(a.) 1300X



(b.) 6500 X

Fig. 58. Compression Failure Specimen, In-hole View,  $0^{\circ}$  Crippled Fibers, Inter-Lamina Failure,  $275^{\circ}$ F.





(a.) 3250X



(b.) 6500X

Fig. 59. Compression Failure Specimen, In-hole View, 0° Crippled Fibers, Inter-Lamina Failure, 300° F.

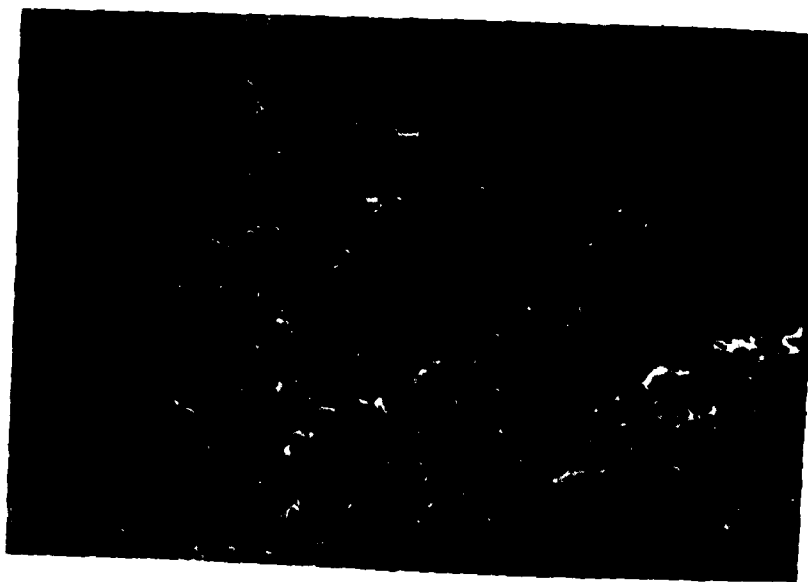
compression loading at elevated temperatures for APC-2, supporting the graphical depiction of laminate strength reduction previously presented.

Changing the viewing perspective from in-the-hole to the top view, compression failure specimens are shown in Fig. 60 and 61. The room temperature specimens indicate a large amount of energy was expended during the fracture process. Examining these figures it is noticed that as temperature increases, fewer fibers are failed toward the hole, indicating that the fibers have experienced less severe loading at elevated temperatures. Reviewing Fig. 44, 45, 49 and 50, it can be seen that an increase in specimen test temperature reduces the amount of out-of-plane crippling and intra-laminar separation of the first  $0^0$  fiber ply. This observation supports the theory that the fibers contain less energy at elevated temperatures than at room temperature. The more energy the matrix-fiber system resists, the larger the energy release on failure; consequently larger displacements, larger intra-laminar separation, and larger zones of crippled fibers indicating better support for fibers from the matrix, as well as better load transfer capability of the matrix.

An interesting verification of the intra-laminar fracture of the first  $0^0$  lamina is shown in Fig. 62. The



(a) RT

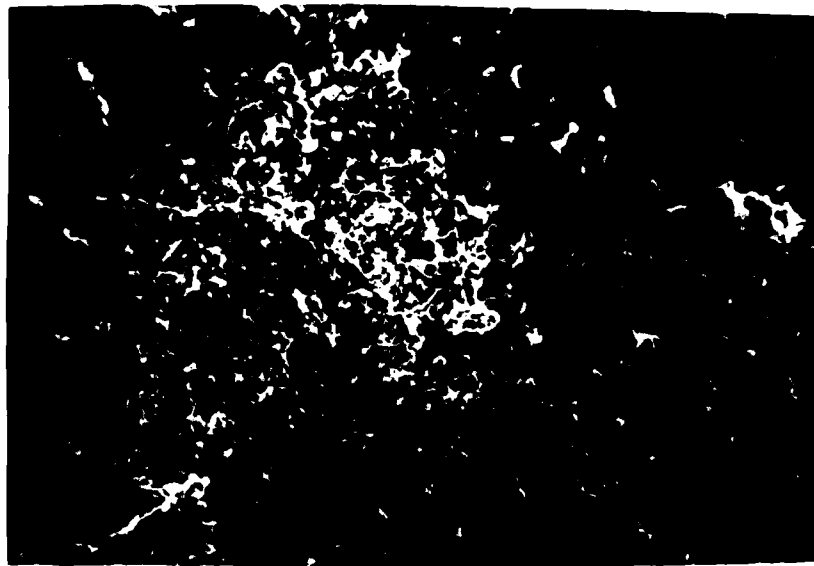


(b) 250°F

Fig. 60. Compression Failure Specimen, Top View.  
130X. (RT and 250°F).



(a) 275<sup>o</sup>F



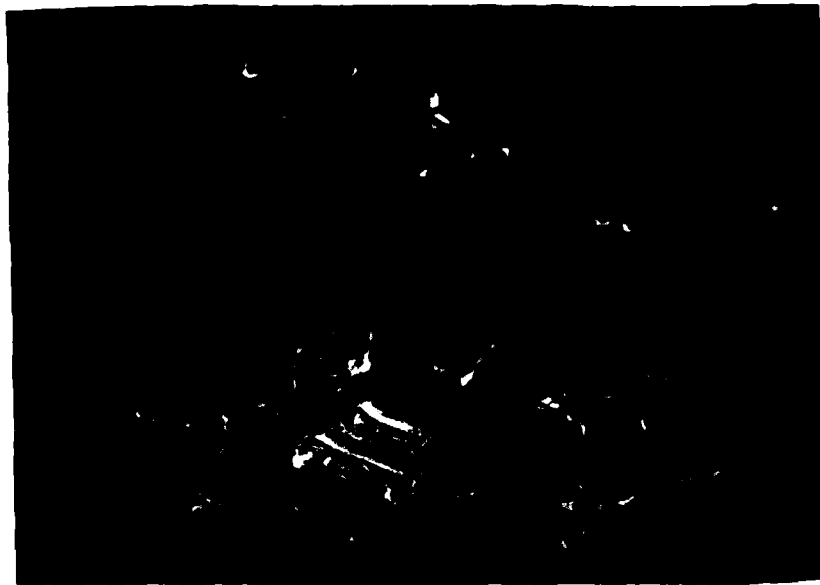
(b) 300<sup>o</sup>F

Fig. 61. Compression Failure Specimen, Top View.  
130X. (275<sup>o</sup>F and 300<sup>o</sup>F).

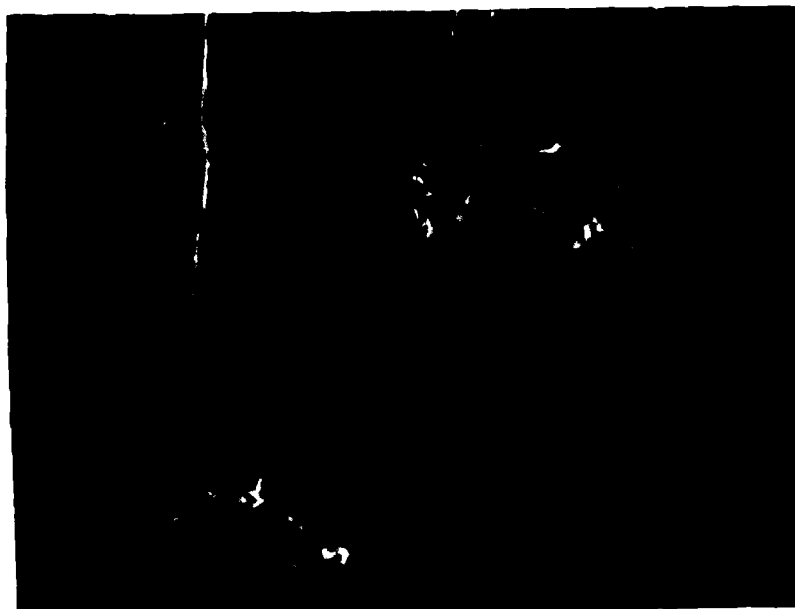
original  $0^{\circ}$  fiber direction is parallel to the length of the page. Note the angles of the failed fibers beneath the top fractured fibers, the fibers have broken toward the cut out. However, the top fractured fibers have buckled out of plane toward the viewer and remain fairly well aligned to the original direction. The lower microphotograph in Fig. 62 is an enlargement of the upper microphotograph. Note the matrix failure mechanisms. The matrix shows that the specimen was tested at room temperature. Due to the relative brittleness of the matrix at that temperature, the matrix demonstrates cracking between fibers, chunks of matrix from compressive forces, and some ductile shearing phenomena.

An examination of fiber end fractures is presented in Fig. 63, 64 and 65. The  $275^{\circ}\text{F}$  test specimen is shown in Fig. 63. The fiber ends point toward the notch. The fiber ends demonstrate that a mixed mode of failure occurred and not a pure tension or compression failure. Rather the fibers have failed from shear, bending, and buckling mixed modes.

To this point, the ends of the crippled fibers nearest the cut out have been examined. The opposite end of crippled fibers is shown in Fig. 64 and 65. These ends demonstrate the compressive build-up of matrix around the fiber. Fig. 65 is a 6500X magnification of the upper left corner of the lower microphotograph in Fig. 64. The fiber can be seen but a large amount of matrix has been compressed by the fiber and the matrix surrounds the fiber.



(a.) 260X



(b.) 650X

Fig. 62. Compression Failure Specimen, Top View,  
RT. Intra-laminar Fracture.

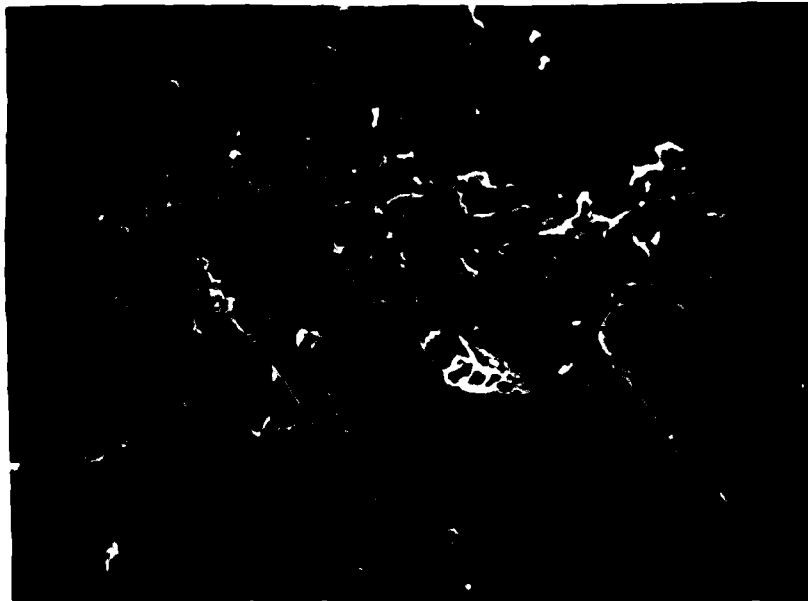


(a.) 3250X

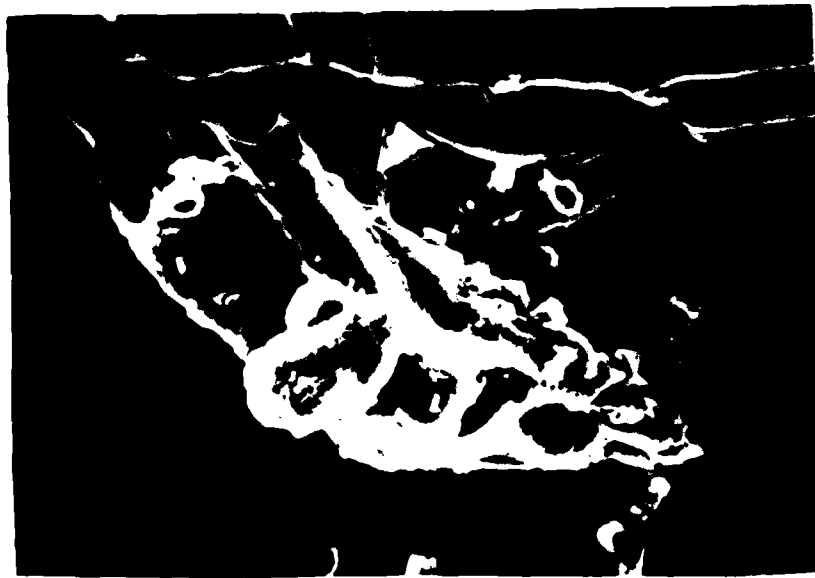


(b.) 6500X

Fig. 63. Compression Failure Specimen, Top View,  
275° F, Crippled Fiber Ends.



(a.) 260X



(b.) 1300X

Fig. 64. Compression Failure Specimen, Top View, 300°F, Crippled Fiber Compressed Ends.





Fig. 65. Compression Failure Specimen, Top View,  
300° F, Crippled Fiber Compressed End,  
6500X.

Compression failure fracture surfaces are characterized clearly by  $0^0$  fiber crippling and inter-lamina ply separation. The matrix shows significant degradation with increase in temperature for compression loading. The matrix degradation leads to reduced fiber-matrix interaction, i.e., the fibers withstand less loading and ultimately demonstrate significant strength reduction in compression.

The initial compressive failure for a notched specimen occurs at the notch where the largest stress concentrations are predicted. The  $0^0$  fibers initially "bend" toward the cut out but do this very locally. Increasing the applied load, the fibers are subjected to greater stresses and these stresses cause displacements. When the energy is sufficient fracture occurs, originating at the cut out and extending outward to the specimen edge.

The progression of crack growth from the cut out outward to the edge of the specimen is also a phenomena of tension failure as will be shown in the following section. Specimen will be seen to fail locally around the hole in a manner very dissimilar to failure at a distance away from the hole. The matrix properties play an important role in this occurrence and will be presented in the following subsection along with experimental strain results.

## 2. Tension Failure Analysis

To complete the microstructural analysis, an evaluation of the experimental tension strain results and

scanning electron microscope microphotographs is presented in this sub-section. Problems were encountered in obtaining sufficient quantities of near-hole and top-hole strain gages due to limited time available for this study and lead time required to manufacture the 0.015" gages. Additional problems, incurred during the experimental process itself, have combined with the logistical problem to severely limit the amount of experimental strain results. To further limit the tension study, the specimens loaded to 90 and 95 percent of average tension failure load did not demonstrate visible external failures. Although lack of external damage occurred, microphotographs of fracture surfaces will sufficiently demonstrate the fracture process. This sub-section contains the strain results for tension specimens which is followed by scanning electron microscope microphotographs.

a. Tension Strain Results

Room Temperature strain data is presented in Fig. 66. The far-field gage results demonstrate that APC-2 has linear response to 4400 pounds or 95 percent of failure load. The side-of-hole gage, however, demonstrates that non-linearity occurs locally, beside the hole, at 3000 pounds, 65 percent of failure load. The lack of external damage at 95 percent combined with the higher strain rate indicates that PEEK matrix is very ductile and capable of distributing load very well.

The limited quantity of strain gages prevented successful accomplishment of the experiment at 250<sup>0</sup>F. The strain results for 275<sup>0</sup>F are presented in Fig. 67. Non-linearity in the specimen begins to occur at the side of the hole at the same time non-linearity occurs throughout the specimen, indicating the same failure mode is occurring throughout the specimen. As discussed in the compression sub-section, fiber degradation is not a likely mode of degradation, rather matrix degradation can be easily demonstrated.

The 300<sup>0</sup>F strain results are shown in Fig. 68. Although non-linearity occurs at less than 50 percent failure load, early gage failure occurs detracting from the integrity of the strain data. It is likely, temperature has effected the gages' bonding ability.

Although strain data is limited for experimental tension specimens, the failure modes of the composite are still discernable using scanning electron microscope microphotographs. The following section presents the tension failure modes as observed in the SEM.

b. Tension Microscopic Analysis

Tension specimen were observed microscopically using a scanning electron microscope. The inspection of fracture surfaces must be consistent from specimen to specimen. That is, the same 90<sup>0</sup> ply must be evaluated for

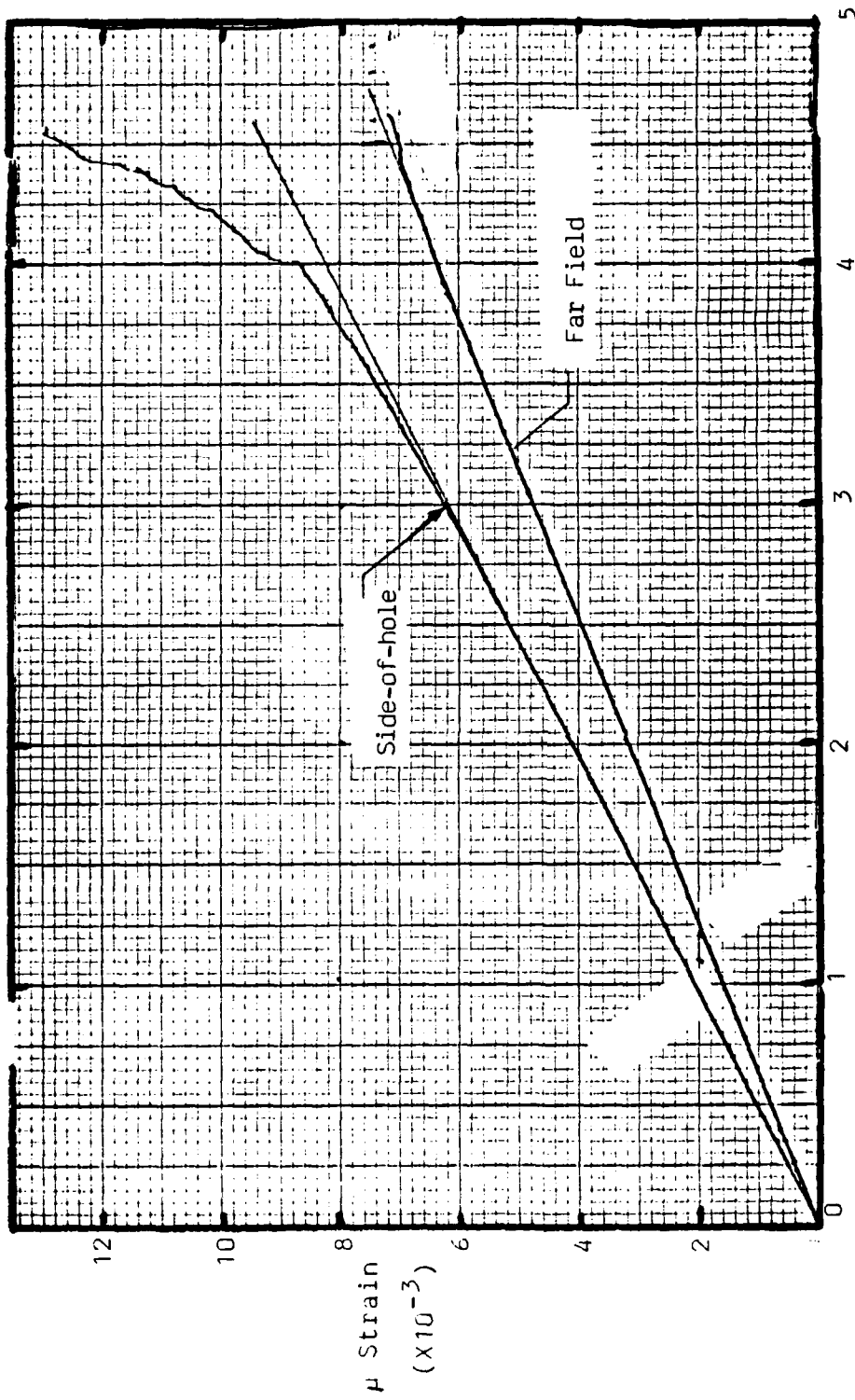


Fig. 66. Strain Results, 0.2" Diameter Cut out, Tension, RT  
Load (Pounds X 1000)

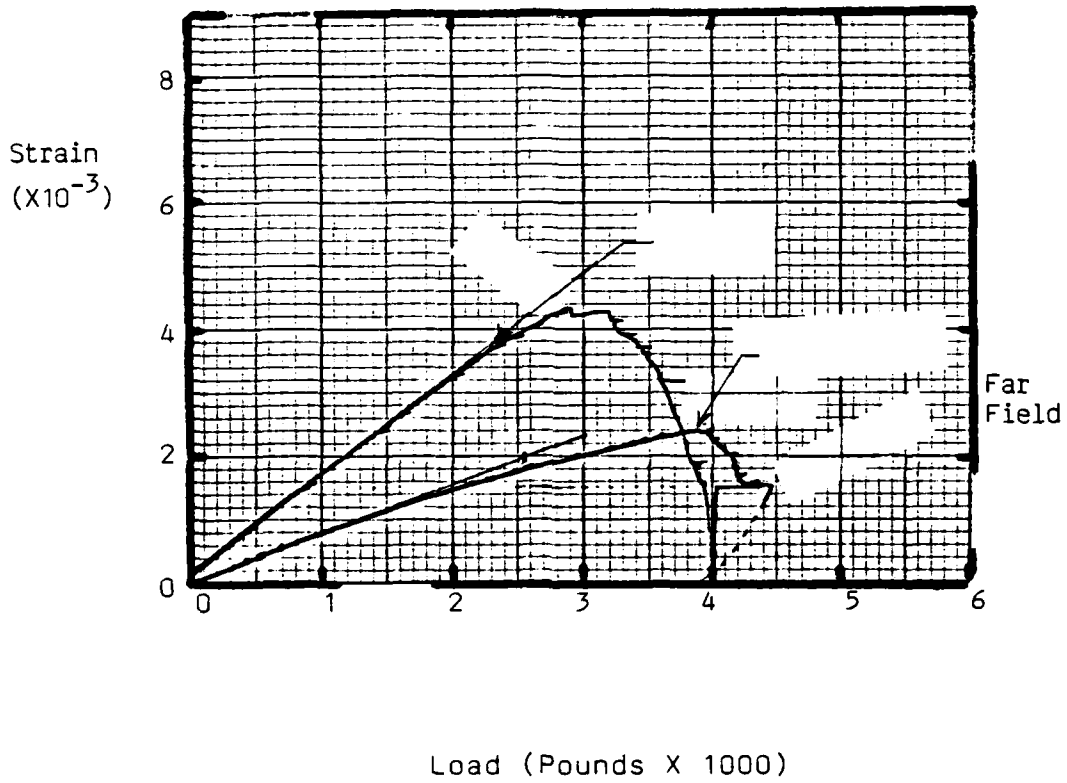


Fig. 67. Strain Results, 0.2" Diameter Cut Out, Tension, 275°F.

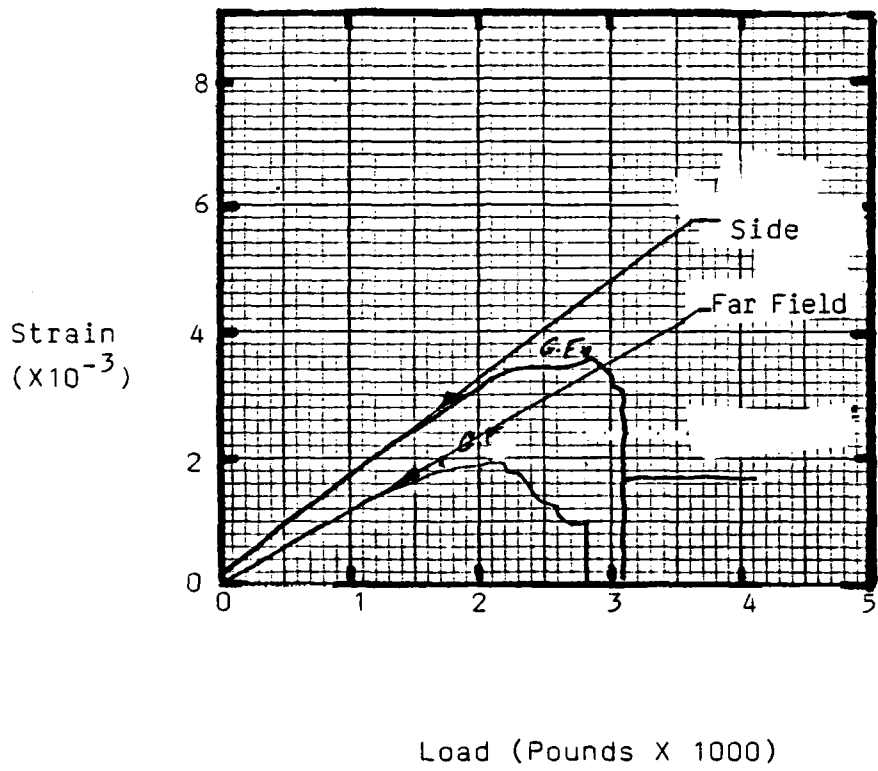


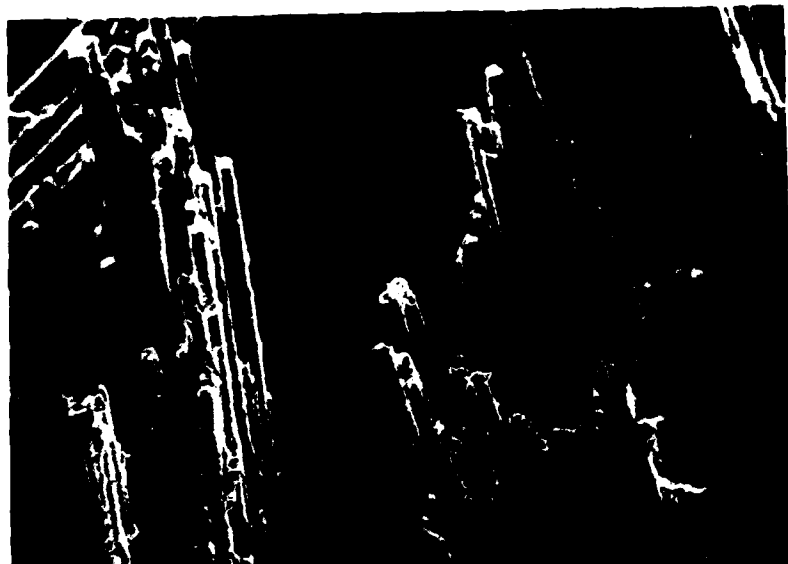
Fig. 68. Strain Results, 0.2" Diameter Cut Out, Tension, 300<sup>o</sup>F.

each specimen and must be evaluated in the same general location. This technique was followed throughout the tension specimen examinations. As mentioned earlier, there are two primary areas of interest, near the hole and away from the hole, and two principal viewing vantage points, top view and a frontal view. The reader may want to make a quick reference to Fig. 36b if uncertainty of viewing method is encountered. The first set of photographs discussed are top of specimen views of the first  $0^0$  ply (Fig. 69-79).

The  $0^0$  fiber fracture surfaces for the first ply, viewed from the top, are shown in Fig. 69-79. Fig. 69 and 70 are near-hole views for each of the test temperatures. Fiber pull-out is evident at each notch location and at each temperature. Fiber pull-out is an indication of plastic deformation and toughness. The brittle Gr/Ep system evaluated by Miller and Wingert [35] does not demonstrate fiber pull-out for brittle fracture mode, but at elevated temperatures the epoxy system was more ductile and fiber pull-out occurred. The extent of fiber pull-out is also an indication of toughness. A tougher material resists crack growth and it can be seen that the PEEK matrix allows and supports large fiber displacements, i.e. fiber pull-out.

Fig. 71 and 72 are magnifications of Fig. 69 and 70 and are presented to depict matrix characteristics. The





(a) RT



(b) 250°F

Fig. 69. Tension Specimen, 0° Fibers, Top View,  
Near Hole. 260X (275°F and 300°F).



(a) 275<sup>o</sup>F



(b) 300<sup>o</sup>F

Fig. 70. Tension Specimen, 0<sup>o</sup> Fibers, Top View,  
Near Hole. (275<sup>o</sup>F and 300<sup>o</sup>F).



(a) RT



(b) 250°F

Fig. 71. Tension Specimen, 0° Fibers, Top View, Near Hole, Matrix. 1300X (RT and 250°F).



(a) 275<sup>o</sup>F



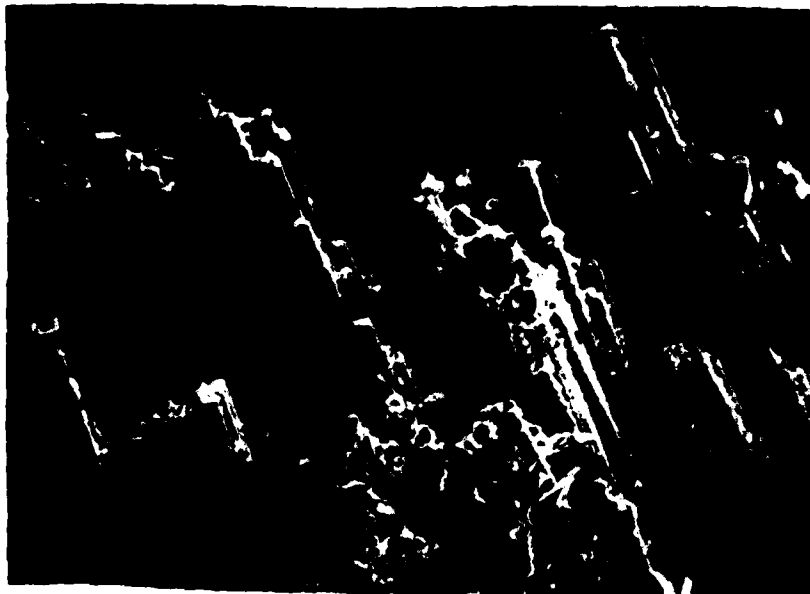
(b) 300<sup>o</sup>F

Fig. 72. Tension Specimen, 0<sup>o</sup> Fibers, Top View, Near Hole, Matrix. (275<sup>o</sup>F and 300<sup>o</sup>F).

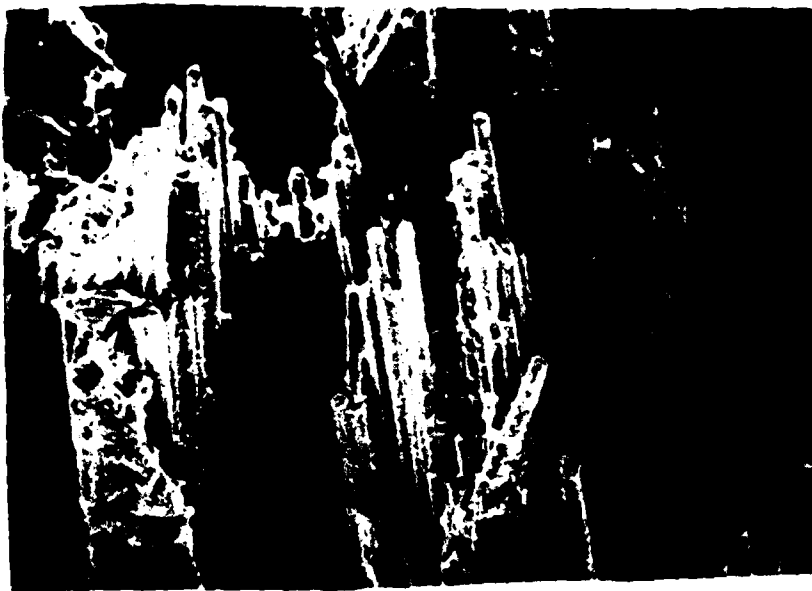
room temperature specimen in Fig. 71 shows some shear stresses have occurred within the matrix as the fibers have been pulled out and "hackles" formed on the side of the fibers. The amount of shearing is minimal when compared to deformations depicted in Donaldson's work [2]. As temperature increases, it appears that less and less shear stresses occur in the fracture modes shown in Fig. 71 and 72. It is obvious also that significant matrix adheres to the fibers at all temperatures, indicating the primary method of matrix failure is cohesive rather than adhesive.

Fig. 73 and 74 are microphotographs of specimen away-from-hole but still top view. First, comparing these figures as temperature elevates from RT to 300<sup>o</sup>F, again the fiber pull-out can be observed. When each temperature specimen in Fig. 73 and 74 are compared to the corresponding near-hole specimen in Fig. 69 and 70, it can be seen that the length of fiber pull-out in the near-hole fibers is greater than the same temperature specimen away from the hole. This is an early indication that a phenomena of stress is occurring at the hole that does not occur farther from the hole.

Fig. 75 and 76 are magnifications of Fig. 73 and 74 and, as such, are far from hole microphotographs, top view. These fibers indicate much higher shearing forces

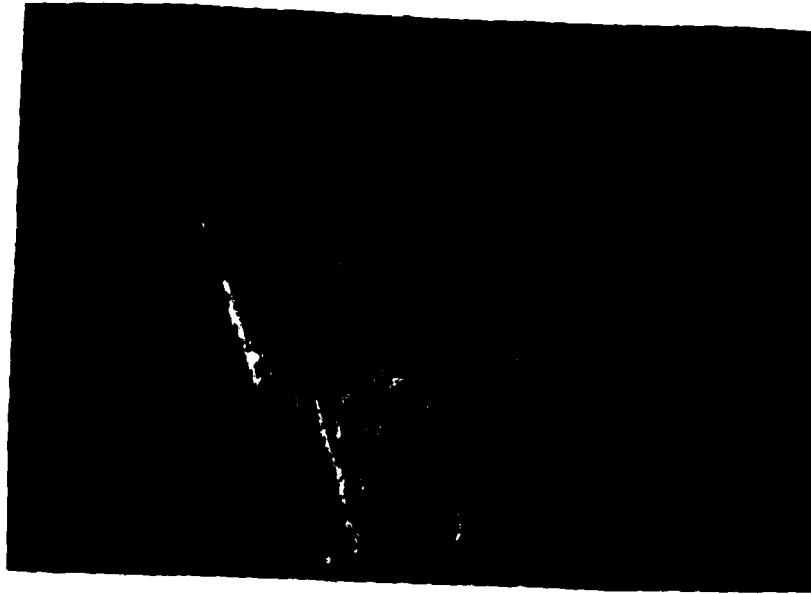


(a) RT



(b) 250°F

Fig. 73. Tension Specimen, 0° Fibers, Top View, Away from Hole. 260X (RT and 250°F).



(a) 275<sup>o</sup>F



(b) 300<sup>o</sup>F

Fig. 74. Tension Specimen, 0<sup>o</sup> Fibers, Top View, Away from Hole. 260X (275<sup>o</sup>F and 300<sup>o</sup>F).



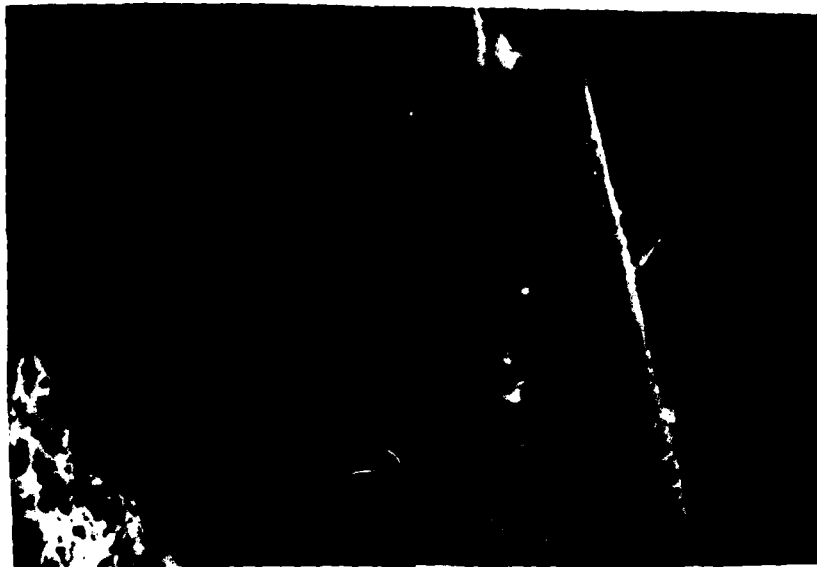
(a) RT



(b) 250°F

Fig. 75. Tension Specimen, 0° Fibers, Top View. Away From Hole, Matrix. 1300X (RT and 250°F).





(a) 275°F



(b) 300°F

Fig. 76. Tension Specimen, 0° Fibers, Top View, Away From Hole, Matrix. 1300X (275°F and 300°F).

and more brittle failure than near the hole for all test temperatures. These hackle-like formations are indicative of brittle failure [3,35].

Fig. 77 is a comparison of 250<sup>0</sup>F specimen near the hole and away from the hole. Note the relatively clean matrix surface and yet ductile nature of PEEK in the near-hole microphotograph. The far-from-hole picture in Fig. 77b demonstrates hackle-like formations indicating shear failure mechanism and compares well with shear mechanisms previously observed [35].

Fig. 78 and 79 are comparisons of near hole (Fig. 78a and 79a) and far from hole (Fig. 78b and 79b) matrix characteristics. The same shear phenomena described for Fig. 77 applies equally well for these microphotographs. Comparing matrix around the fiber end exposed in Fig. 77a with the matrix around the fiber end exposed in Fig. 78a, the matrix degradation with temperature from 250<sup>0</sup>F to 275<sup>0</sup>F can be seen. At 250<sup>0</sup>F the matrix is still capable of extensive plastic deformation. Comparisons of Fig. 77b, 78b, and 79b clearly show matrix degradation. As temperature increases, the matrix becomes more "fluid" and is less capable of transferring loads and resisting loads. This reduction in load capabilities would indicate a reduction in strength for elevating temperatures should be seen from experimental data. The reduction in strength shown in Fig. 14 concurs with the microstructural failure mode.



(a) Near Hole



(b) Far From Hole

Fig. 77. Tension Specimen,  $0^{\circ}$  Fibers,  $250^{\circ}\text{F}$ ,  
Top View. 3250X (Near hole and away  
from hole).



(a) Near Hole

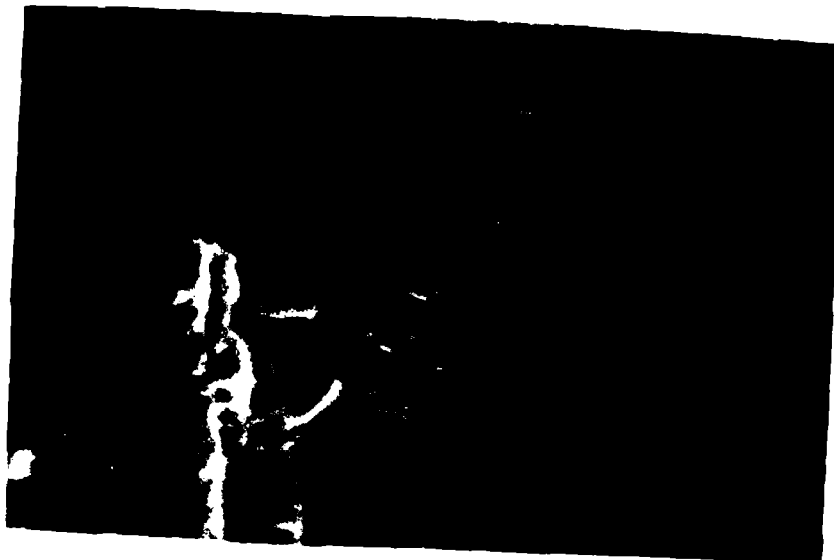


(b) Far From Hole

Fig. 78. Tension Specimen,  $0^{\circ}$  Fibers,  
 $275^{\circ}\text{F}$ , Top View. 3250X (Near hole  
and away from hole).



(a) Near Hole



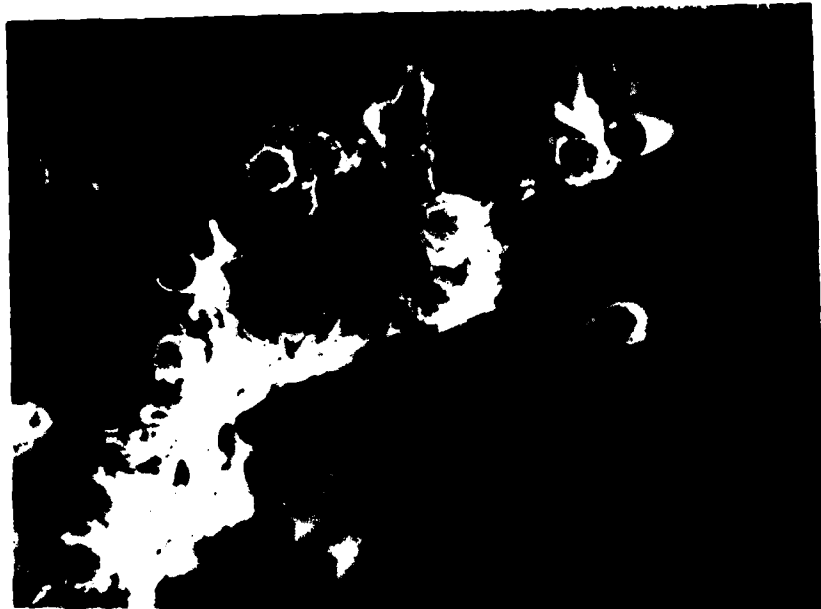
(b) Far From Hole

Fig. 79. Tension Specimen,  $O^0$  Fibers,  $300^0F$ ,  
Top View. 3250X (Near hole and away  
from hole).

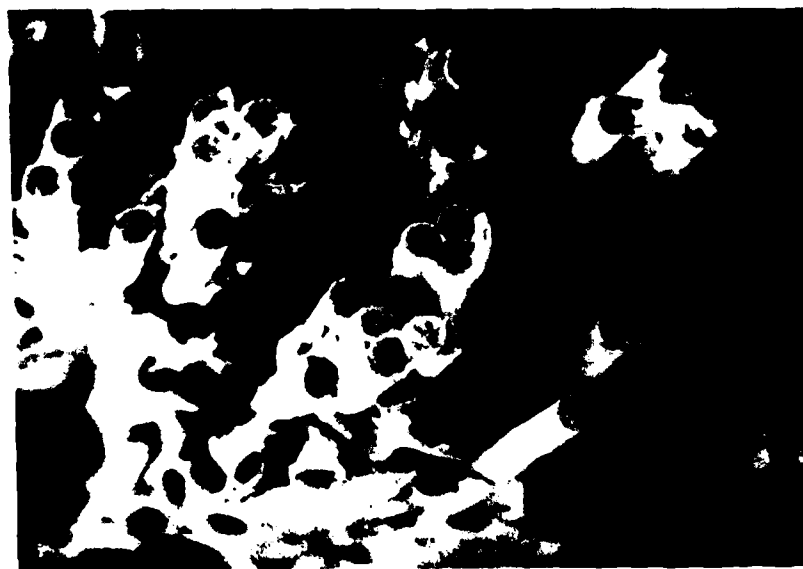
The variation in fracture modes between near-the-hole microphotographs and away-from-the-hole microphotographs must be further evaluated before conclusive explanations can be formed. Additionally, the extent of fiber pull-out for the  $0^0$  fibers should be examined.

Changing view points for the  $0^0$  fibers is necessary to examine more extensively the fiber pull-out and the hole effect. Fig. 80-87 are not top views but are either view A or View B as shown in Fig. 36b respectively. Consequently, all these microphotographs, Fig. 80-86, are  $0^0$  fibers within the laminate. Since the laminate is symmetric, the inner  $0^0$  ply should experience equivalent loadings.

Fig. 80 and 81 are near-hole specimens for each of the four test temperatures taken at as close to the same angle as possible. It is evident in these microphotographs that the length of fiber pull-out increases with temperature. It is also evident that the fibers have failed on an individual basis and not as groups. This individual fiber failure is indicative of a ductile matrix where load distribution can easily take place. The more brittle Gr/Ep specimen [35] demonstrated significant cooperative fiber failure and almost no fiber pull-out at room temperature. Load redistribution efficiency would also be an indication of notch sensitivity. A more brittle matrix would not be capable of the efficient load redistribution of this PEEK matrix. The notch sensitivity discussed in the graphical



(a) RT



(b) 250°F

Fig. 80. Tension Specimen, 0° Fibers, Front View, Near Hole. 650X (RT and 250°F).



(a) 275<sup>o</sup>F



(b) 300<sup>o</sup>F

Fig. 81. Tension Specimen, 0<sup>o</sup> Fibers, Front View, Near Hole. 650X (275<sup>o</sup>F and 300<sup>o</sup>F).



presentations indicated APC-2 to be less notch sensitive than APC-1 and Gr/Ep and these microphotographs substantiate that finding.

Fig. 82-85 are presented to examine the matrix characteristics for the various temperatures. The room temperature specimens in Fig. 82 depict a ductile matrix distributing load to fibers at varying fiber pull-out lengths. Close examination of Fig. 82b shows that the matrix is still very efficient and that failure occurs at least partially adhesively. Examining Fig. 83, 84 and 85, it can be seen that degradation of the matrix itself occurs. It is noticed that the 300<sup>o</sup>F specimen still has extensive matrix adhering to the fiber. From these microphotographs, (Fig. 80-85) it can be seen that the matrix mode of failure changes from adhesive at room temperature to cohesive at elevated temperature. This indicates that as temperature increases the matrix-to-fiber crystalline bond is stronger than the matrix bonding within itself.

Continuing the comparison between near-hole and far-from-hole microphotograph, the microphotographs for the far-from-hole specimen, Fig. 86 and 87, corresponding to the same temperature specimen in Fig. 80 and 81 are compared. The far-from-hole fibers at each of temperatures in Fig. 86 and 87 demonstrate much less fiber pull-out than the near-hole fibers. The fibers away from the hole seem to fail in



(a) 1300X



(b) 3250X

Fig. 82. Tension Specimen,  $0^{\circ}$  Fibers, Front View, Near Hole, RT. (1300X and 3250X).

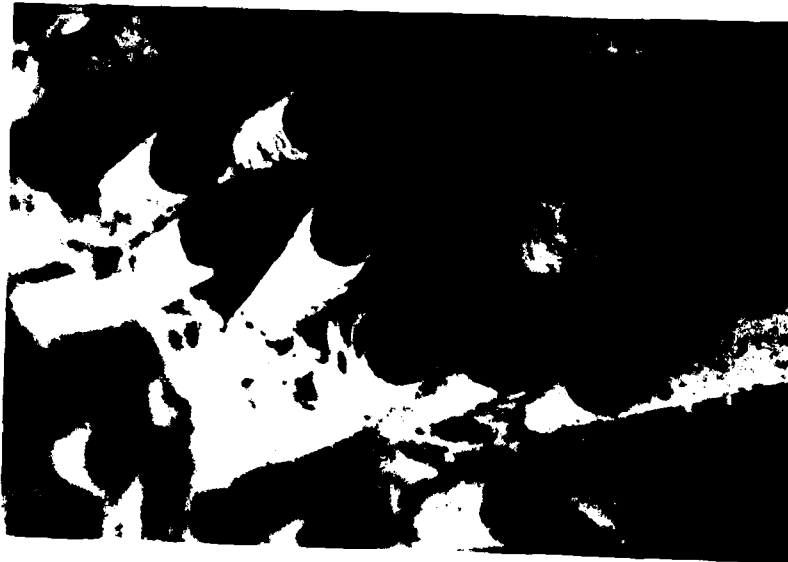


(a) 1300X



(b) 3250X

Fig. 83. Tension Specimen,  $0^{\circ}$  Fibers, Front View, Near Hole,  $250^{\circ}\text{F}$  (1300X and 3250X).



(a) 1300X



(b) 6500X

Fig. 84. Tension Specimen,  $O^{\circ}$  Fibers, Front View, Near Hole,  $275^{\circ}\text{F}$ . (1300X and 6500X).

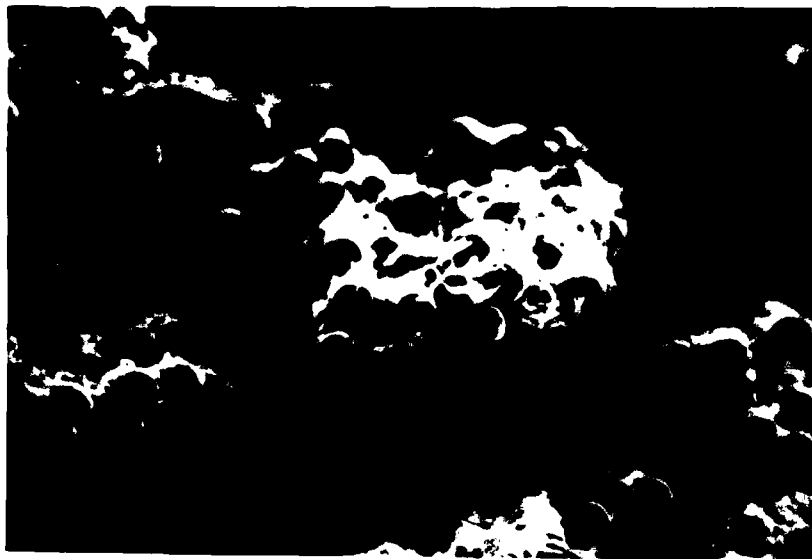


(a) 1300X

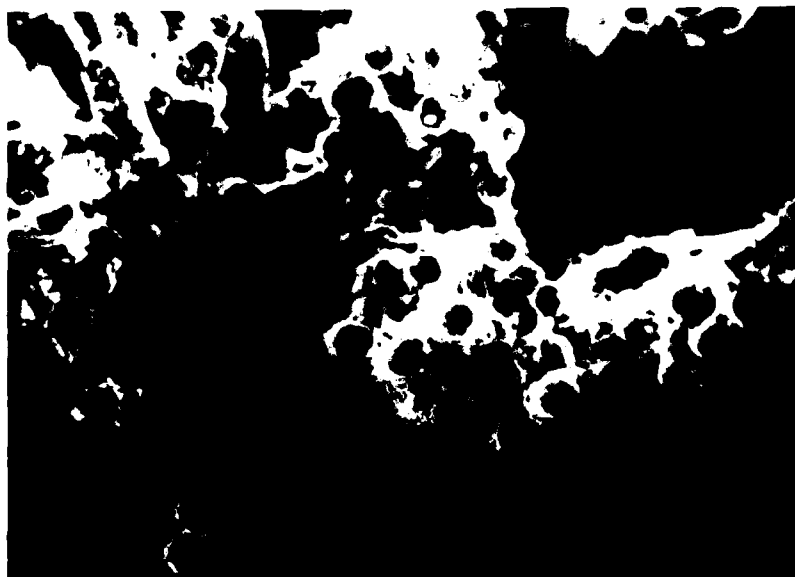


(b) 3250X

Fig. 85. Tension Specimen,  $0^{\circ}$  Fibers, Front View, Near Hole,  $300^{\circ}$ F. (1300X and 3250X).



(a) RT



(b) 250°F

Fig. 86. Tension Specimen, D<sup>0</sup> Fibers, Front View, Away From Hole. 650X (RT and 250°F).



Fig. 87. Tension Specimen,  $0^{\circ}$  Fibers, Front View, Away from Hole.  $275^{\circ}\text{F}$ ,  $650\times$ .

bundles, again a sign of a more brittle failure away from the hole compared to failure at the hole. The hypothesis at this point would be that failure near the hole occurs over the period of loading the specimen and failure away from the hole occurs during the dynamics of catastrophic failure. Thus one might say that the fracture occurs "slower" at the hole than away from the hole, or, conversely, the crack or fractures grows faster away from the hole. For this hypothesis to be accurate, the  $90^{\circ}$  plys must also demonstrate a "faster" growth away from the hole.

The  $90^{\circ}$  plys examined in this report are the two center  $90^{\circ}$  plys. Before comparing the  $90^{\circ}$  plys near-the-hole and away-from-the hole, an examination must be made for each case individually. One would expect that failure of the  $90^{\circ}$  lamina in a tension experiment would exhibit mode I failure. However, Fig. 88, when compared to Donaldson's mode I failures [2] for APC-1, are not similar in fracture patterns. Fig. 89a is somewhat similar to APC-1 mode I, but other modes of failure occur in Fig. 89 that are not observed in mode I failure.

Donaldson observed in brittle failures the angle of hackles in a failure mode was an indication of the amount of shear stress experienced by the matrix, a flat hackle experienced more shear stress than a vertical hackle, and the hackle angle appeared to progress from flat angle and pure shear load to vertical angle hackle and mode I failure





(a) RT



(b) 250°F

Fig. 88. Tension Specimen, 90° Fibers, Front View, Near Hole. 650X (RT and 250°F).



(a) 275<sup>o</sup>F



(b) 300<sup>o</sup>F

Fig. 89. Tension Specimen, 90<sup>o</sup> Fibers, Front View, Near Hole. 650X (275<sup>o</sup>F and 300<sup>o</sup>F).

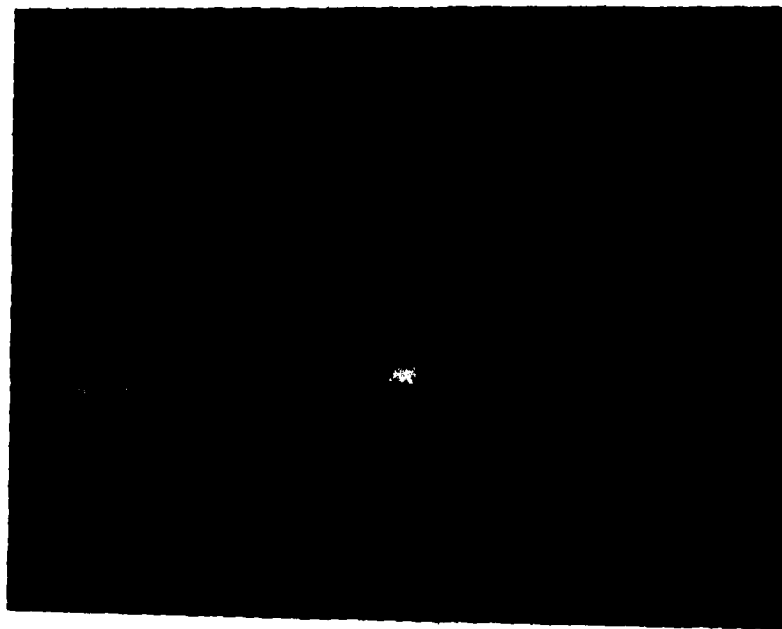
load. In a ductile material, the formation of hackles is not as well defined. Although formations such as those seen in Fig. 89b are extremely close to hackles in formation, the hackles in brittle failures are fairly uniform for a given region. This is not the case in Fig. 88 and 89. In fact, these figures indicate that more than mode I failures occurred near the hole. Evidently, there are Poisson's ratio effects, compressive and/or shearing forces, within the  $90^{\circ}$  ply due to inter-laminar strains and stresses, that cause more than a single mode of failure.

Observing the microphotographs in Fig. 90 and 91 which are magnifications of Fig. 88 and 89, the degradation of matrix with respect to temperature variations is obvious. In Fig. 90 and 91, the matrix degrades from a ductile, useful polymer at room temperature to a "fluid", non-load bearing polymer at  $300^{\circ}\text{F}$ .

The far-from-hole  $90^{\circ}$  plies are presented in Fig. 92 and 93 for the four test temperatures. The room temperature specimen demonstrates mode I failure similar to that seen for APC-1 with a small region of hackle-like formations indicating that possibly, a very localized shearing action has taken place on a single fiber or two. Progressively viewing Fig. 92 and 93 as temperature increases, it is noticed that the matrix is fairly smooth, indicating cohesive failure within the matrix in a mode I failure. The matrix is examined further in Fig. 94 and 95. The



(a) RT



(b) 250°F

Fig. 90. Tension Specimen, 90° Fibers, Front View, Near Hole, 1300X. (RT and 250°F).



(a) 275°F

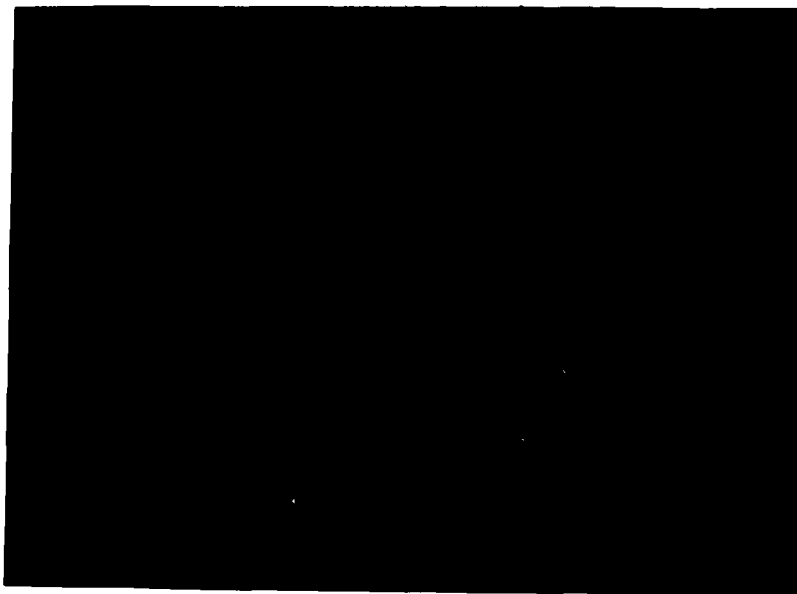


(b) 300°F

Fig. 91. Tension specimen, 90° Fibers,  
Front View, Near Hole, 1300X.  
(275°F and 300°F).

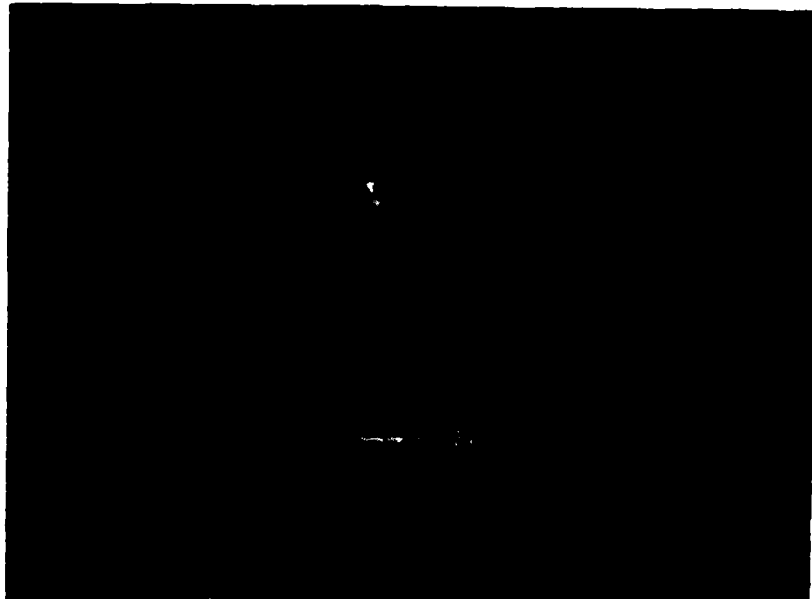


(a) RT

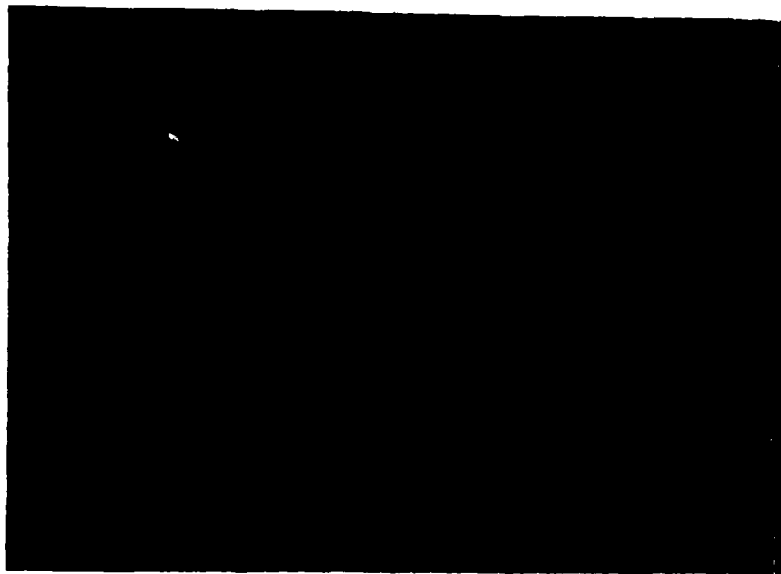


(b) 250°F

Fig. 92. Tension Specimen, 90° Fibers, Front View, Away From Hole. 650X (RT and 250°F).

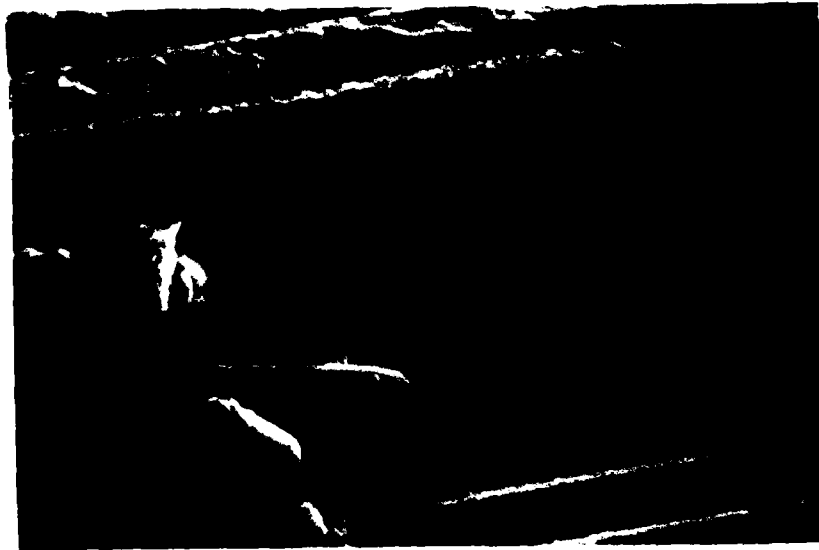


(a) 275<sup>0</sup>F



(b) 300<sup>0</sup>F

Fig. 93. Tension Specimen, 90<sup>0</sup> Fibers, Front View, Away From Hole.



(a) RT



(b) 250°F

Fig. 94. Tension Specimen, 90° Fibers, Front View, Away From Hole, Matrix. 1300X (RT and 250°F).





(a) 275<sup>0</sup>F



(b) 300<sup>0</sup>F

Fig. 95. Tension Specimen, 90<sup>0</sup> Fibers, Front View, Away From Hole, Matrix. 1300X (275<sup>0</sup>F and 300<sup>0</sup>F).

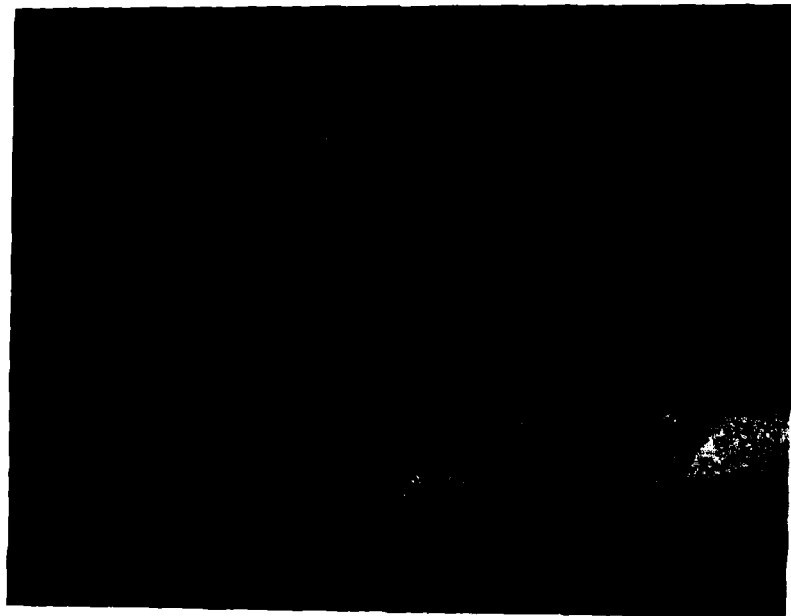
matrix seems to form "stars" in the room temperature specimen mode I failure in Fig. 94, concurring with the findings of others for mode I. At 250<sup>0</sup>F, the matrix is smooth textured indicating that matrix coherence has decreased and matrix degradation has occurred. Examining Fig. 95, the matrix is seen to be smooth with some shearing evident and obvious. Matrix degradation occurs at elevated temperatures.

Comparison between near hole failure modes in Fig. 88 and 89 can now be made to far-from-hole failure modes in Fig. 92 and 93 for each of the test temperature conditions. The near-hole microphotographs show that more ductility has occurred during fracture mode at this location as compared to the far-from-hole microphotographs, and present more than one mode of failure as compared to predominantly mode I failure away from the hole. The previous hypothesis of slow crack growth at the hole followed by faster crack growth away from the hole is supported by results from these 90<sup>0</sup> specimen microphotographs.

The final microphotographs to examine are for the 45<sup>0</sup> plys. The extent of examination required to fully evaluate 45<sup>0</sup> plys is excessive for this report. That is, there are several possibilities of +45 and -45 lamina within the specimen and not every specimen demonstrates failure planes that are observable consistently throughout the temperature ranges tested. Fig. 96 shows two specimen failures at low magnification, note the difficulty in examining both 45



(a) Hole to Right



(b) Hole to Left

Fig. 96. Tension Specimen, Low Magnification, 20X.

plys at the edge of each of the cut outs. Four of the  $45^{\circ}$  plys can be seen but the opposite sign  $45^{\circ}$  plys can not be so easily examined. Note the way the opposite sign  $45^{\circ}$  plys leave the area of the hole, these  $45^{\circ}$  plys continue to extend from the  $90^{\circ}$  plys to the side of the specimen. This makes viewing the original  $45^{\circ}$  plys an extreme problem. In this light, only a representative example is shown in Fig. 97 and 98, both figures are the same specimen  $250^{\circ}\text{F}$  with the latter figure a magnification of the first. Fig. 97 shows that a shear slide has occurred within this  $45^{\circ}$  ply. The fiber bundle on the left side has slipped forward with respect to the fiber bundle on the right side and the area depicting the former parallel faces is shown in the center of Fig. 97a. Fig. 98a shows clearly the shearing stresses have formed hackle-like formations very well. Viewing the ends of the fibers (Fig. 97b and 98b), an unusual phenomenon for a tension specimen is observed. A couple of possible theories for this occurrence are presented. First, at this temperature, the  $45^{\circ}$  plys rotate a slight amount to align with the direction of load. This phenomenon has been observed locally in lab specimens but appears nowhere in publications that were read. Assuming the  $45^{\circ}$  plys rotate to align with the  $0^{\circ}$  fibers and then the specimen catastrophically fails, the  $45^{\circ}$  plys would regain the elastic deformation that occurred prior to fracture. During this realignment, the



(a) 260X

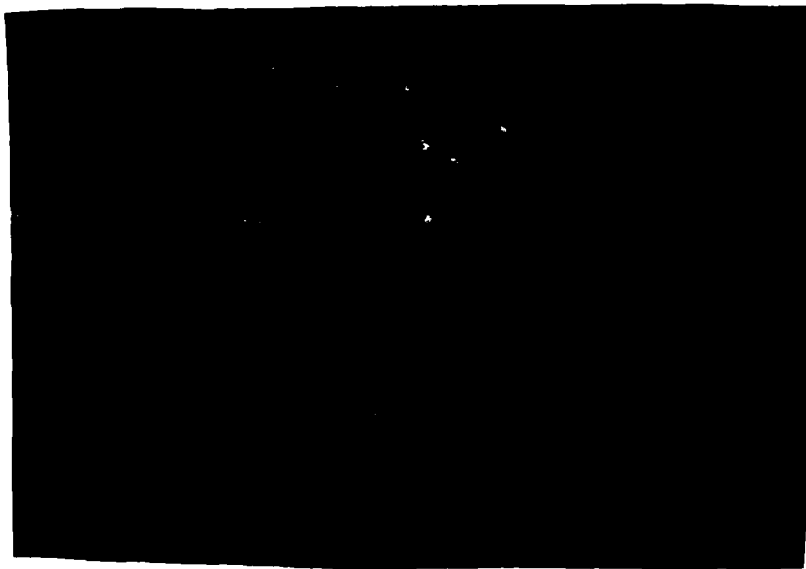


(b) 650X

Fig. 97. Tension Specimen,  $45^{\circ}$  Fibers  
Front View, Away From Hole,  $250^{\circ}\text{F}$ .



(a) Shear



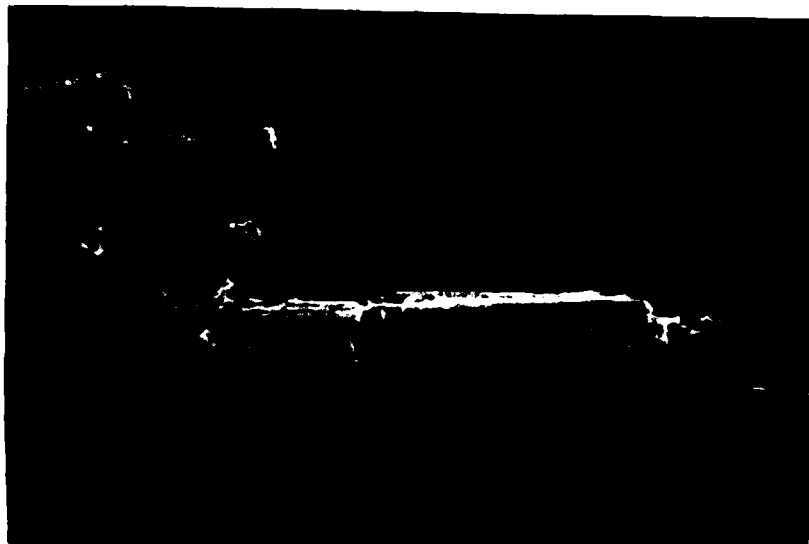
(b) Fiber Ends

Fig. 98. Tension Specimen,  $45^{\circ}$  Fibers, Front View, Away From Hole,  $250^{\circ}\text{F}$ ,  $1300\times$ .

fiber ends rub against the other side of the failed specimen and smear the fiber ends. A second theory would be that the fibers are under a compressive load due to some inter-laminar stresses and/or Poisson's ratio effects. The first theory has more physical evidence, however.

During the scanning of specimens in the SEM, several interesting observations occurred and three of these are depicted in Fig. 99, 100, 101 and 102. Fig. 99 and 100 are the same specimen (275<sup>0</sup>F, tension, 45<sup>0</sup> ply). Note, the interesting formation of hackle-like matrix deformation between the two fibers. Fig. 101 shows matrix degradation at 275<sup>0</sup>F quite clearly, the matrix becomes very fluid. This matrix degradation is also depicted in Fig. 102 as very plastic deformation.

The primary tension strength of APC-2 is derived from the properties of the graphite fibers. The extent of effectiveness of the fibers is determined by the support the matrix provides. As the matrix coherently degrades the overall strength of the APC-2 laminate decreases. The matrix provides good load distribution around and to the fibers at room temperature but this capability is decreased as the matrix degrades for elevated temperatures.



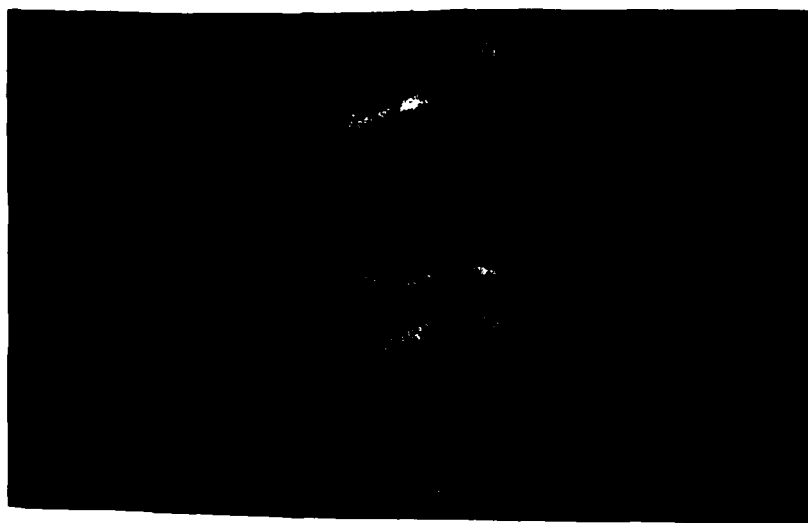
(a) Fiber Ends



(b) 3250X

Fig. 99. Tension Specimen,  $45^{\circ}$  Fibers, Front View, Away-From-Hole,  $275^{\circ}$ F.





(a) 6500X

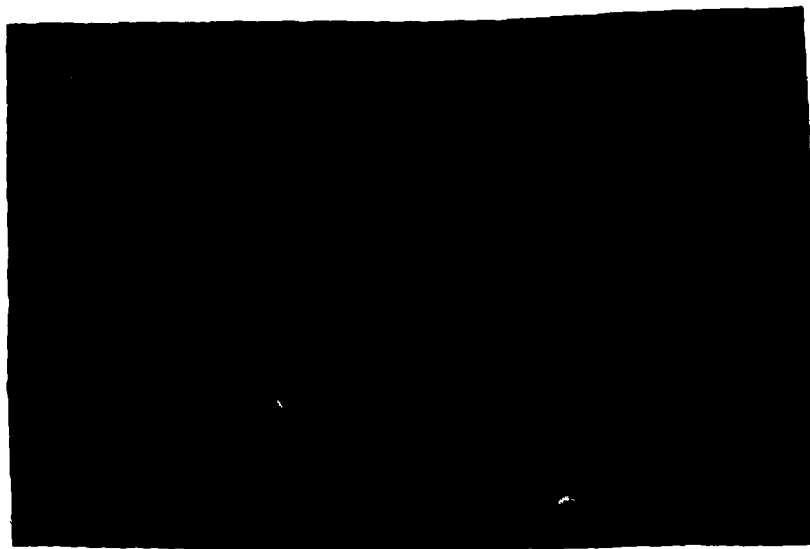


(b) 9750X

Fig. 100. Tension Specimen,  $45^{\circ}$  Fibers, Front View, Away-From-Hole,  $275^{\circ}$ F. (High magnification).

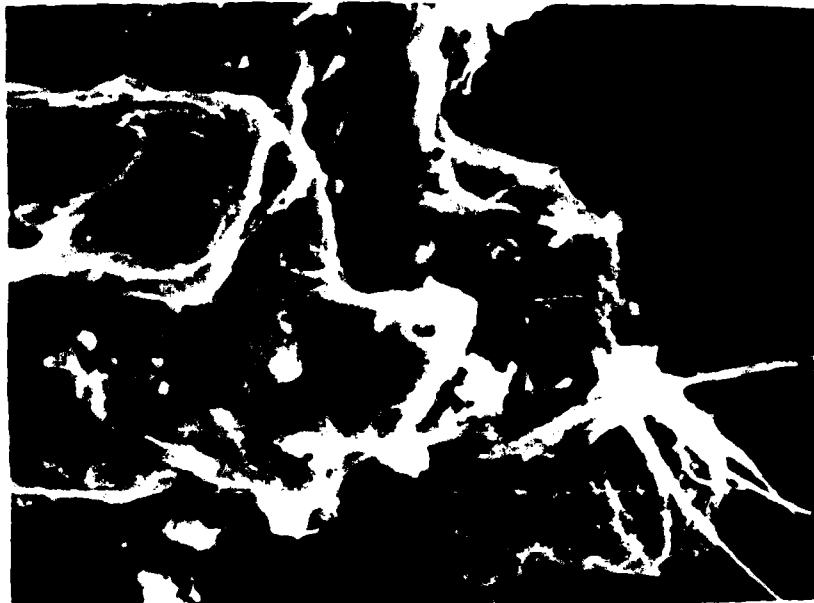


(a) 3250X



(b) 6500X

Fig. 101. Tension Specimen,  $45^{\circ}$  Fibers, Front View, Matrix Plasticity.



(a) 3250X



(b) 6500X

Fig. 102. Tension Specimen,  $45^{\circ}$  Fibers, Front View, Matrix Degradation.

## V. Conclusions

The vast expanse of experimental results and SEM microphotographs allow several conclusions to be drawn concerning APC-2 as a composite and APC-2 as compared with Gr/Ep and APC-1. The conclusions drawn from this experimental study are as follows:

1. APC-2 tension strength is only slightly affected by temperature increases up to the  $T_g$  for a given notch size.
2. Tension strength of APC-1 and APC-2 are comparable except at large (0.4" and 0.6") diameter holes, where APC-2 exhibits higher failure strengths.
3. APC-2 is less sensitive to notch size than APC-1 when larger radius (0.4" and 0.6") cut outs are considered for tension loading conditions.
4. APC-2 is less sensitive to notch size than Gr/Ep when tension and compression loading are considered.
5. The characteristic length ' $d_0$ ' is less sensitive to notch size in APC-2, for tension and compression, as compared to APC-1 and Gr/Ep, demonstrating better matrix load distribution characteristics in APC-2.

6. The characteristic length ' $a_0$ ' is not as notch sensitive in APC-2, for tension and compression loading, compared to APC-1 and Gr/Ep, confirming the better matrix load distribution characteristics of APC-2.

7. The parameters C (notch sensitivity) and m (exponential parameter) from Pipes' three parameter model of failure prediction are not constants for a given material when temperature variations occur.

8. The notch sensitivity factor, C, for APC-2 is less than the values for APC-1 and Gr/Ep when tension loading is considered.

9. The two parameter and three parameter prediction models are sufficient for a specific temperature but are not as effective when temperature variations are considered, thus no general failure prediction model has been presented to date.

10. APC-2 compression strength is significantly and consistently reduced by temperature increases up through the  $T_g$ .

11. Compression strength of APC-2 is more than compression strength of APC-1 for temperatures through the  $T_g$ .

12. APC-2 has higher strength for notched specimens than Gr/Ep for room temperature conditions when compression loading is

considered, even though the Gr/Ep has a seven percent fiber volume advantage over APC-2.

13. Matrix degradation with increasing temperature reduces the overall strength of a APC-2 for tension and compression through cohesive failure of the matrix.

14. Under compression loading, the  $0^0$  fibers at the cut out fail initially and the failure mode (crack) progresses from the notch to an outside edge perpendicular to load direction.

15. The tougher thermoplastic, PEEK, does not provide improved performance in laminates with holes when crippling of the fibers is a dominant compression failure mode.

16. The crystallization process continues at temperatures above the  $T_g$  and thus, larger amounts of matrix adhere to the fibers.

17. Crack growth in tension specimens initiates at the cut out and progresses toward the outside edge.

18. The crack growth rates for tension specimen are slower at the notch than away from the notch.

## VI Recommendations

Although this study is extensive in detailing the failure modes of APC-2 for tension and compression loadings, in evaluating three failure prediction methods, and in comparing failure strengths of three composite materials, there are still deficiencies that require further assessment. To advance the state of art in these areas, the following recommendations are presented.

(1) The specific failure mechanisms of individual fiber direction plys should be studied for notched specimen. A study of failure mechanisms for laminates of the same direction ( $0^{\circ}$  and  $90^{\circ}$ ) and symmetric directions ( $+45^{\circ}$  and  $-45^{\circ}$ ) would lead to individual failure mechanisms. Then, individual failure mechanisms could be compared to the more complex laminate system failure mechanisms evaluated in this study.

(2) It is possible to determine individual fiber failure direction using high magnifications on the scanning electron microscope. This procedure consumes a significant amount of time, but it can be used to describe the fiber failure pattern for a fractured laminate. If the fibers fail individually, there may be a randomness to the fracture directions. However, if the fibers fail in groups, there may be a general direction of crack growth that can be determined. This method could be used to evaluate transition

areas where different crack growth rates occur. An evaluation of a brittle epoxy matrix composite and a thermoplastic matrix composite is recommended to further define the crack growth rate transition area.

(3) A general purpose failure prediction method capable of handling various temperature states for a given composite is needed for field use. A detailed analysis of composites, tested to various temperatures, is required to determine specific temperature effects. Through this analysis, a material parameter such as the thermal coefficient of expansion might be defined.



## Bibliography

1. Williams, J.G., "Effect of Impact Damage and Open Holes on the Compression Strength of Tough Resin/ High Strain Fiber Laminates", NASA Technical Memorandum 85756, (February 1984).
2. Donaldson, S.L., "Fractography of Mixed Mode I-II Failure in Graphite/Epoxy and Graphite/Thermoplastic Unidirectional Composites", AFWAL-TR-84-4186, (June 1985).
3. Malik, B., Palazotto, A.N. and Whitney, J.M., "Notch Strength of GR/PEEK Composite Material at Elevated Temperatures", AIAA paper No. 85-0648, (1985).
4. Rybicki, E.F. and Schmuesser, D.W., Three Dimensional Finite Element Stress Analysis of Laminated Plates Containing a Circular Hole, AFML-TR-76-96, (Aug. 1976).
5. Barker, R.M. et al, "Stress Concentration Near Holes in Laminates", Engineering Mechanics, Vol. 3, (June 1974).
6. Cruse, T.A., "Tensile Strength of Notched Composites", Journal of Composite Materials, Vol. 7, p. 218, (1973).
7. Knoish, H.J. and Whitney, J.M., "Approximate Stresses in an Orthotropic Plate Containing a Circular Hole", Journal of Composite Materials, Vol. 9, 157-158, (April 1975).
8. Morris, D.N. and Simond, R.A., The Effect of Extreme Temperatures on the Elastic Behavior of Graphite/ Polyimide Composites, NASACR 172143, (1983).
9. Greszczuk, L.B., "Stress Concentrations and Failure Criteria for Orthotropic and Anisotropic Plates with Circular Openings", Composite Materials, Testings and Design, American Society for Testing Materials, ASTM STP497, Philadelphia, Pa, (1972).
10. Whitney, J.M. and Nuismer, R.J. "Stress Fracture Criteria for Laminated Composites Containing Stress Concentrations", Journal of Composite Materials, Vol 8, (July 1974).
11. Whitney, J.M. and Nuismer, R.J., "Uniaxial Failure of Composite Laminates Containing Stress Concentrations", ASTM STP 593, American Society for Testing and Materials, (1975).

12. Waddoups, M.E. and others. "Macroscopic Fracture Mechanics of Advanced Composite Materials", Journal of Composite Materials, Vol 5, p. 446, (1971).
13. Tirosh, J., "On the Tensile and Compressive Strengths of Solids Weakened (Strengthened) by an Inhomogeneity", Journal of Applied Mechanics, p. 449, (September 1977).
14. Nuismer, R.J. and Hahn, H.T. presented at the American Society for Testing and Materials, "Composite Reliability Conference", Las Vegas, Nevada, (15-16 April 1974).
15. Karlak, R.F., "Hole Effects in Related Series of Symmetrical laminates", Proceedings of Failure Modes in Composite III, American Society of Metals, Chicago, (1977).
16. Whitney, J.M. and Kim, R.Y., "Effect of Stacking Sequence on the Notched Strength of Composite Laminates", AFML-TR-76-177, (November 1976).
17. Pipes, R.B., Gillispie, J.R. and Wethhold, R.C., "Superposition of the Notched Strength of Composite Laminates", Polymer Engineering and Science, Vol 19, No. 16, (December 1979).
18. Nuismer, R.J. and Labor, J.D., "Application of the Average Stress Failure Criteria: Part I-Tension", Journal of Composite Materials, Vol 12, 238-249, (July 1978).
19. Nuismer, R.J. and Labor, J.D., "Application of the Average Stress Failure Criteria: Part II-Compression", Journal of Composite Materials, Vol 13, 49-60, (January 1979).
20. Rhodes, M.D., Mickulas, M.M. and Medowan, P.E., "Effect of Orthotropic Properties and Panel Width on the Compression Strength of Graphite/Epoxy Laminates with Holes", AIAA paper No. 82-0749, (1982).
21. Jones, D.P., Leach, D.C. and Moore, D.R., "Mechanical Properties of Poly-ether-ether-ketone for Engineering Applications", Polymer, Vol 26, (August 1985).
22. Donaldson, S.L., "Fracture Toughness Testing of Graphite/Epoxy and Graphite/PEEK Composites", Composites, Vol 16, No 2, (April 1985).

23. Hartness, J.T., "An Evaluation of Polyetheretherketone Matrix Composites Fabricated from Unidirectional Prepreg Tape", SAMPE Proceedings of 29th Symposium and Exhibition, Mar 1984
24. Hartness, J.T. and Kim, R.Y., "A Comparative Study on Fatigue Behavior of Polyetheretherketone and Epoxy With Reinforced Graphite Cloth", SAMPE Proceedings of 28th Symposium and Exhibition, Mar 1983
25. Leach, D.C. et al, "Delamination Behavior of Aromatic Polymer Composite APC-2", Presented at ASTM Symposium on Toughened Composites, Houston, Tex, (March 1985).
26. Leach, D.C. and Moore, D.R., "Toughness of Aromatic Polymer Composites", Presented at "Composites: Materials and Engineering", University of Delaware, (September 1984).
27. Pipes, R.B., Wetherhold, R.C. and Gillispie, J.W., "Notched Strength of Composite Materials", Journal of Composite Materials, Vol 13 (April 1979), pp 148-160.
28. Timoshenko, S.P. and Goodier, J.M., Theory of Elasticity, Second Edition, McGraw-Hill, New York, p. 78, (1951).
29. Irvin, G.R., "Fracture Dynamics", Fracturing of Metals, ASM, Cleveland, (1948).
30. Lekhnitakii, S.G., Anisotropic Plates, Translated from the Second Russian Edition by S.W. Tsai and T. Cheron, Gordon and Breach, Science Published, Inc., New York, p. 157, (1968).
31. Blundell, D.J. et al, "Cryatalline Morphology of the Matrix of PEEK-Carbon Fiber Aromatic Polymer Composites, 1. Assessment of Crystallinity", SAMPE Quarterly, Vol 16, No 4, (July 1985).
32. Cottrell, A.H., The Mechanical Properties of Matter, Robert E. Krieger Publishing Co., Hunington, N.Y., (1981).
33. Kumer, S., and Anderson, D.P., "Crystallization and Morphology of Poly (aryl ether ether ketone)", Accepted for Publication in forth coming 1986 issue of Polymer magazine
34. Jones, R.M., Mechanics of Composite Materials, Scripta Book Co., Washington D.C., (1975).

35. Miller, A.G. and Wingert, A.L., "Fracture Surface Characterization of Commercial Graphite/Epoxy Systems", American Society for Testing and Materials, ASTM STP 696, Philadelphia, Pa (1978).
36. Nuismer, R.J. and Brown, G.E., "Progressive Failure of Notched Composite Laminates Using Finite Elements", Advances in Engineering Science, 13th Annual Meeting Society of Engineering Sciences (1976).

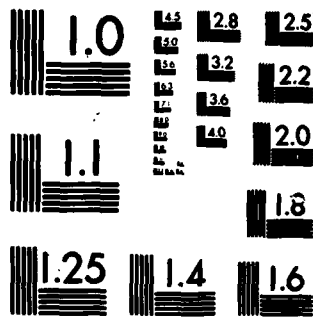
AD-A164 033    COMPARISON OF NOTCH STRENGTH BETWEEN GR/PEEK (APC-1 AND 3/3  
APC-2) AND GR/EPO. (U) AIR FORCE INST OF TECH  
WRIGHT-PATTERSON AFB OH SCHOOL OF ENGI..    J E RAMEY  
UNCLASSIFIED    DEC 85 AFIT/GAE/AR/85D-12    F/G 11/4    NL

END

FILED

100

DTIC



MICROCOPY RESOLUTION TEST CHART  
NATIONAL BUREAU OF STANDARDS-1963-A

Vita

Joe Ernest Ramey, Jr. was born 23 September 1950 in Coeburn, Virginia. In February 1969, he married Freda Sutherland and later that month joined the U.S. Air Force. After 12 years enlisted time, he graduated from Texas A&M University with a Bachelor of Science degree in Aerospace Engineering. He attended Officer Training School and was commissioned a second lieutenant in April 1981. He then worked at the Warner Robins Air Logistic Center as a structural engineer for the C-130 aircraft. In June of 1984, he entered the Air Force Institute of Technology in the Graduate Aeronautical Engineering Program.

Permanent Address: Rt.1, Box 89  
Coeburn, Va. 24230

UNCLASSIFIED

SECURITY CLASSIFICATION OF THIS PAGE

AD-A164033

REPORT DOCUMENTATION PAGE

1a. REPORT SECURITY CLASSIFICATION <b>UNCLASSIFIED</b>		1b. RESTRICTIVE MARKINGS	
2a. SECURITY CLASSIFICATION AUTHORITY		3. DISTRIBUTION/AVAILABILITY OF REPORT Approved for public release; distribution unlimited.	
2b. DECLASSIFICATION/DOWNGRADING SCHEDULE		5. MONITORING ORGANIZATION REPORT NUMBER(S)	
4. PERFORMING ORGANIZATION REPORT NUMBER(S) <b>AFIT/GAE/AA/85D-12</b>		7a. NAME OF MONITORING ORGANIZATION	
6a. NAME OF PERFORMING ORGANIZATION <b>School of Engineering</b>	6b. OFFICE SYMBOL (If applicable) <b>AFIT/ENY</b>	7b. ADDRESS (City, State and ZIP Code)	
6c. ADDRESS (City, State and ZIP Code) <b>Air Force Institute of Technology Wright-Patterson AFB, Ohio 45433</b>		9. PROCUREMENT INSTRUMENT IDENTIFICATION NUMBER	
8a. NAME OF FUNDING/SPONSORING ORGANIZATION	8b. OFFICE SYMBOL (If applicable)	10. SOURCE OF FUNDING NOS.	
8c. ADDRESS (City, State and ZIP Code)		PROGRAM ELEMENT NO.	PROJECT NO.
11. TITLE (Include Security Classification) <b>See Box 19</b>		TASK NO.	WORK UNIT NO.
12. PERSONAL AUTHOR(S) <b>Ramey, Joe E. Jr.</b>			
13a. TYPE OF REPORT <b>MS Thesis</b>	13b. TIME COVERED FROM _____ TO _____	14. DATE OF REPORT (Yr., Mo., Day) <b>1985 December</b>	15. PAGE COUNT <b>192</b>
16. SUPPLEMENTARY NOTATION			

17. COSATI CODES			18. SUBJECT TERMS (Continue on reverse if necessary and identify by block number) <b>Composite Materials, APC-1, APC-2, Gr/Epoxy, Peek, Notched Strength Comparison, SEM Fracture Surfaces, Point Stress Failure Criterion, Average Stress Failure Criterion, Pipes, Three Parameter Failure Criterion.</b>
FIELD <b>11</b>	GROUP <b>04</b>	SUB. GR.	

19. ABSTRACT (Continue on reverse if necessary and identify by block number)

**Title: COMPARISON OF NOTCH STRENGTH BETWEEN GR/PEEK (APC-1 AND APC-2) AND GR/EPOXY COMPOSITE MATERIALS AT ELEVATED TEMPERATURES**

**Thesis Chairman: Dr. Anthony Palazotto**

Approved for public release LAW-SPR 85-11  
 JOHN E. WOLAVEN 16 JAN 86  
 Dean for Research and Professional Development  
 Air Force Institute of Technology (AGS)  
 Wright-Patterson AFB - OH 45433

20. DISTRIBUTION/AVAILABILITY OF ABSTRACT UNCLASSIFIED//UNLIMITED <input checked="" type="checkbox"/> SAME AS RPT. <input type="checkbox"/> DTIC USERS <input type="checkbox"/>		21. ABSTRACT SECURITY CLASSIFICATION <b>Unclassified</b>	
22a. NAME OF RESPONSIBLE INDIVIDUAL <b>ANTHONY W. PALAZOTTO, PROFESSOR</b>		22b. TELEPHONE NUMBER (Include Area Code) <b>513-255-3517</b>	22c. OFFICE SYMBOL <b>AFIT/ENY</b>



UNCLASSIFIED

SECURITY CLASSIFICATION OF THIS PAGE

Abstract:

Thermoplastics have been developed to improve fracture toughness compared to the widely used thermosetting polymers such as epoxy systems. A semi-crystalline thermoplastic, poly-ether-ether-ketone(PEEK), matrix has been developed with significant toughness improvement over thermosets. A review of literature resulted in very little information related to the Aromatic Polymer Composite-2 (APC-2) which is formed from graphite fibers (60% volume) and PEEK. The experimental study reported herein was conducted to investigate the high temperature strength (tension and compression) of APC-2 laminates with holes. The experimental data was then used to determine parameters necessary to predict failure stress trends for the average stress failure criterion, point stress failure criterion, and a three parameter model failure criterion. The comparison of experimental and predicted failure strengths are depicted graphically. The failure modes of APC-2 are also studied utilizing the scanning electron microscope.

**END**

**FILMED**

**386**

**DTIC**